PROTEUS

ADAPTIVE MICROFLUIDIC - AND NANO - ENABLED SMART SYSTEMS FOR WATER QUALITY SENSING

WP5- Validation of the first version of Proteus integrated system

D5.2

Sensing performances, reliability in lab testing, energy management, and model deployments

Author : **Bérengère Lebental**

March, 6th 2016

www.proteus-sensor.eu

This project has received funding from the European Union's H2020 Programme for research, technological development and demonstration under grant agreement No 644852

Editor:	Bérengère Lebental, IFSTTAR	
Deliverable nature:	R-Report	
Dissemination level:		
Contractual/actual delivery date:	M18	M25
Suggested readers:	Consortium partners	
Version:	V1.0	
Keywords:		

Disclaimer

This project has received funding from the European Union's Horizon 2020 Programme for research, technological development and demonstration under grant agreement n° 644852.

Copyright notice

Revision History

Revision	Date	Description	Author (Organisation)
V0.1	20/06/2016	Creation	Bérengère Lebental (IFSTTAR)
V0.2	21/11/2016	Updated TOC	Bérengère Lebental (IFSTTAR)
V0.3	25/11/2016	IFSTTAR, ESIEE, WINGS, NIPS, AQUALABO, UNINOVA contributions	Bérengère Lebental (IFSTTAR)
V0.4	01/02/2017	Revised TOC;	Bérengère Lebental (IFSTTAR)
V0.4	20/02/2017	ESIEE, UI, UNINOVA, IFSTTAR contributions. Homogenization by IFSTTAR	Bérengère Lebental (IFSTTAR), Tarik Bourouina (ESIEE), Bruno Almeida, Miguel Costal (UI), Joao Oliveira (UNINOVA)
V0.5	03/03/2017	Review by UI and SMAS	Bruno Almedia (UI), Paulo Nico (SMAS)
V1.0	06/03/2017	Final version before submission	Bérengère Lebental (IFSTTAR)

Table of content

Executive summary

The first version of Proteus node (PNODE V1 in short, described in D5.1) contains the following components:

- a replaceable “sensor cap” integrating a CMOS chip and a sensor chip with 7 different types of MEMS and CNT sensors into a single compact, waterproof packaging
- an electronic card V1.2 enabling both operation of the sensor cap, notably wired and wireless data gathering up to a water management system, and multi-source energy harvesting to power the full PNODE.

The present deliverable D5.2 reports first on new validation results for the different building blocks of this D5.1 prototype (7 different types of sensors, analog to digital conversion by the CMOS chip, piezoelectric vortex generator). These building blocks are described for the most part in the deliverables D3.1, D3.2, D3.3 that predate deliverable D5.1.

Then we present the lab validation of the sensor cap in chapter 3: description of the different versions of caps under test, description of the sensor analog front end, description of the test bench for chemical and thermal sensitivity analysis. Linear sensitivity to temperature, pH, chlorine and chloride are demonstrated, though the selectivity between the different CNT sensors needs to be investigated further and probably enhanced. The conductivity sensor still remains to be investigated in the lab.

After a description of Sense-City water loop and a description of the integration strategy of the PNODE in Sense-City water management system, the validation results of the PNODE in Sense-City are proposed: temperature-compensated, linear sensitivity of temperature, pressure, conductivity, pH, chlorine and chloride sensors are observed, though additional data and data processing would provide valuable insight. A lower bound for the precision level of ach of the sensors is provided. Energy harvesting is also demonstrated in Sense-City, as well as prediction capability at water management system level.

Finally, the different outcomes are summarized. Additional validation steps are listed for the current version of the PNODE, while optimization routes are proposed, to be explored in the deliverable D2.2 (design).

1 Introduction

The first version of Proteus node (PNODE V1 in short, described in details in D5.1) contains the following components:

- a replaceable “sensor cap” integrating a CMOS chip and a sensor chip with 7 different types of MEMS and CNT sensors into a single compact, waterproof packaging
- an electronic card enabling both operation of the sensor cap, notably wired and wireless data gathering up to a water management system, and multi-source energy harvesting to power the full PNODE.

The present deliverable D5.2 reports first (chapter 2) on new validation results for the different building blocks of this D5.1 prototype. These building blocks are described for the most part in the deliverables D3.1, D3.2, D3.3 that predate deliverable D5.1.

Then we present the lab validation of the sensor cap in chapter 3, accompanied by some more details on the mode of operation of the sensor cap by the electronic card.

After a description of Sense-City water loop, the chapter 4 presents the validation results of the PNODE in Sense-City.

Chapter 5 summarizes the different outcomes and proposes optimization routes

2 Lab validation of separate building blocks

2.1 Generalities

The PNODE includes the following hardware buildings blocks, which are described in details in other building blocks:

- A 1cm² silicon sensor chip with 7 types of sensors (description in D3.1): temperature, pressure, flow rate, conductivity sensors based on microelectronics/MEMS technologies; pH, chlorine, chloride sensors (3 of each type on each chip) based on carbon nanotubes technologies.
- A CMOS chip designed as the analog front end of the sensor chip (description in D3.2).
- A V1.2 electronic card operating the CMOS and the sensor chip (description in D3.3 and D5.1; complement in the following chapter 3 of D5.2)
- A mechanical housing for the sensor head on the one hand, called sensor cap and assembling sensor and CMOS chips, and for the electronic card on the other hand (description in D5.1)
- A energy harvester implanted inside the pipe based on piezoelectric vortex generation (description in D5.1)

The following sections described the validation of the different types of sensing elements in the sensor chips (sections 2.2 to 2.5), of the CMOS chip (section 2.6) and of the energy harvester (section 2.7) before integration of these different subparts into a PNODE, and notably before signal conditioning via a dedicated electronic card.

2.2 Temperature sensors

As a reminder from D3.1, the temperature sensor consists in a platinum resistor whose resistance varies linearly with respect to temperature: R(T)=R0 (1+αT). A 4-point measurement of the resistance ensures precision because the resistance is measured locally without including parasitic wiring resistance that may vary due to local heating from other chip devices.

A 4-point measurement consists in measuring the voltage drop at the resistor terminals while injecting a constant current of small value (less than 1 mA) so that to avoid self-heating of the resistor. The ratio of measured voltage over injected current values gives the value of the resistance and hence the value of temperature.

The resistors were designed to exhibit a resistance of about 1000 Ohm at room temperature (Figure 1). Calibration of a temperature sensor (before sensor caps assembly) was performed using an injected current of 500µA (using a LM317 as a current regulator) and a 16bit DAQ-board. The resistance of the resistor was then measured while dipping the probe into water at different temperatures. We obtained the following calibration curve (Figure 2):

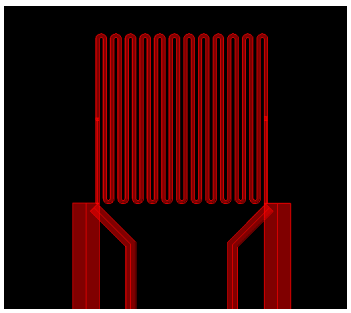

Figure 1; MEMS Temperature sensor layout

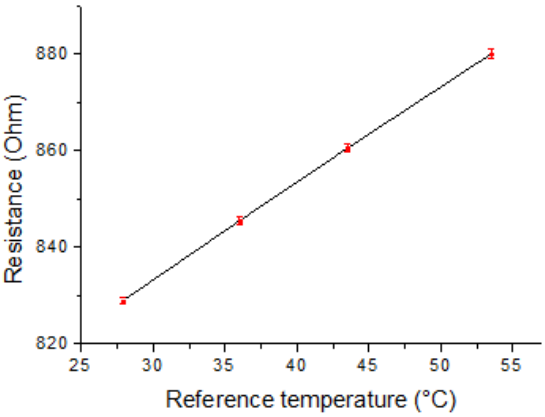

Figure 2: Calibration curve of a temperature sensor

Typical values for the R_0 and α parameters are 773 Ohm and $2.61 \times 10^{-3} °C^{-1}$ respectively. The precision is lower than 0.5°C. The actual room temperature resistance R_0 is lower than expected, due to variation in metal thickness and metal conductivity compared to the expected values. It is acceptable as it can be compensated during the calibration phase of the sensor. If not calibrated, the sensor will exhibit a systematic error in the form of an offset.

2.3 Conductivity sensors

This section presents lab testing results of conductivity sensors performed at ESIEE after completion of the MEMS chip fabrication. We present the experimental setup and the protocol used to conduct these experiments. Then, we present the results obtained on the 3 different versions of the fabricated conductivity sensors. These measurements are performed at the MEMS chip level. They will serve as a basis for comparison for further measurements that will be done at the PNODE level after complete assembly of the prototype.

2.3.1 Experimental setup

The conductivity sensors consist of four *independent* platinum electrodes, which are directly in contact with water (Figure 3). The corresponding reading circuit uses these 4 pole electrodes as follows: the inner two electrodes are used to read a voltage and the current is applied between the outer electrodes.

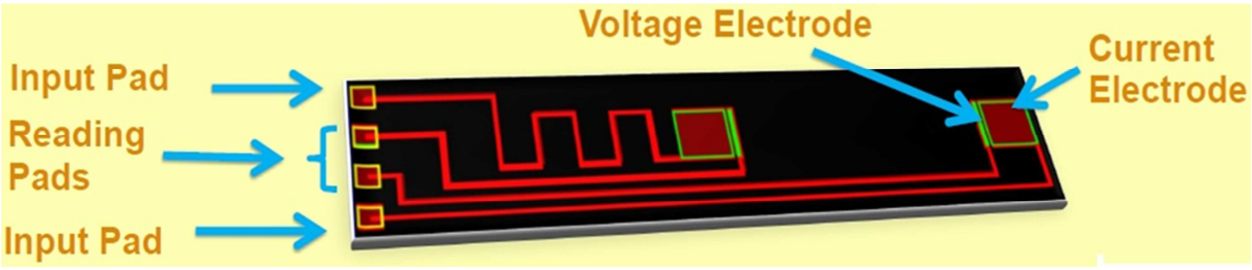

Figure 3: Schematic description of the 4-pole electrode arrangement for conductivity sensors. The two input pads are used to inject AC current into water, and the tow (inner) reading pads are used to read the corresponding voltage difference. The ratio of current over voltage is proportional to water conductivity.

The input and the output reading pads are connected through wire bonding to a PCB (Printed Circuit Board-Figure 4). The two input pads are the outer electrodes and are used for AC current injection and are referred as the current electrodes, while the two inner electrodes are used to read the corresponding voltage difference used for calculating the water conductivity.

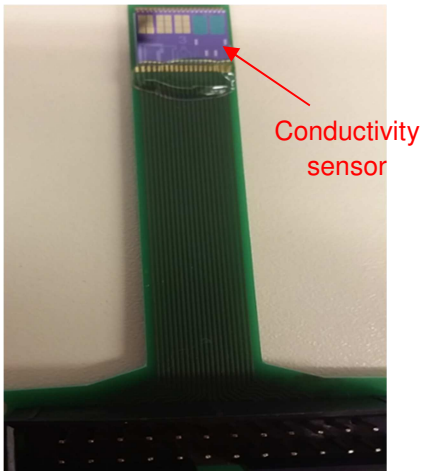

Figure 4: Multi sensor chip mounted on a PCB. Here subversion 3.

The amplitude of the excitation current *I* is maintained at a constant value of *1 μA* throughout the experiment. The corresponding voltage amplitude *V* is acquired and reversed. It is indicative of the water conductivity σ_w. Indeed, *1/V* is directly proportional to σ_w as expressed in the following relation*:*

$$\frac{1}{V} = \sigma_w\left(\frac{S}{IL}\right)$$

It is worth mentioning that the AC frequency needs to be chosen carefully within a certain frequency range. Typical values for optimum operation of our devices were found to be 5 kHz or 10 kHz.

It is also important to keep the excitation current amplitude at reasonably low values (here *1 μA)* so as to avoid severe electrolytic phenomena including the electro-erosion of the platinum electrodes, which might affect the device long-term reliability.

2.3.2 Data acquisition

The NI-6259 acquisition board was used. It has an acquisition frequency of 49 KHz, which was enough to proceed to our measurements for AC signals whose frequency range extends from 30 Hz to 20 KHz. The LabVIEW Graphical User Interface setup and its components are shown in the figure below (Figure 5).

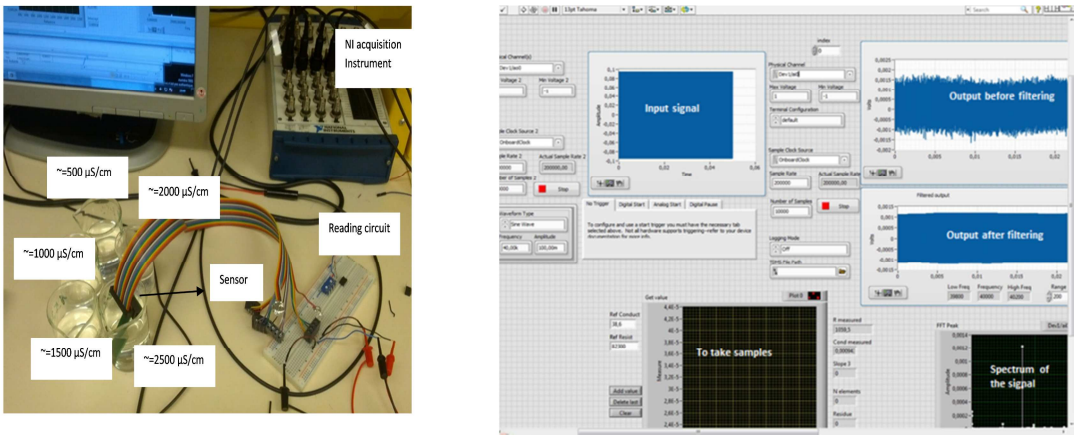

Figure 5. Experimental setup developed for conductivity measurements and corresponding Graphical User Interface

2.3.3 Procedure for testing and calibration

The experiments for testing and calibration of the conductivity sensors were performed using five water samples with different conductivity. The different levels of conductivity were obtained by adding different amount of Sodium chloride (NaCl) in pure water to approximately reach the following values: 500μS/cm, 1000μS/cm, 1500μS/cm, 2000μS/cm, 2500μS/cm. The exact conductivity of the samples was precisely measured using a reference conductivity sensor (calibrated beforehand using water conductivity standards).

It is essential to ensure that those conductivity values remain constant and uniform during the whole experiment. One also needs to maintain constant the temperature of the electrolytes. Conductivity measurements are strongly affected by the temperature of the samples. The conductivity reading of a salt solution of Sodium chloride typically changes every 2% for every centigrade degree. Therefore, the conductivity of a salt solution at 15°C can be expected to be about 20% different than the value at 25°C. Hence, it is important to take note of the temperature reading or the reference temperature with every conductivity reading recorded.

In general, it is very difficult to collect and store the samples much lower than ~147 μS/cm. These samples are easily affected by the contamination and by carbon dioxide absorption. Ideally, the sample container must be scrupulously clean and exclude the atmosphere. This is consistent with the smallest value of reference conductivity taken in this set of experiments.

2.3.4 Results on the 3 sensor versions

Then sensor responses were acquired while manually changing the frequency of the excitation AC signal. The frequency varies from 30 Hz to 20 KHz and the conductance is noted then the graph is plotted using excel sheets.

We compared the three versions of conductivity sensors, named 2.1, 2.2 and 2.3 (Figure 6). For each sensor and each water sample (with different water conductivity) 20 samples were taken and the average of those 20 values was calculated. The graphs were drawn based on those data.

From the frequency responses, the working frequency range of the sensor can be identified. We have selected 3 values of the AC frequency and made a representation of the corresponding curves of the measured conductivity as a function of the reference conductivity.

It was found from the latter curves that excellent linearity (with a linear regression coefficient R^2 of at least 0.991) is obtained on version 2 and version 3 of the conductivity sensors, while version 1 has very poor linearity (R^2 in the order of 0.2) certainly due to the square shape of the corresponding electrodes.

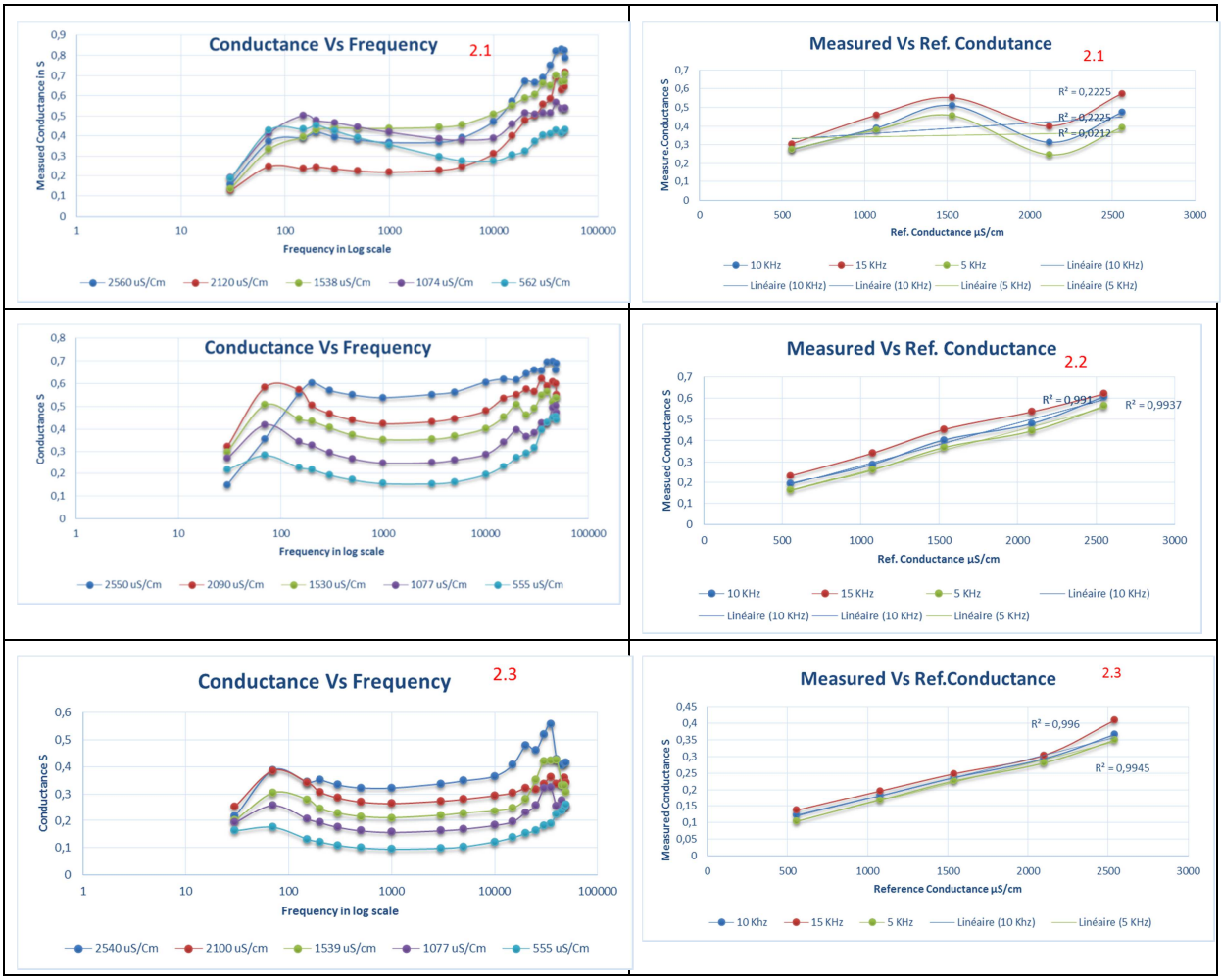

Figure 6. Experimentally measured responses of the conductivity sensors (from top to bottom, 2.1, 2.2., 2.3). The left column gives the frequency responses of the sensors immersed in five different solutions of known and pre-calibrated water conductivity. The second line gives the calibration curves at different fixed values of the AC voltage frequency. The latter results show that excellent linearity is obtained on version 2 and version 3 of the conductivity sensors, while version 1 has very poor linearity.

2.4 Pressure and flow rate sensors

2.4.1 Description of the test bench

For the lab testing performed at ESIEE, we used the setups shown in the Figure 7 below for the evaluation of flow-rate sensors and pressure sensors.

For flow-rate measurements (Fig. 1a), the sensor was inserted into a 32-mm diameter PCV pipe. A square-shaped plastic box with one open side was used as a water reservoir in which a variable speed water pump was submerged. A closed loop was built between the PVC pipe, the water reservoir and the pump by 16-mm diameter flexible pipes, which were connected to the PVC by adjusters. Hot-wire anemometric operation scheme was used for velocity and flowrate measurement. To ensure a good anemometric operation, a constant current source was used to supply the current to the 4-probe heater resistor. The source was built using LM317. LabVIEW was used for data acquisition. For each flowrate value, the voltage drop due to the flow cooling was measured. The resistance drop with respect to the zero-velocity situation was then calculated and related to the temperature and hence to the flow fluid velocity.

For pressure sensor measurements, we used an electronically tunable hydrostatic pressure source (FLUIGENT SA) feeding pressurized air into a closed glass bottle containing the pressure sensor. Even the pressure source is capable of producing a pressure level up to 7 bars, we preferred not exceeding 4 bars in this experiments for safety reasons. Our main objective at this stage was to provide preliminary evaluation of the fabricated pressure sensors. It is also worth mentioning that the measured responses were obtained under hydrostatic air pressure. Evaluation under water environment is in principle accessible through the use of an intermediate water reservoir (shown in the right side of the photo of Figure 1b) so as to transmit the hydrostatic air pressure to the closed bottle filled with water.

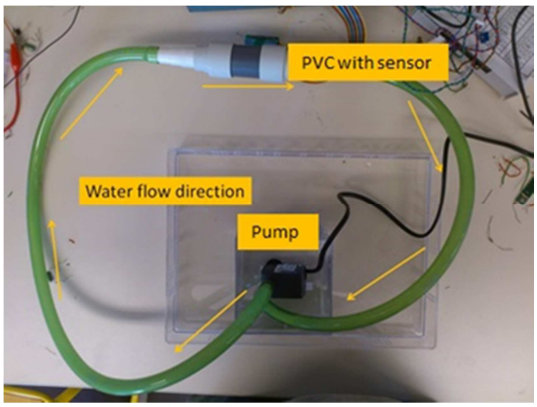

(a)

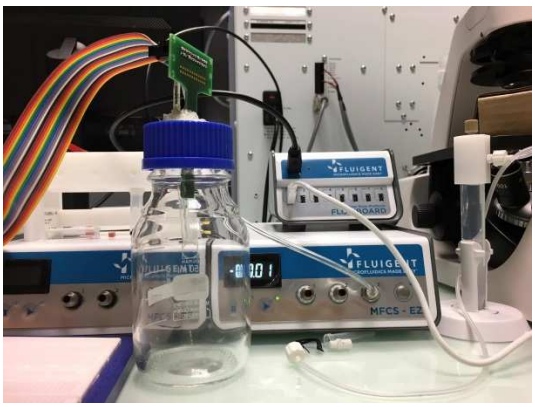

(b)

Figure 7. Experimental setups used for (a) flow-rate sensor measurements, (b) pressure sensor measurements.

2.4.2 Flow rate sensors

As a reminder, the multi-parameter sensor (Fig. 8) has a MEMS chip size of 1x1 cm in which the footprint of each sensor is no more than millimeters. All sensors are based on resistive read-out and all of them, except the pressure sensor, are easily obtained by metal micro-patterning with the combination of Ti, Pt and gold. Hence, when using glass as a substrate material, flow-rate sensors were easily co-integrated with temperature sensors and water conductivity sensors. On the other hand, when using silicon as a substrate material, further co-integration of a pressure sensor was possible. It required several additional steps, which include patterning of polysilicon strain gauges and backside etching of the silicon bulk. The later step was used to produce thin membranes of silicon, not only for the pressure sensor but also to some of the flow-rate sensors aiming to reduce their thermal conductance. In each case, the membrane is acting either as a mechanically flexible structure or as a thermal insulating layer, respectively. It is important to understand et this point that even glass has intrinsic better thermal properties with respect to the performance of the flow-rate sensor, however, silicon has absolutely need to be used as it allows co-integration of the pressure sensor on the same chip. Hence, the main challenge here is to co-integrate a flow-rate sensor with a pressure sensor, while keeping good performance and reasonable power consumption.

We considered in this study of the flow-rate sensor, the three different configurations explored to date schematically depicted in Figure 9: (i) glass, (ii) silicon and (iii) silicon membrane. This comparative study aims to make an evaluation of the thermal insulation, also targeting the best tradeoff between sensitivity and power consumption.

The experimental measurement results (Fig. 10) confirm the expected trends. Even with the rather high conductivity of silicon, compared to glass, it appears that a small but perfectible reduction of thermal conductance is obtained on silicon through the use of a membrane.

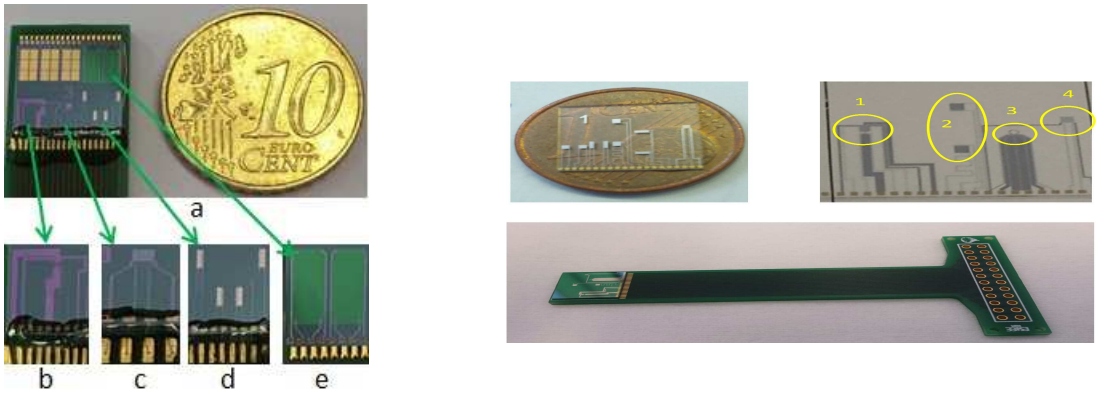

Figure 8. Left) Reminder on the details of (a) fabricated silicon multi-parameter sensor chip including (b) flow-rate sensor, (c) temperature sensor, (d) 2 conductivity sensors, (e) 2 pressure sensors – Right) Similar chip on glass substrate co-integrating all sensors except the pressure sensor

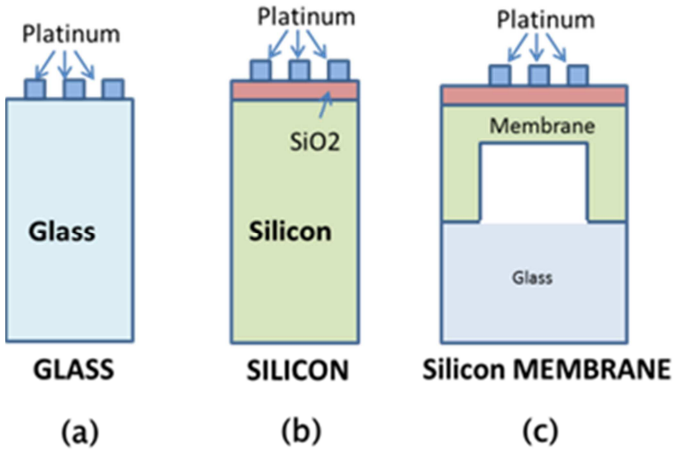

Figure 9: The 3 different configurations considered to date for the flow-rate sensor aiming to study the impact on thermal conductance and hence on power consumption.

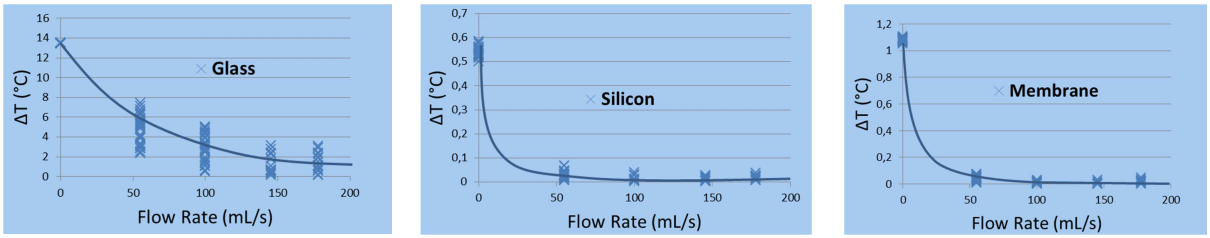

Figure 10: Measured responses of the flow-rate sensor corresponding to the 3 configurations (a), (b) and (c) described in Figure 9, illustrating the best performance for glass substrate, the worst for pure silicon substrate, and an intermediate response for silicon membrane.

2.4.3 Pressure sensors

Figure 11 below gives an illustration of typical responses of version 1 and version 2 of the pressure sensors, corresponding to (twin) rectangular and square shaped membranes, respectively. In both cases, an excellent linearity is observed in the explored pressure range up to 4 bars of absolute pressure, with a regression coefficient of 0,998 for both variants of the pressure sensors.

It is worth mentioning that in these figures, the values of the pressure in the horizontal axis denotes the absolute pressure. This value was evaluated from the differential pressure produced in our setup, assuming a value of 1 bar for the atmospheric pressure during measurement.

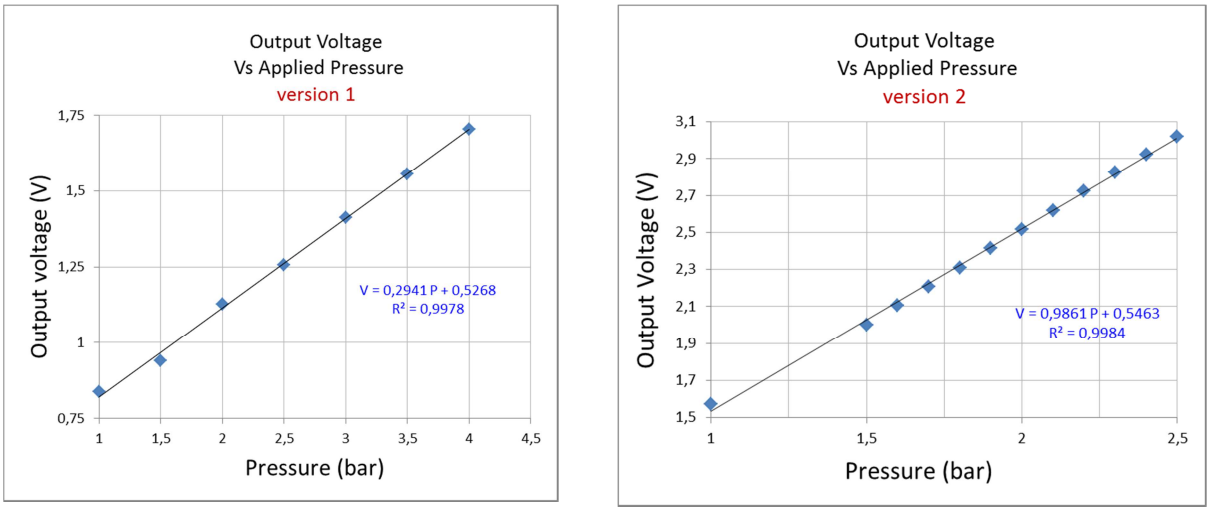

Figure 11: Measured responses of the two versions of the pressure sensors, based on rectangular (version 1) and square membranes (version 2). Excellent linearity is observed in both cases with a regression coefficient of 0,998.

2.5 CNT sensors

The following sections show the sensitivity of CNT sensors fabricated according to the process described in deliverable D3.1.

2.5.1 Experimental setup

The CNT chips are bonded onto dedicated PCBs as shown in Figure 12. The bondings are insulated from water using the UV curing optical resist NOA61 from Thorlabs. Solutions with predefined amount of chemicals are prepared beforehand in beakers. For pH testings, NaOH or HBr are dissolved in deionized water. For free chlorine testing, dilution of bleach (NaOCl) in DI water is used. For the chloride sensors, KCl salt is dissolved in DI water.

During testing, the chip under test is plunged into a given beaker. From one beaker to the next, the chip is rinsed with deionized water. The temperature of each beaker is monitored when the chip is in it. The average temperature during each trial is registered.

The electrical response of the individual sensors is measured using a Keithley 2601 sourcemeter in single channel mode: a current is applied on one of the channels and the voltage of the channel is measured. The excitation consists of rectangular current pulses at 10μA at frequency 0.25 Hz (period 4s) with duty cycle 50% (2s ON, 2s OFF).

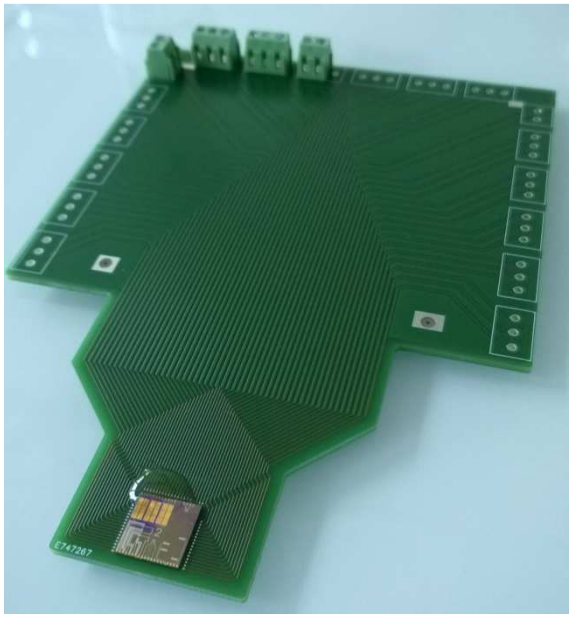

Figure 12: CNT sensor chip bonded onto a dedicated PCB

2.5.2 pH sensors

The pH sensors are made using pristine CNTs (without functionalization). Figure 13 shows SEM images of these well-dispersed CNTs.

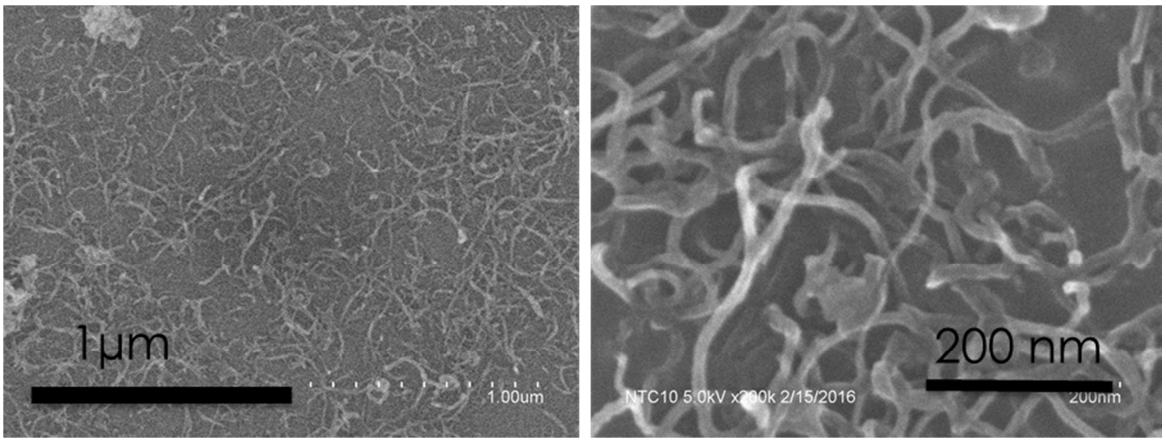

Figure 13: SEM images of a deposition of non-functionalized (pristine) CNT deposition

Figure 14 shows the relative resistance variation of one of the pH sensor as a function of pH (with respect to the resistance at pH 7). The sensors are not sensitive to pH below pH 8. Above pH 8, the resistance increases linearly with the pH ($\Delta R/R(\%)=16pH-140$), with high correlation factor ($R^2=0.93$).

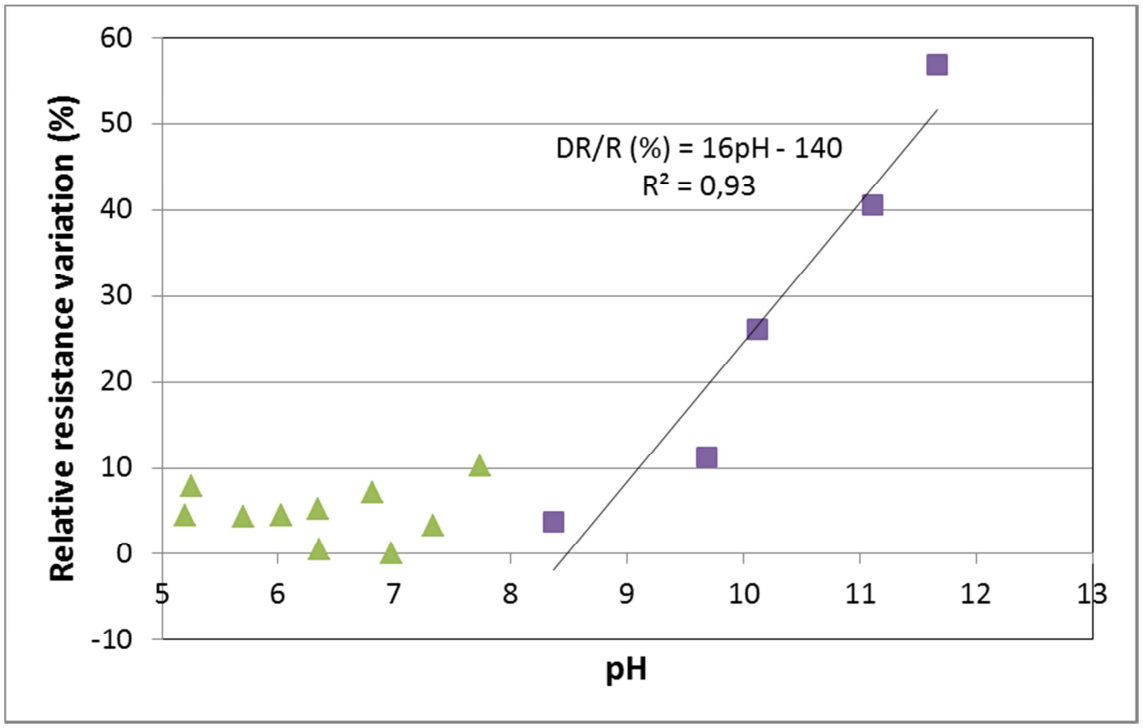

Figure 14: Relative resistance variation as a function of pH. The reference resistance is 27kΩ measured at pH 7.

2.5.3 Chlorine sensors

The chlorine sensors are made using CNT functionalized with the CF-OX-14, a conjugated polymer with formula displayed in Figure 15a.The oxime function is responsible for the sensitivity to hypochlorite ions. The hypochlorite ion is one of the forms of chlorine in water, notably prevalent at higher pH. Figure 15b is the SEM image of deposition of CNT functionalized with CF-OX-14.

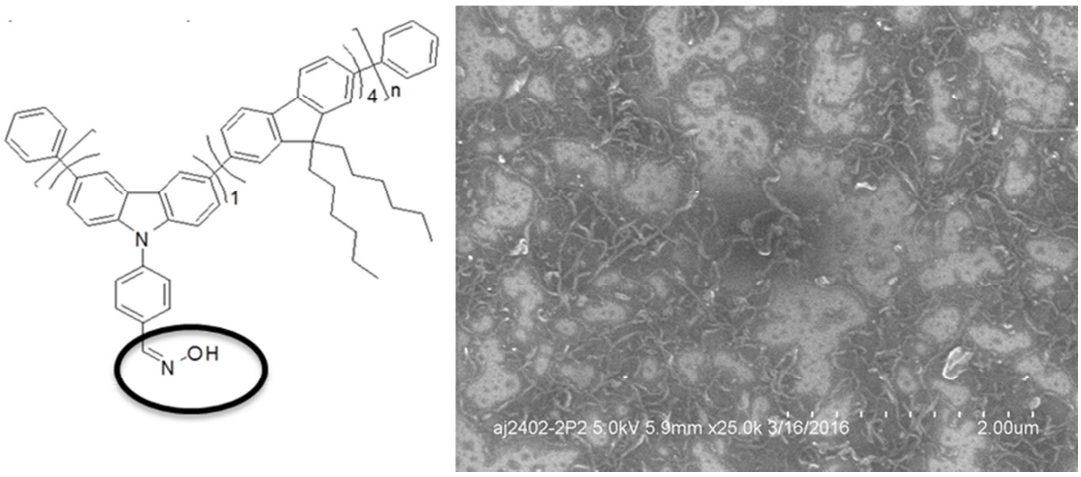

Figure 15: a) CF-OX-14 molecule used to functionalize CNT for hypochlorite detection .b) SEM image of a deposition of CNT functionalized with CF-OX-14.

Figure 16 shows the sensitivity of one of the resulting devices to the free chlorine concentration (total chlorine content, including hypochlorite ions ClO^- and hypochlorous acid HClO). The free chlorine concentration is controlled by the volume of added bleach (NaOCl). There is an increase by 12% of the resistance over the whole range of concentration of interest. Sensitivity to active chlorine alone was not tested.

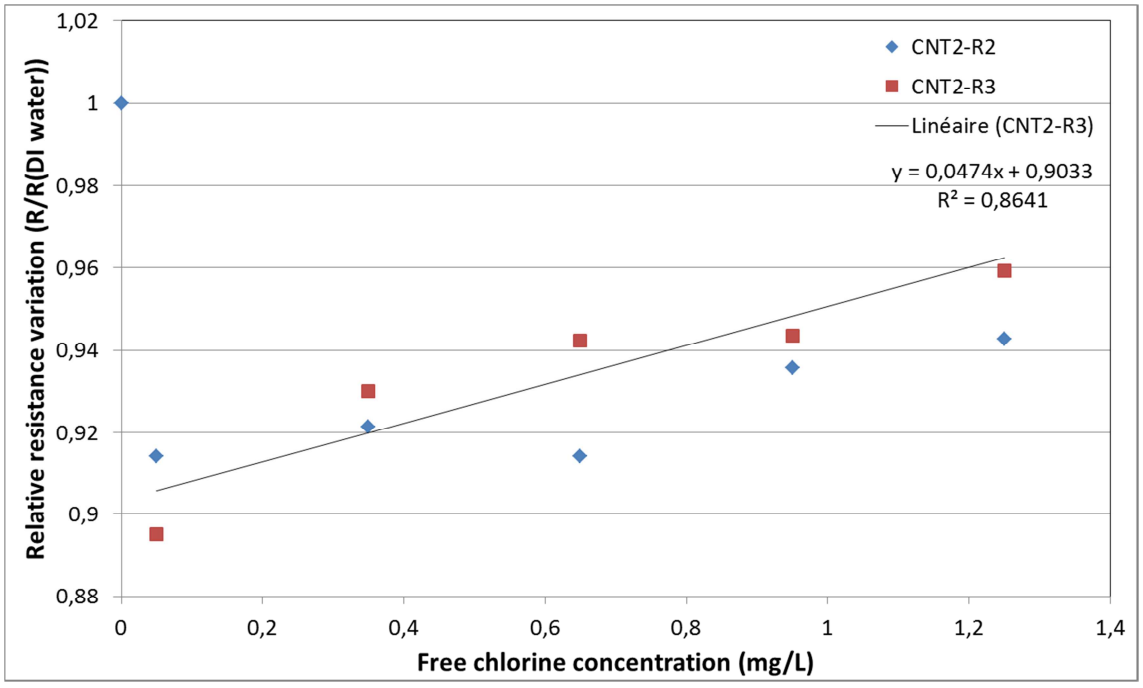

Figure 16: Resistance increases linearly as a function of the free chlorine concentration.

2.5.4 Chloride sensors

The chloride sensors are made using CNT functionalized with the FF-UR-14, a conjugated polymer with formula displayed in Figure 17a.The pair of urea functions is responsible for the sensitivity to chloride ions. Figure 17b is the SEM image of deposition of CNT functionalized with FF-UR-14.

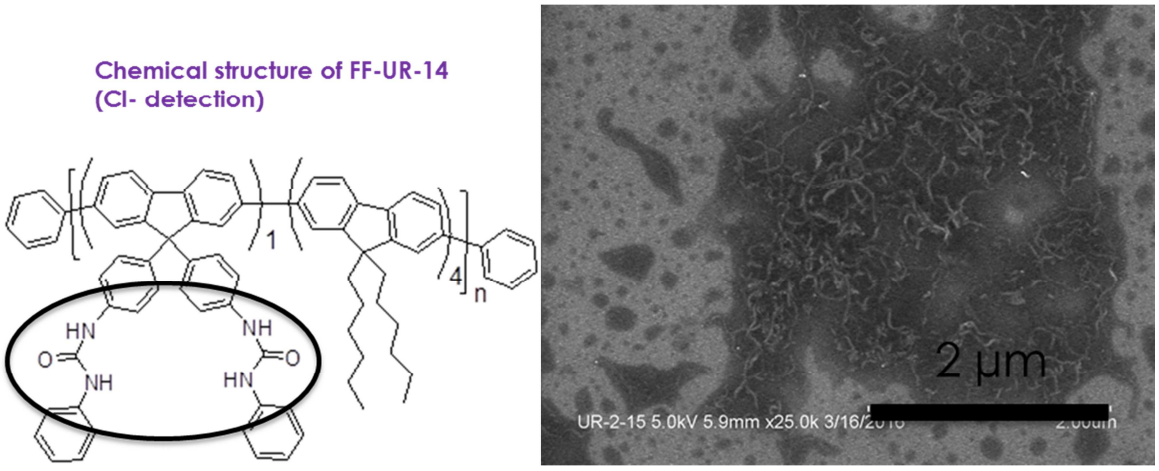

Figure 17: a) FF-UR-14 molecule used to functionalize CNT for chloride detection. b) SEM image of a deposition of CNT functionalized with FF-UR-14.

Figure 18 shows the strong sensitivity (50%) of one of the resulting devices to the concentration of chloride ions, at low chloride concentration (1.5mg/L; only 0.5% of the full range of interest). The sensitivity at higher concentrations was not studied. Note that in mg/L, we have [Cl-]=0.6[NaCl].

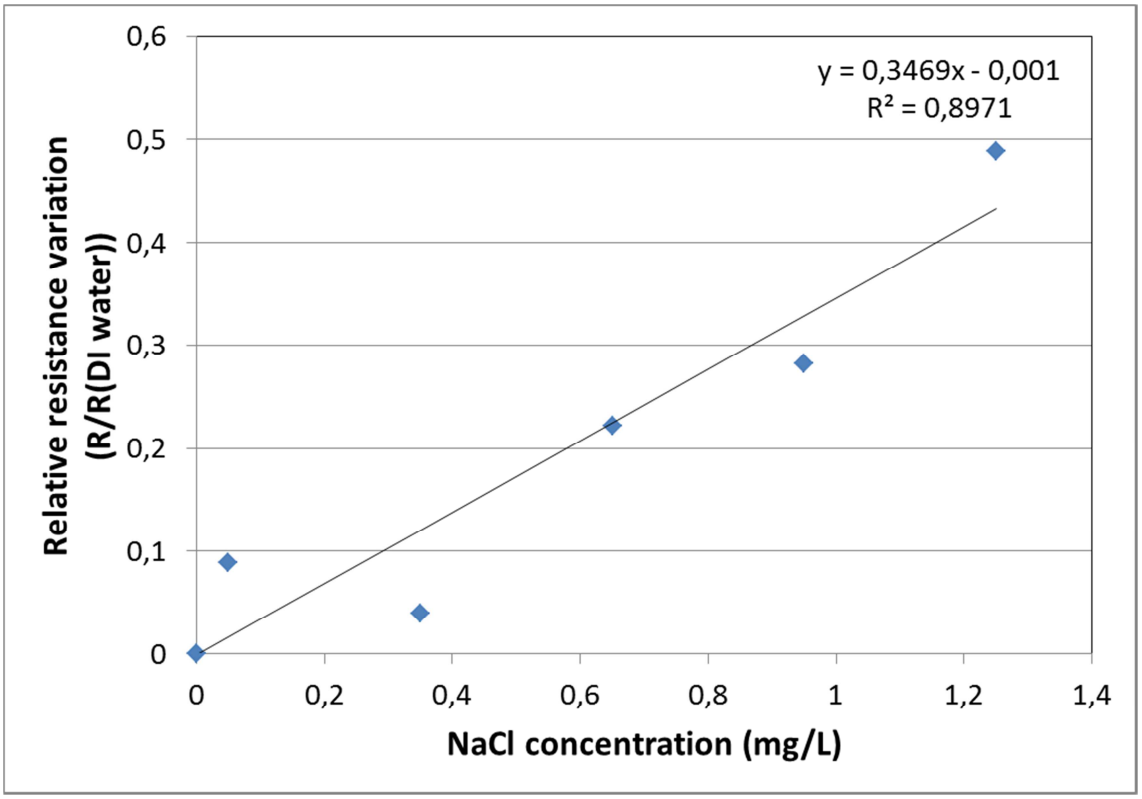

Figure 18: Linear resistance increase as a function of the NaCl concentration. In mg/L, [Cl-]=0.6[NaCl]

2.6 Analog-to-digital conversion on CMOS

Previous lab validation of each building block of the analog front-end (AFE) included in the first version of the CMOS chip (PROTEUS1) was reported in D3.2: namely programmable gain S&H, programmable filter, sigma delta modulator (SDM) for the analog to digital converter (ADC), and DC-DC converter. The experimental results have shown that the circuits are fully operational and they achieve a performance very close to the initial design requirements. The complete analog chain formed by these blocks is show in Figure 18 and the spectrum of the signal at the output is depicted in Figure 19, for a 4kHz input signal. The signal at the output reflects the processing of the bandpass filter (4kHz-5kHz) and the effect of the 20dB gain of the input sample and hold, considering an input signal as low as -55dBV. Besides the frequency component at 4kHz, the bandpass filter response can be observed as well. In addition, the linearity is maintained at high level, since harmonics (2^{nd}, 3^{rd}) are kept at low levels.

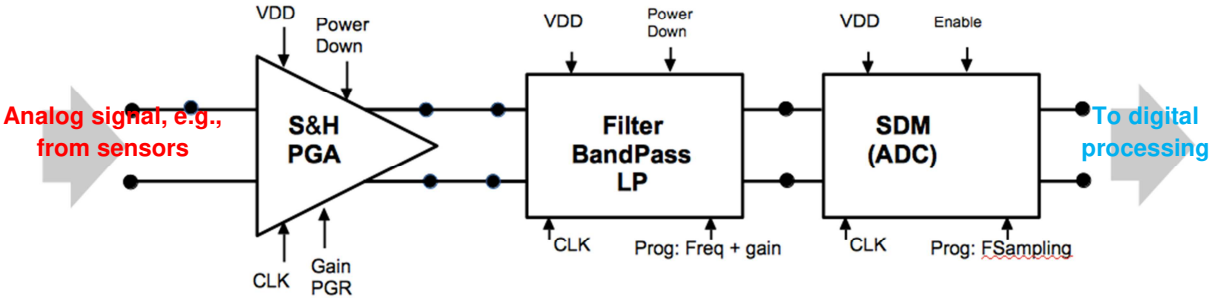

Figure18: Analog front-end channel.

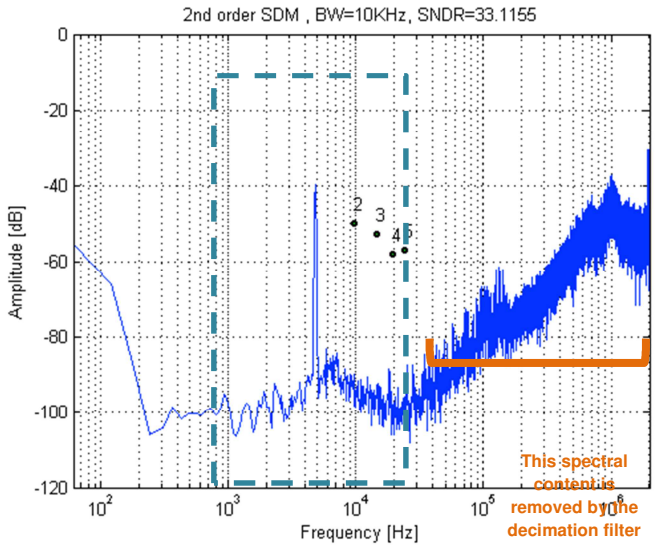

Figure 19: Signal spectrum at the output of the analog front-end channel, before decimation filter.

The first version of the CMOS chip integrates the most challenging analog building blocks while the digital processing part is performed externally. To accommodate both, a support board (SB V1.2), whose block diagram is depicted in Figure 20, was designed and implemented (described in D3.3 and D51). In addition, the full assembled PNODE is formed by this support board, an energy harvester module and a caps module, which is exposed to water. This caps board integrates a sensor chip and a CMOS chip (PROTEUS1), in which a sigma-delta modulator is used to perform the analog-to-digital conversion. Is this component that is responsible to quantize the signals coming from the sensors (with or without analog pre-processing) and deliver it to the digital section for further processing.

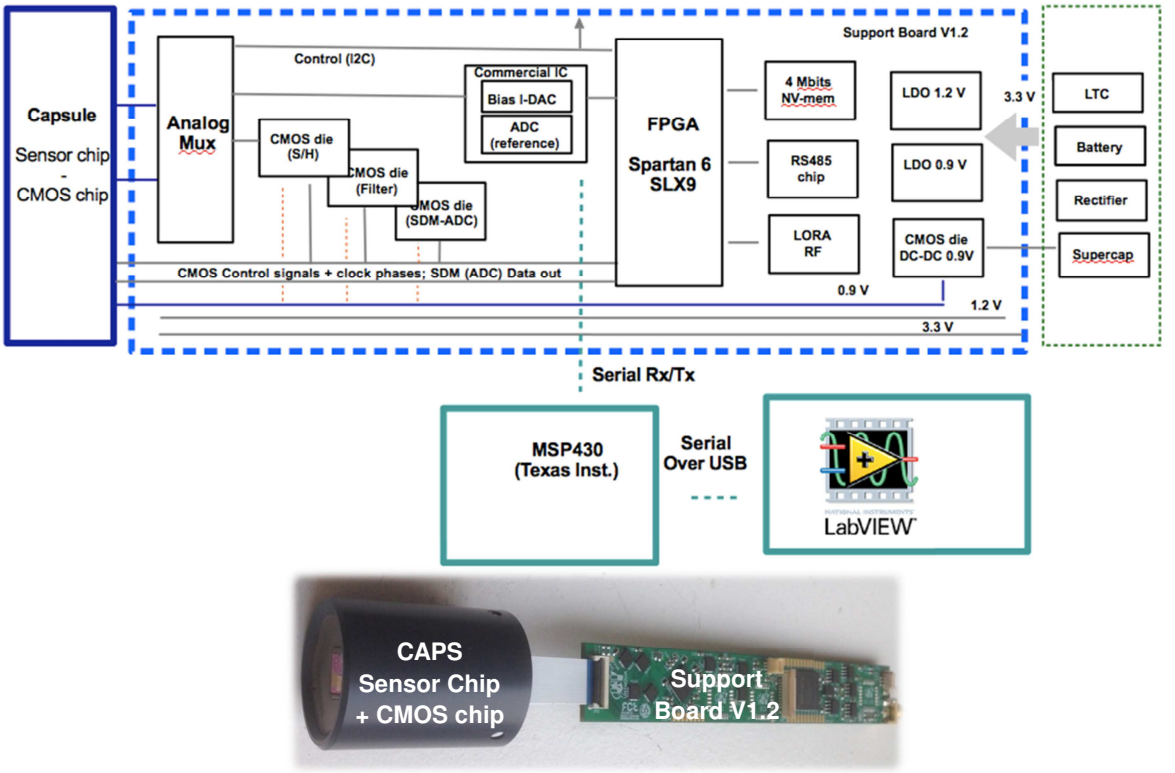

Figure 20: Block diagram of the PNODE v1.2, including caps and support board.

The support board of Figure provides several entry points used for testing and backup purposes. Notably the AFE can be directly accessed by an external microcontroller (in this case an MSP430) which formats the data to be provided to a LabView program or to be sent to a water monitoring system (WMS) through a wire or wireless Modbus link.

Using a direct access to the AFE available in support board V1.2 and for evaluation purpose, the output stream was firstly acquired from the sigma-delta modulator and processed by a MATLAB program which performs the low-pass decimation filtering and formats the data to be visualized in a graphic (for better observation). For example, after decimation the 12 bits binary output word (e.g., 0000100010011011) is represented as a real number adjusted to the full scale of the ADC (e.g, 0.57).

The setup used for the experimental tests is represented in Figure 21. Complementing the main signal processing using the PNODE (represented with green lines), an alternate path using the SDM of the CMOS chip used in the dedicated lab testing board, described in D3.3 was also added. The output data stream is acquired by a digital oscilloscope (with logic analyzer capability) from which the data is

gathered and provided to the referred MATLAB program. As stated before this program performs low-pass filter decimation and then formats the results to be presented in a graphical and human readable representation.

Figure 21: Experimental setup of the PNODE v1.2, including caps and support board.

The experimental results (Figure22) are obtained for two of input signals types. Representing an analog signal obtained at the output of the conductivity sensor, after amplification, the first test signal corresponds to a sinusoid with 5 kHz and peak to peak amplitude of 400 mV and 600 mV, respectively. For the DC input signal case, corresponding to the signal obtained from the remaining sensors, an alternative approach was used for testing purpose, only. The DC variation was emulated by using a slow triangle signal, with 10 Hz and 600mVpp of amplitude.

The results at the output show the digital stream provided by the sigma-delta modulator (blue lines), corresponding to variations between two voltage values. Applying this stream to a decimation filtering operation yields the signal represented in green. It is clear that the information of the original signal is preserved, to be then further processed by the microcontroller. As a reminder, each point in the green line represents a 12bit digital binary word. It has been converted to a real number in order to be graphically represented.

Type of signal	Input signal	Output of the SDM before (blue) and after low-pass filter decimation (green)
AC signal 5 kHz input signal with 400 mVpp amplitude	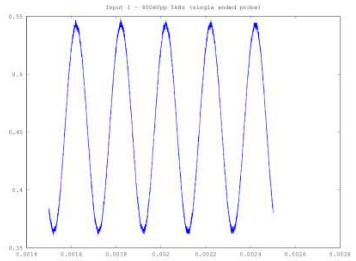	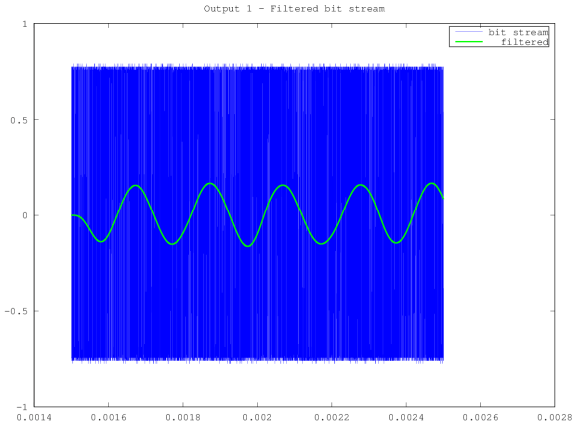
AC signal 5 kHz input signal with 800 mVpp amplitude	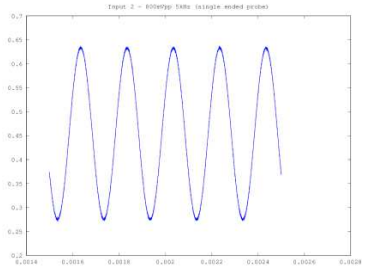	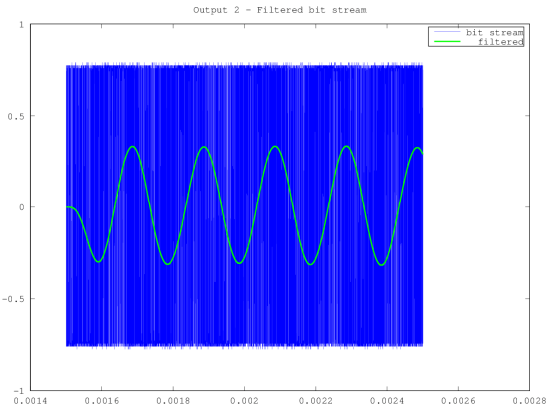
Low Frequency 10 Hz signal using a slow signal triangle wave, to evaluate the DC behaviour of the system	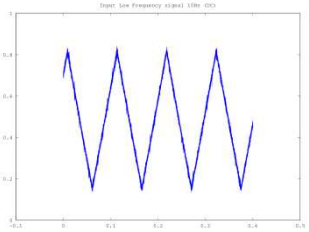	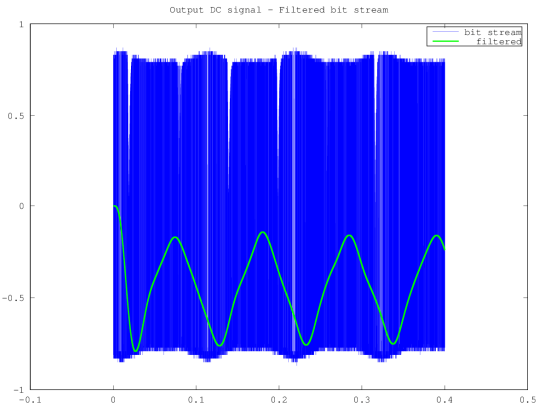

Figure 22: Output of the SDM before and after decimation-filtering.

2.7 Energy harvester: piezoelectric vortex generator

2.7.1 Description of test bench

The first validation of the piezoelectric vortex generator (PVG) was carried out in a water loop test bench realized at NiPS laboratory at Physics department at University of Perugia, which is showed in Figure 23. In this experimental setup, the PVC pipe measures 2 inches and the water speed can range between 0.3 and 0.8 m/s, which corresponds to the actual range of most of the SMAS water pipes of the drinking water network. The water flowrate is measured through a Parker Flowmeter (PET) with capacity of 100L/min and max 10 bar of pressure. The piezoelectric generator is inserted into a chamber with a small window that allows the observation of the oscillation of the cylindrical mass. The output voltage of the generator is connected to an electrical load and then acquired through a data acquisition card (DAQ) of National Instruments (USB-6356 16bit 1Ms/s) with a LabView program. In particular the tests were previously made with simple electrical resistance ranging from few kOhm to MOhms in order to find the optimal load impedance. Subsequently, the piezoelectric generator was coupled to a supercapacitor and to the power management circuit of the PNODE in order to validate the behavior of the voltage regulator. Tests were achieved by varying the flowrate and the electrical load. We have also tried different geometries of the oscillating body. Some test was also performed directly at the SMAS drinking water network to prove the resistance of the piezoelectric element in the real case.

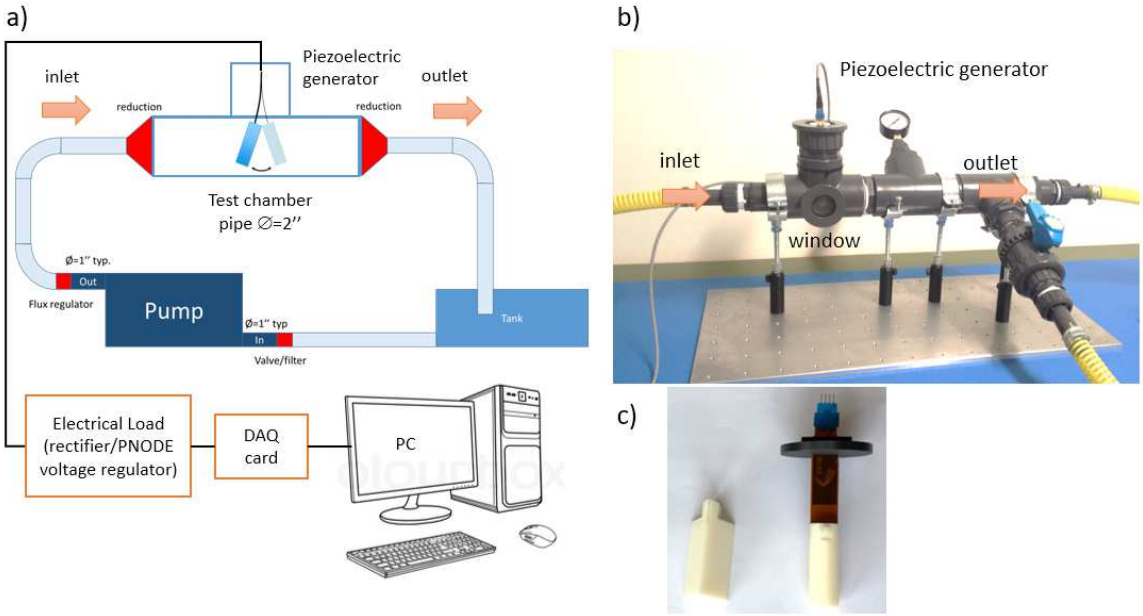

Figure 22 - Water loop test bench: a) scheme and b) photograph of the setup and c) piezoelectric generator (NiPS laboratory, University of Perugia).

2.7.2 Harvesting performances

Figure 23 shows how the natural frequency of the cantilever is red-shifted by the presence of a tip mass. In fact, the cylinder itself can be in first approximation only considered as a further mass attached to the tip. The measurements have been carried out in air, fixing the cantilever to a vibrating table. The table was subjected to a transversal motion with a white frequency spectrum between 1 and 1000 Hz, with acceleration below 0.1 g. As in all the following measurements, we acquired the time signal by a DAQ card and by FFT, we obtained the frequency spectrum.

a)

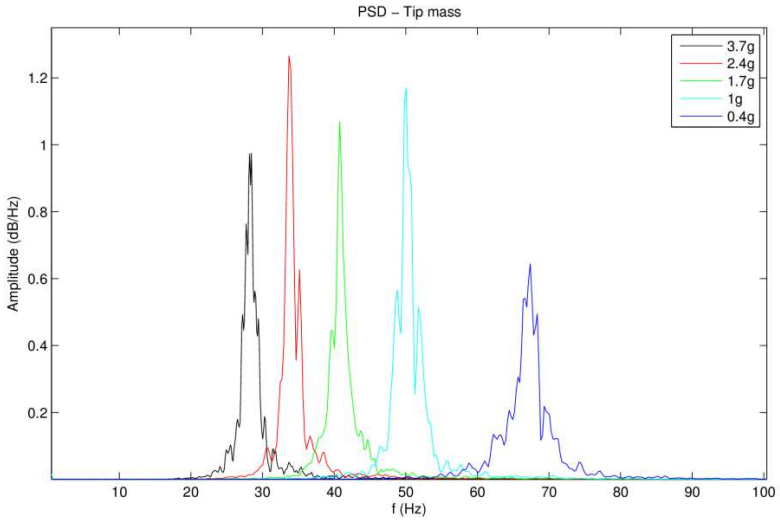

b)

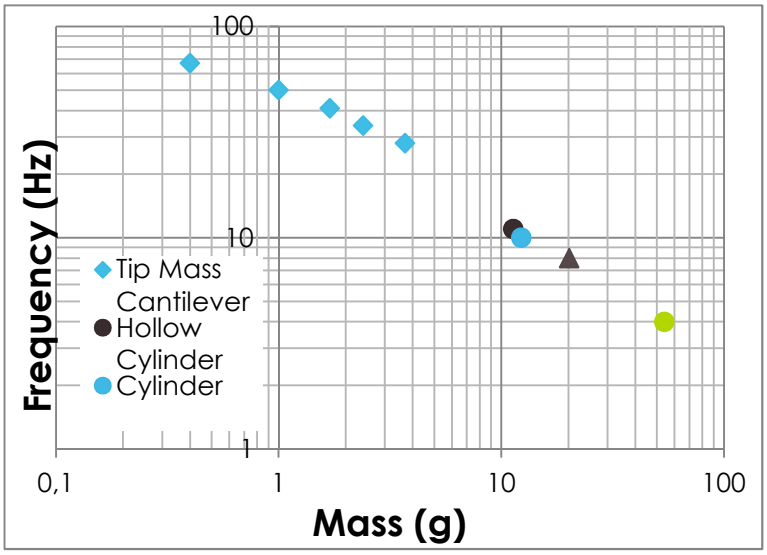

Figure 23–a) Power spectrum of the PVG as a function of the mass attached to the tip. b) Tuning of the natural frequency of the cantilever

In water there is a much higher viscous force (velocity dependent), which further decreases (and broadens) the resonance. Figure 24 compares the frequency spectrum of the cantilever in air and in still water when excited at all frequency by an impulsive force. Due to the higher viscous damping of water, the resonant frequency shifts from 8.6 (Δv ~0.5 Hz) to 6.5 Hz (Δv ~.9 Hz)

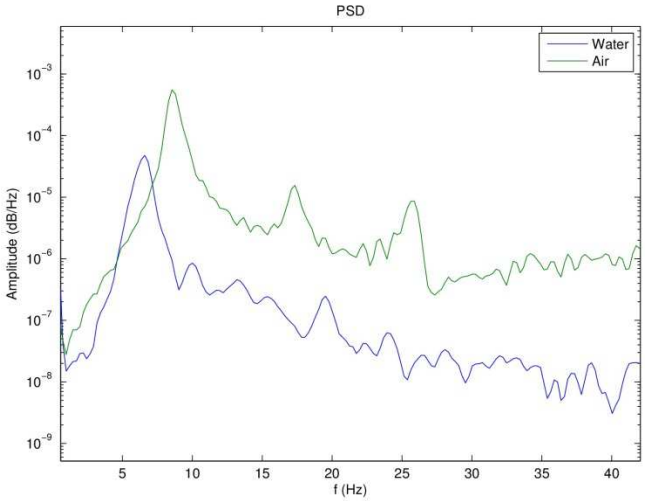

Figure 24 – Power spectrum of the PVG in air and water.

It is apparent that, by changing the mass, we can tune the cantilever up to the frequency (7-30Hz) we expect to have for the forcing in the range of velocity 0.5 - 3 m/s.

Figure 25a) shows the voltage signal acquired in time from the piezoelectric cantilever termination at different water speed. The signal is nearly sinusoidal with a well-defined resonance at about 6-8 Hz (Δv ~1 Hz). At the highest water speed, the elongation of the cantilever is such that it hits the walls of the chamber. This gives rise to sharp and intense electrical signals. Moreover, in the power spectrum a new peak at high frequency becomes well manifest, which we attribute to a high order mode of the piezoelectric beam. The observed low frequency mode testifies a good agreement between the forcing and the natural forcing of the cantilever.

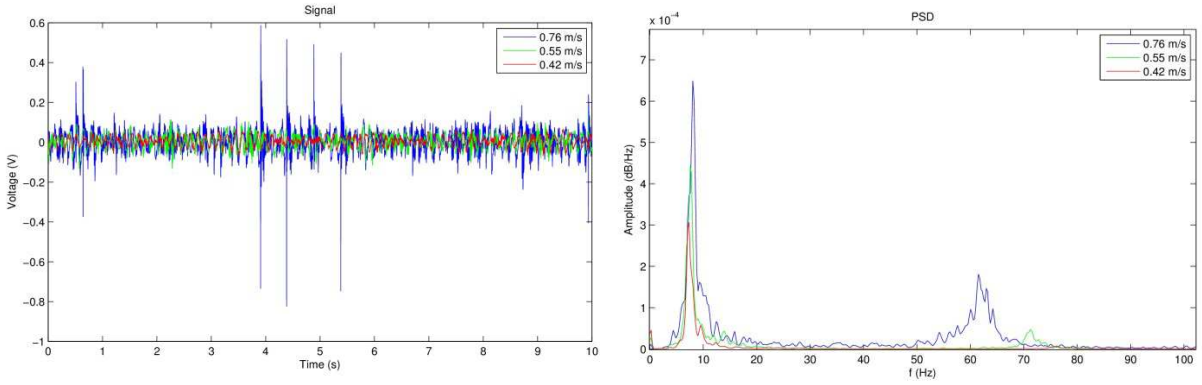

Figure 25 – a) Time Signal of the PVG for several water speed and b) Power spectrum obtained by FFT of the signal.

Figure 26a) reports the observed main frequency in the power spectrum as a function of the water speed. As we are very near the natural frequency of the cantilever and both the forcing and the

mechanical cantilever resonance are not very sharp we have a convolution of the two. This gives rise to a peak, which is not exactly proportional to the water speed as expected for the pure forcing. We could better appreciate such expected behavior in a PVG with a slightly larger (D= 25mm) and much heavier Teflon cylinder. In this case (Figure 26b), as the natural frequency is below 2 Hz and the minimum forcing frequency is about 4 Hz we had enough separation between them, at least from 0.4 m/s and the linear dependence between water speed and cantilever frequency could be observed.

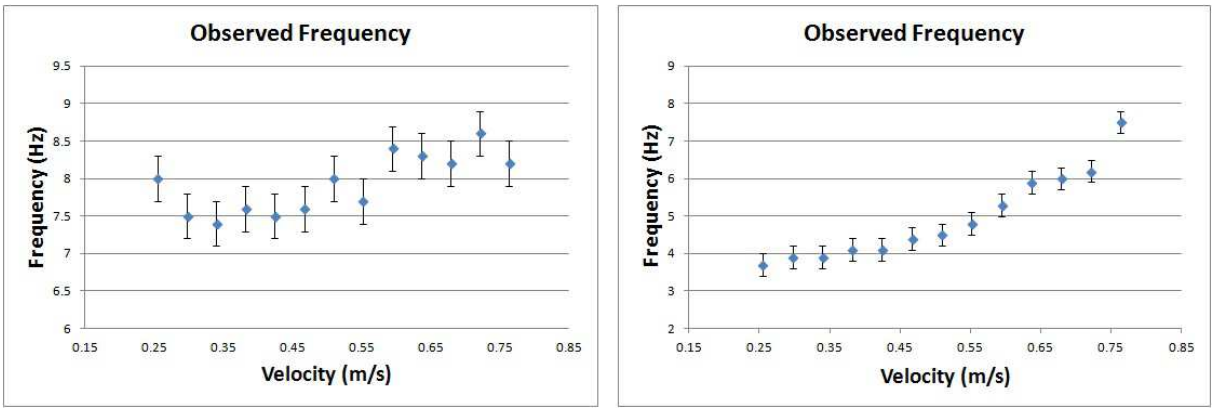

Figure 26 – Frequency position of the low frequency peak of the PVG generator a) for the 17 mm ABS cylinder and b) for the 25 mm Teflon cylinder.

As shown in Figure 27, the frequency of the high order mode decreases with the water speed. This is due to the increased damping of the water. This effect is scarcely visible in the low frequency mode, as it is masked by the much more relevant effect of the superposition between natural and forcing frequency. In fact, the damping coefficient for the oscillatory motion of the cylinder can be expressed as the sum of the damping term for still water and a term linearly dependent on the water speed [Norwegian Deepwater Program: Damping of Vortex-Induced Vibrations, K. Vikestad, C. M. Larsen and J. K. Vandiver, OTC11998].

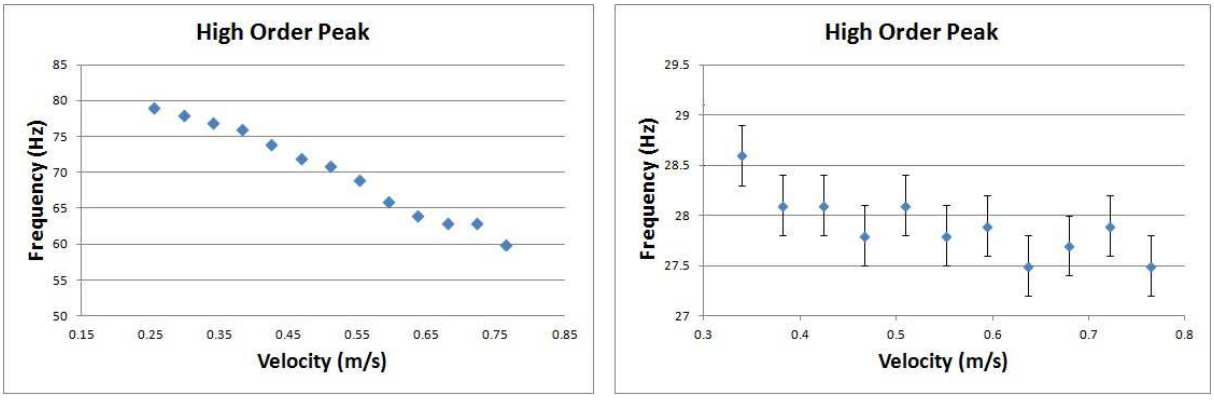

Figure 27 – Frequency position of the high frequency peak of the PVG generator for the 17 mm ABS cylinder and b) for the 25 mm Teflon cylinder.

In order to find the optimal load of the device we recorded the output power as a function of a resistive load at the highest velocity (0.78 m/s). The measurement for the 25 mm cylinder shows that the optimal load is about 200 kΩ, in agreement with the expectations considering that, as we are out of the resonance, most of the energy is concentrated in the high frequency mode. For the 17 mm cylinder, the optimal load is about 1 MΩ. (Figure 28)

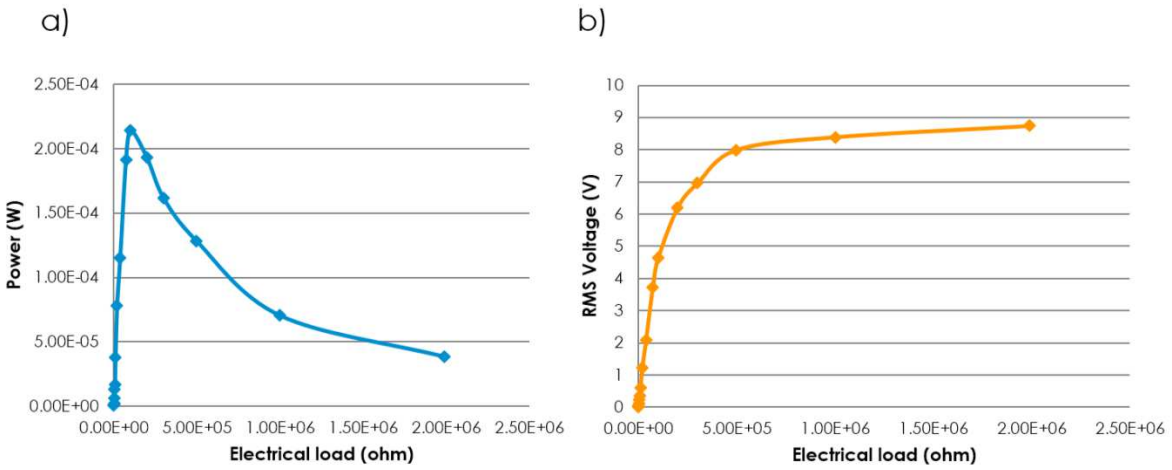

Figure 28 – a) Electrical output power and b) RMS voltage vs electrical load generated by the PVG. A max of 230 micro Watts were generated at optimal load of 208 kΩ

3 Assembled sensor caps validation strategy

3.1 Sensor caps under test

The detailed description of the sensor caps is provided in deliverable D5.1. Each sensor cap contains a dedicated electronic board with wirebonded CMOS and sensor chips sensors and the corresponding connectors in a dedicated housing. The gold wirebondings on the sensor caps are covered with the thixotropic epoxy resist H70E-4. The final step of assembly for each cap is the coating around the sensor chip, it has to make the cap waterproof while protecting the full cap board and leaving the sensor chip exposed to the water.

In total, 15 cap boards were assembled, among which only 8 feature CNT deposition on the sensor chips. Out of the 15 boards, 12 were assembled into actual sensor caps (including all of the boards with CNT sensors). These 12 caps feature different characteristics depending on the type of sensor chips, the presence of CNT sensors or not, and the type of coating.

Sensor chip versions: Three different versions, 1, 2 and 3, of the sensor chips are used, as shown in Figure 29. The chips are labeled physically with the mark 1, 2 and 3. The number refers to the model of conductivity sensor on the chip as described in chapter 2, section 2. Version 1 and 2 have the square pressure sensor as described in chapter 2, section 3, while version 3 has the rectangular pressure sensor.

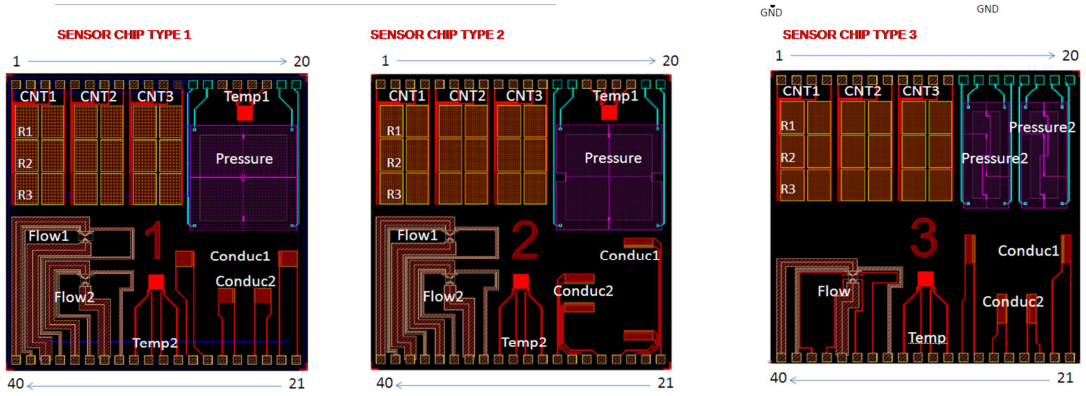

Figure 29: Three different versions of the sensor chips

CNT sensors: The CNT sensors available on the sensors chips were fabricated according to the process reported in deliverable D3.1. The parameters used were the following: cartridge temperature 60°C, cartridge voltage 13V, drop spacing 5µm, chip at ambient temperature. The number of CNT layers in each device is 28, with a rinsing time between each layer of 15s in methanol and 15s in acetone and a drying time of 7 minutes at 150°C. CNT1, 2 and 3 are respectively chloride, chlorine and pH sensors.

The CNT sensors were prepared along 2 batches of 4 chips. The first batch failed (unexpected change in chip thickness from previous chip versions), so the deposition was cleaned and redone. At the end, the printing was successful but the resulting CNT sensors were shown to be only marginally successfully connected at caps level (probably because of poor surface state preventing proper wirebonding). Among this batch of 4 chips, only the chip of cap #4 (version 3 chip) features 4 out of 9

operational CNT sensors. For the 2nd batch, the process went smoothly and all resulting caps have 9 out of 9 operational CNT sensors (#5 – version 3 chip, #7 version 2 chip, #6 version 1 chip, #8 version 1 chip).

Coating strategy: two references of bi-component epoxy resin were tested over 13 assembled caps, resulting in three versions of caps (see table below).

Coating strategy	Type 1: Use of the same resist for globtop and for surrounding area	Type 2: DAM and FILL process : use of two resins	Type 3: Use of two resins without DAM.
Globtop :Resin #1	H70E-4	H70E-4	H70E-4
Dam : Resin #2	/	H70E-4	/
Fill : Resin #3	H70E-4	302-3M	302-3M
Number of deposition steps	2	3	2
Final visual aspect of the cap	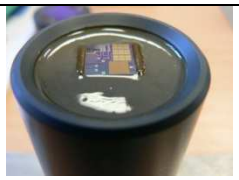	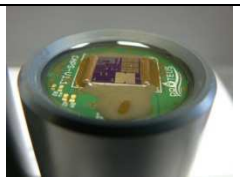	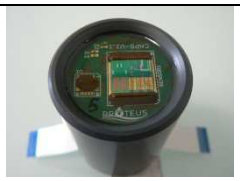

All the 5 caps with successfully assembled CNT sensors are of coating type 3.

3.2 Analog front end and associated software

As stated in D5.1 and D3.3, the PNODE system for version 1, is composed by the aggregation of a Capsule, which includes the sensor chip and one CMOS chip, and a support board which provides the external interface services and additional processing capabilities to the capsule. In particular, for lab testing, the PNODE needs to connect to a LabView program, specially developed for the task. Figure 30 shows a simplified block diagram of the configuration that was tuned for the lab testing phase. The capsule connects to the support board through two flat cables. The analog multiplexers in the support board facilitate the sensor selection and signal routing to the FGPA or to one of the additional CMOS extra die or to the commercial reference ADC acquisition patch. The digitized value is provided to an external MSP430 microcontroller, used as a Modbus gateway which is responsible for sending it to a Labview program running in a computer, see Figure1 to 34 .

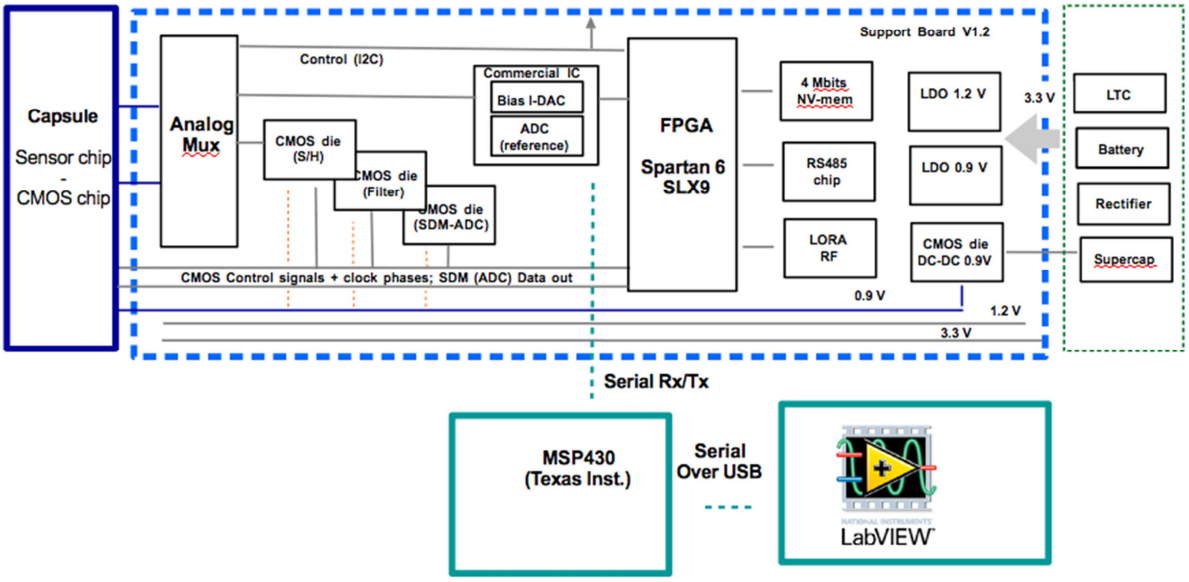

Figure 31 System block diagram.

The software running in the Labview framework is composed by a kernel where several modules were implemented, namely the one responsible for the Modbus interface. This is interface is also used to send the appropriate commands to select the sensor that is intended to measure. The usability is facilitated by GUI interface from which the sensor is selected and the acquired data can be visualized, as shown in Figure 32.

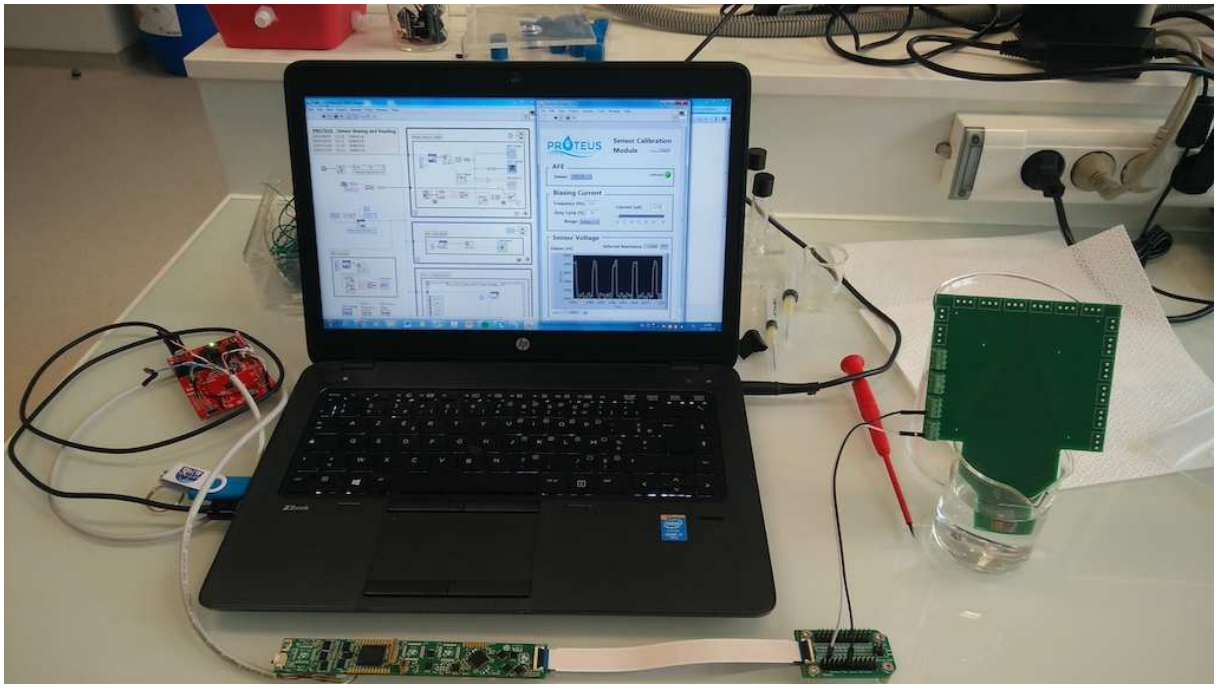

Figure 32: Labview interface for the PNODE connected to sensor lab board.

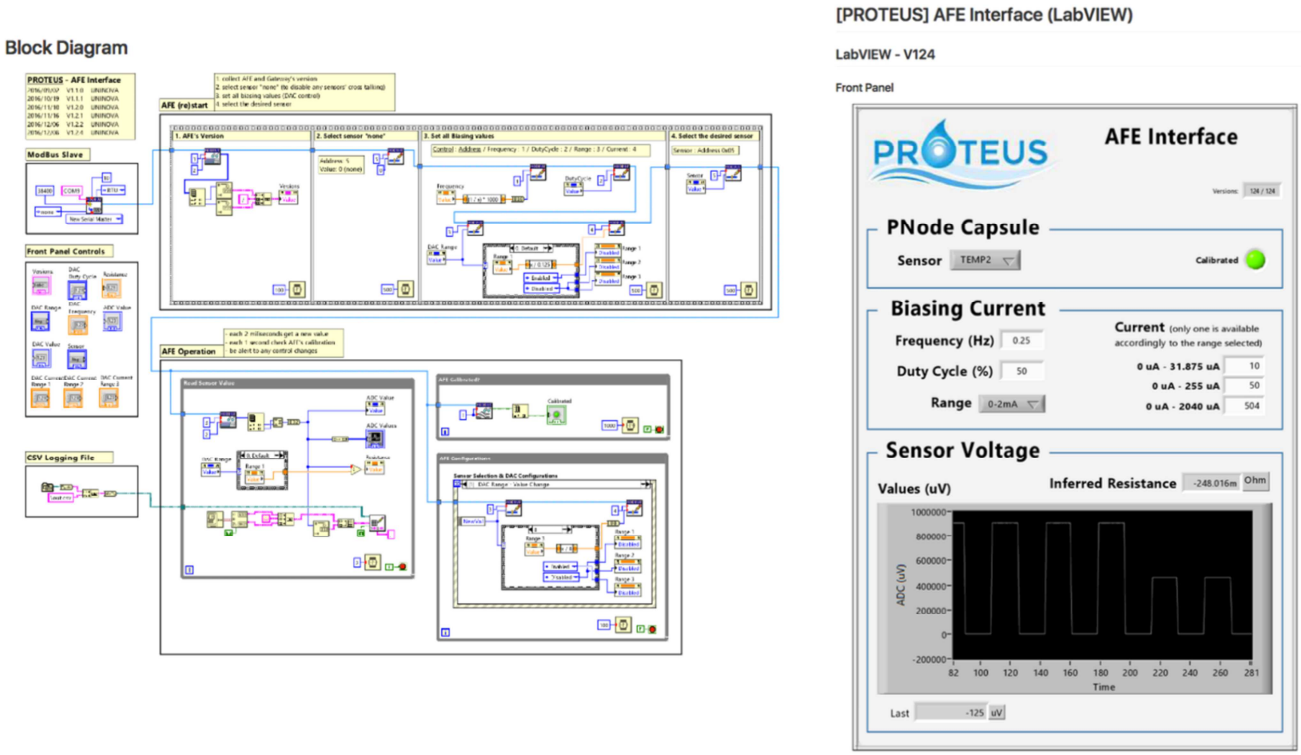

Figure 33: Labview code: PNODE Labview Interface.

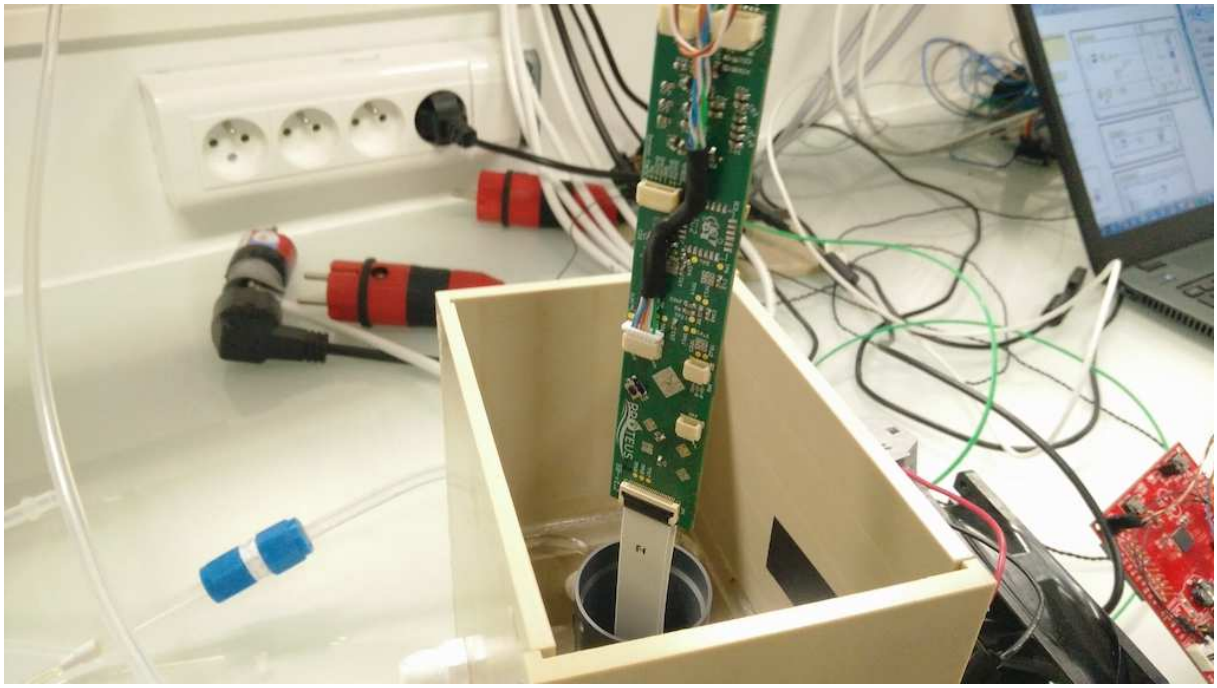

Figure 34: Electronic card V1.2 connected to the caps.

Depending on the type of sensor, the system is reconfigured accordingly, as explained next.

CNT and Temperature Sensors

Electrically, both CNT and MEMS temperature sensors are variable resistors. By using a current biasing approach shown in Figure , the use of an external Wheatstone bridge can be avoided. The sensor output voltage, which is processed by the ADC, is determined by the programmable source current **Ibias** multiplied by the value of the resistor (including baseline level plus the variation). Moreover, this topology can extend the overall dynamic range since for N bits ADC and N bits current source, the dynamic range of the readout interface is extended to N+M bits. Additional bits of the current source are used for calibration purpose.

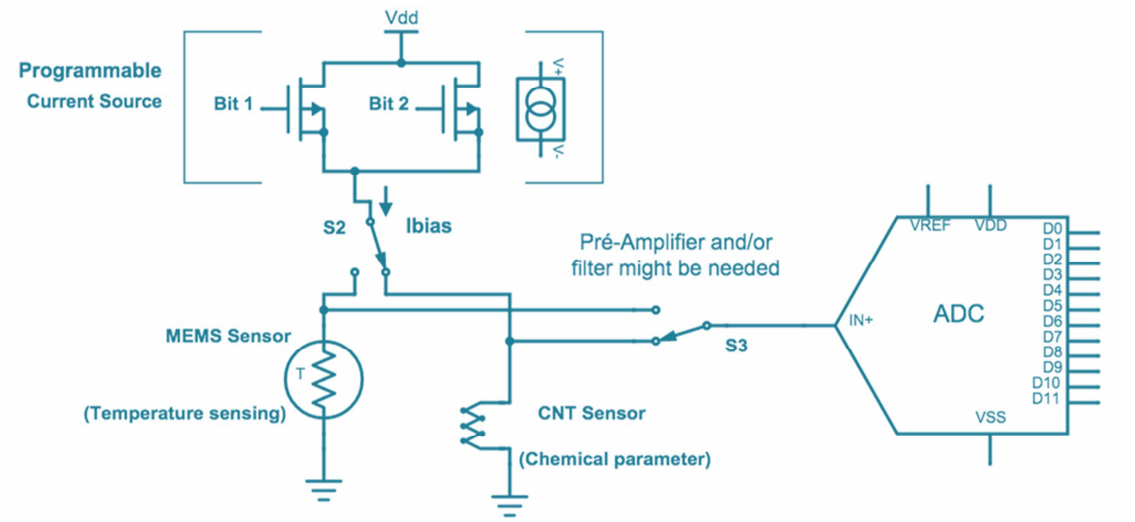

Figure 35: Interface for the CNT and Temperarure (MEMS) sensor.

The process of sensor data acquisition is based on the approach depicted in Figure.

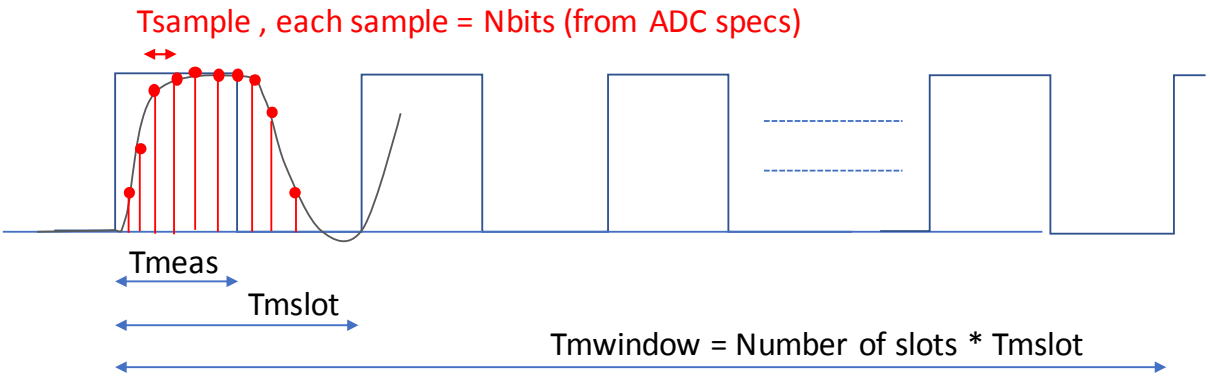

Figure36: Sensor data acquisition approach

During measurement time window ($T_{mwindow}$) several measurements slots are executed. A number of 10 is initially assumed. During the measurement time slot (T_{mslot}) the sensor is biased (i.e., a current is turned on and a voltage appears between the sensor terminals) during a measurement time spot (T_{meas}). During the remaining time (i.e., T_{mslot}-T_{meas}) the sensor is "turned off", to minimize higher order effects, such as self-heating, aging effects, among others.

To detect the transient behavior of the sensor time response, which is needed to determine the settled value, the output sensor voltage must be sampled at a rate higher than $1/T_{mslot}$. A minimum of samples during T_{meas} (or T_{mslot}) must be defined.

The actual configuration of the AFE of PNODE V1.2 does not apply any pre-processing (for example, average) on the acquired data. It sends directly to the serial port, a stream of "raw data" of 12-14 bits resolution, for a sampling rate higher than 1 kbps.

Consider a T_{mslot} of 4 s (that is, measurement repetition of 0.25 Hz), a duty cycle of 50% (i.e., T_{meas} = 2s), and ADC sampling rate of 1kPs (i.e., 1ms between samples) with a resolution of 14 bit. In this case the number of acquired samples during T_{mslot} is 4000. Considering that each one is a 14-bit word, then (if no compression is used) an effective transmission raw data rate of approx 19.2kbps is needed to send all the information via a serial port.

As referred previously, the AFE is configured to send raw data without any pre-processing, as for example, moving averaging. It is therefore needed to define the strategy of acquiring data and obtain a representative value for each $T_{mwindow}$ interval. The first assumption is that averaging must be done among all settled values. How to define stable values (see figure below): after reaching 63% of final value.

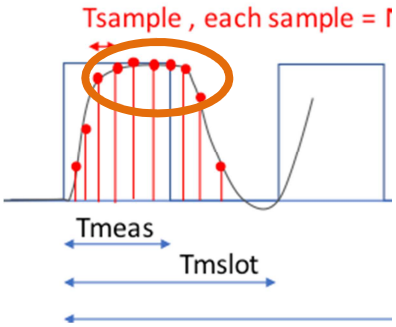

Figure37: Sensor data acquisition approach

One important remark is that more information is acquired with the actual AFE in LAB mode configuration (high data sampling rate and high resolution). Thus, the acquired signal can be seen to be noisier.

Measurement parameters taken into account:

- Levels of biasing currents for each sensor
- Number of slots during calibration phase and during normal operation state
- Allowed range values for T_{mslot}
- Duty cycle value
- Pre-processing data (averaging, moving average, settling time determination)

MEMS Pressure Sensor

A similar approach to the previous one is applied for the MEMS Pressure sensor. As explained in D2.1, the MEMS resistive type elements that compose the pressure sensor are disposed in a Wheatstone bridge structure and therefore a current can also be used to bias the sensor, as shown in Figure . The main difference from the previous sensor cases, is that the now the AFE front-end channel acquires a fully differential DC voltage. All the remaining aspects related with measurement parameters are maintained, namely:

- Levels of biasing currents
- Number of slots during calibration phase and during normal operation state
- Allowed range values for T_{mslot}
- Duty cycle value
- Pre-processing data (averaging, moving average, settling time determination)

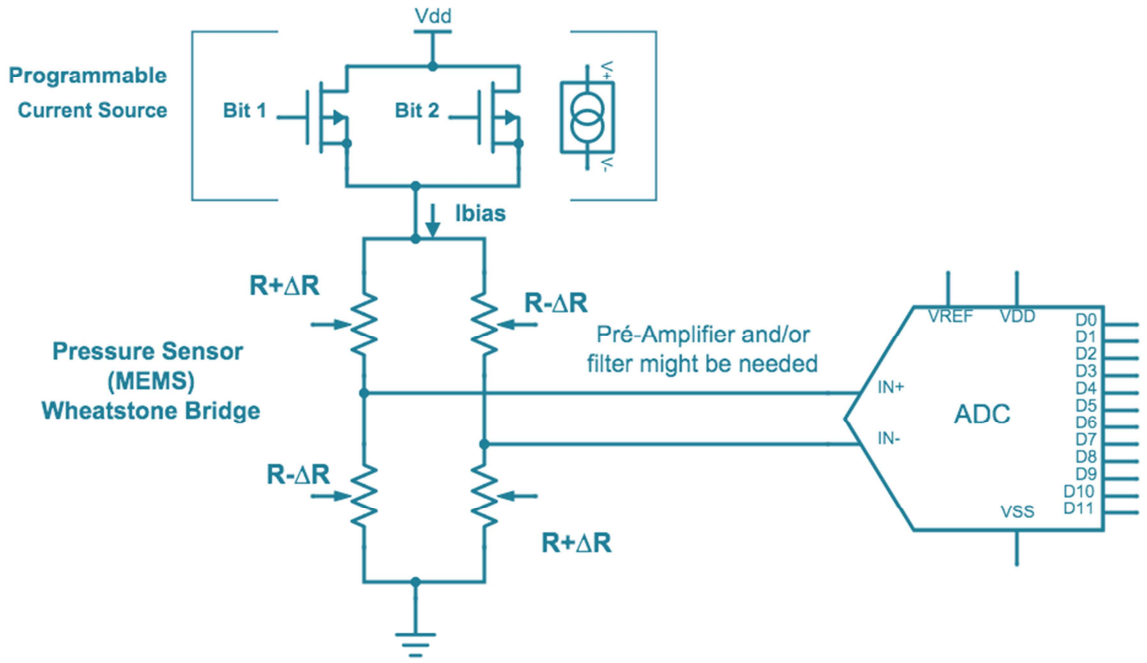

Figure 38: AFE Interface MEMS based pressure sensor.

MEMS Conductivity Sensor

The capacitive nature of the frequency response of the conductivity sensor suggests using an AC measurement setup to determine indirectly the value of the impedance from which it is possible to extract the water conductivity. The configuration developed is represented in Figure 39639. Here, a sinusoidal signal generated by a voltage or current Digital-to-Analog Converter (DAC) is injected in the sensor. The resulting output signal voltage is acquired by the ADC. Despite not being represented in Figure 396, preceding the ADC a bandpass filter is used to prepare the signal for digitalization.

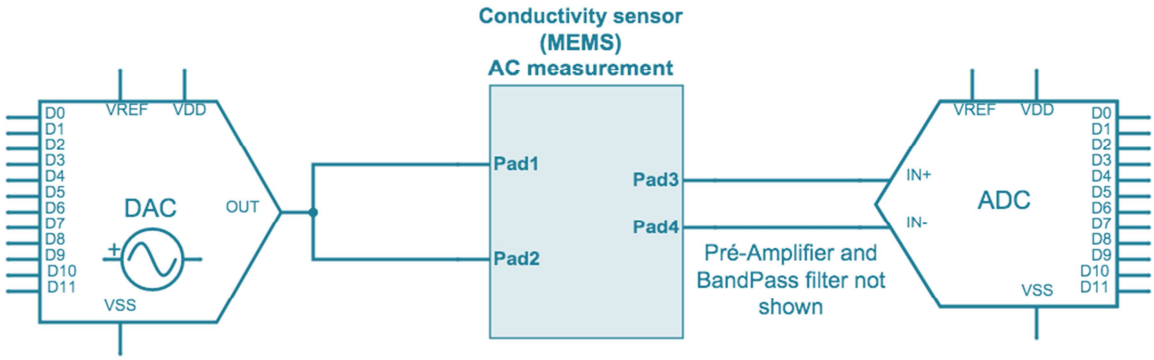

Figure 396: AC measurement interface for the MEMS based Conductivity sensor.

The same time slot definition, previously described, is maintained for this type of sensor. However, the excitation signal is no longer a DC signal but rather a sinusoidal, with frequency between 1 kHz and 10 kHz, Figure 40.

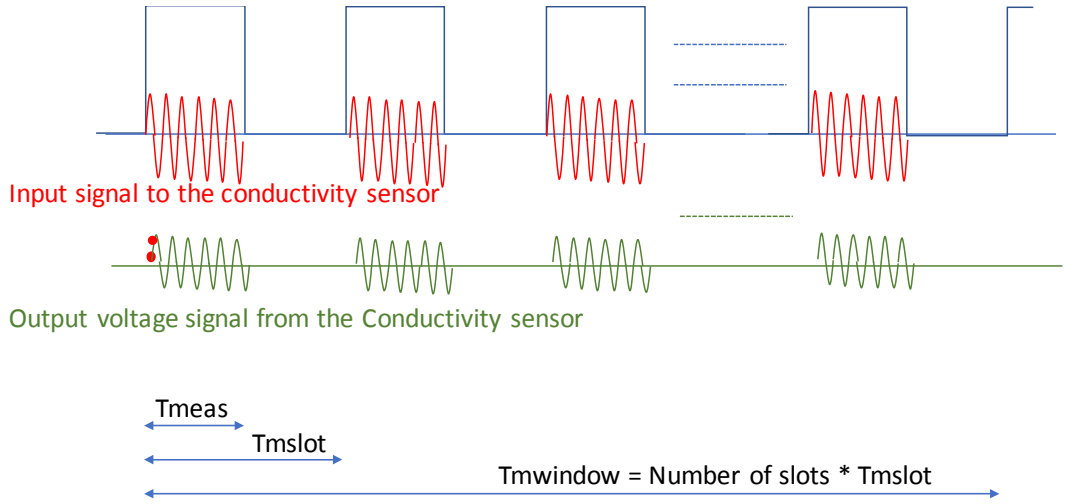

Figure 40: Sensor data acquisition approach during sensor calibration.

Preliminary functional sensor tests, indicates that only the output voltage amplitude is needed to be obtained, since it directly indicates the conductivity level. When compared with the resistive based sensors, it is needed to ensure:

- Sample at higher rate, namely, higher than 10 kHz
- T_{meas} includes several periods of the excitation signal
- An amplitude detector should be applied to the acquired signal
- Averaging applied to the amplitudes samples values

Measurement parameters taken into account:

- AC signal amplitudes for driving the sensor
- Number of slots during calibration phase and during normal operation state
- Allowed range values for T_{mslot}
- Duty cycle value
- Pre-processing data (averaging, moving average, settling time determination)

3.3 Lab calibration test bench

3.3.1 Objectives and requirements

The objectives of Proteus require the systematic testing in the lab of a large number of chips on PCB and of a large number of assembled sensor caps for calibration purposes and for analysis of selectivity and ageing features. A dedicated lab test bench was developed for the temperature and chemical calibrations.

The bench has to withstand the chemical, thermal and chemical constraints imposed by the set of parameters considered in Proteus (for instance deliverable D1.1). The most exacting parameters to manage are the range of pH (pH 5 to pH 10, limits the use of certain polymers) and the presence of free chlorine (forbids the use of most metals). The high level of pressure (requires strong mechanical robustness of all the hydraulic systems) are considered also for further extension of the bench to pressure calibration.

To enable analysis of sensitivity and perturbing factors (cross-sensitivity), it needs to enable the change each of those parameters while keeping the other parameters as constant as possible (for instance, checking the sensors response to free chlorine at constant temperature), and while monitoring in real time as much parameters as possible in the solution (for instance, measuring the conductivity and temperature while doing an essay on sensitivity to chloride).

To save time for the operator, the level of automation must be as high as possible, and the bench must be compliant to testing several devices at the same time.

3.3.2 Features of the bench

Based on these requirements, we proposed the following system-level design (Figure 41). A set of solutions are injected into the bench, and can be stirred continuously. The level of filling is determined by a dedicated level sensor and used to control the solution injection system. The solution filling the bench can be sent to waste automatically after use. The temperature can be controlled. The static pressure of the bench will also be controllable in a later version.

It was decided not to manage here the flowrate control, as it requires large volume of fluids circulating into a large network of pipes. As such it was not compatible with the rest of the installation. Sensitivity analysis to flow rate and pressure are addressed for the current version in Sense-City loop, better suited for such test (see section 3.4).

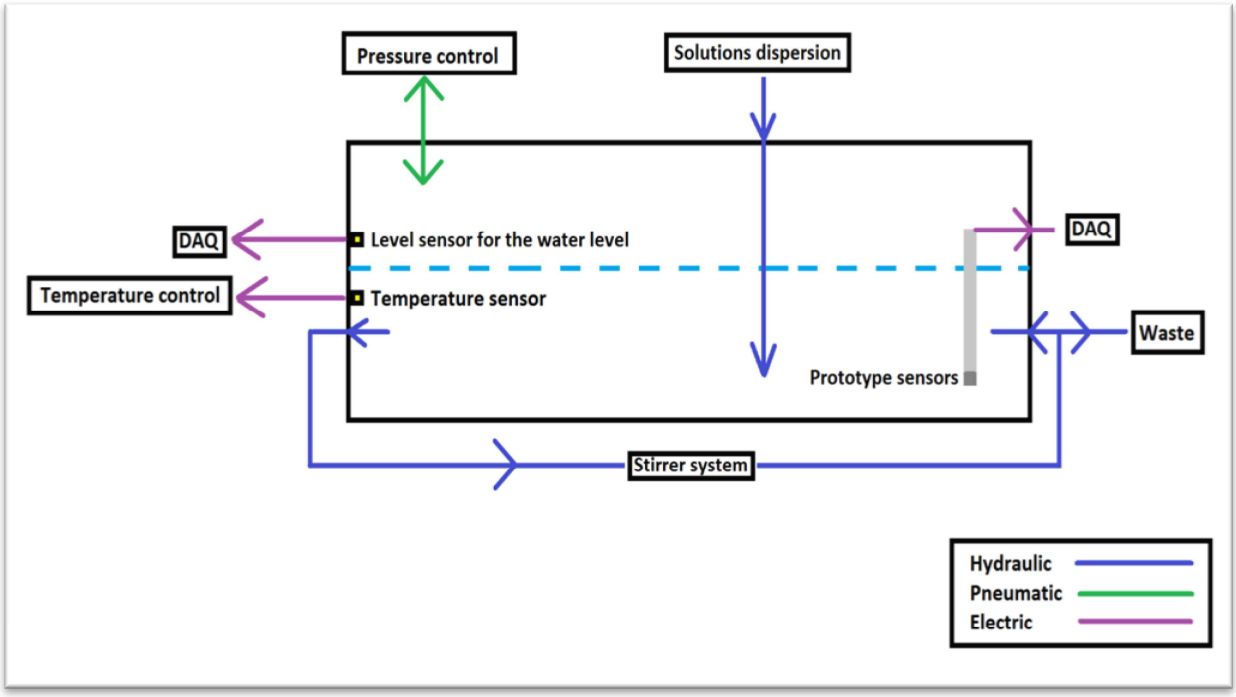

Figure 7: Architecture of the testbench

3.3.3 Geometry and materials

The geometrical characteristics of the bench are shown in Figures 42 to 46: a rectangular box with a slopped bottom (to evacuate fluid) is designed with size large enough to welcome 5 PCB (supporting sensing chips) in parallel, or 3 sensor caps together with 2 reference sensors. The PCBs and the sensor caps are supported by specially designed racks that are inserted inside the box. The material of the box is PEEK, selected for its resilience to most chemicals, while the rack is made using laser machined Plexiglas covered with resist for protection against chemicals.

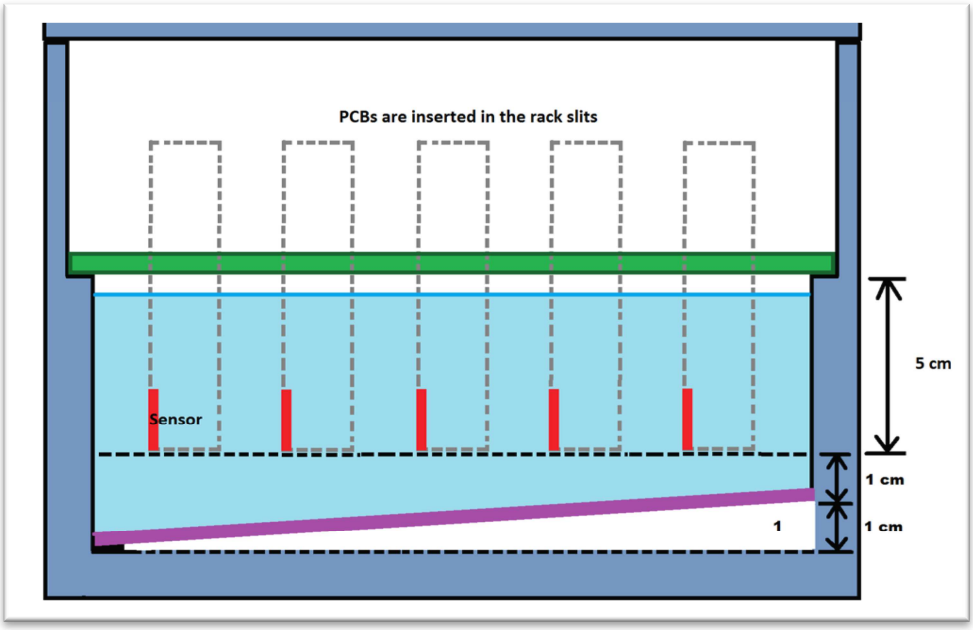

Figure 42: Side view of the geometry of the bench (configuration for 5 PCB)

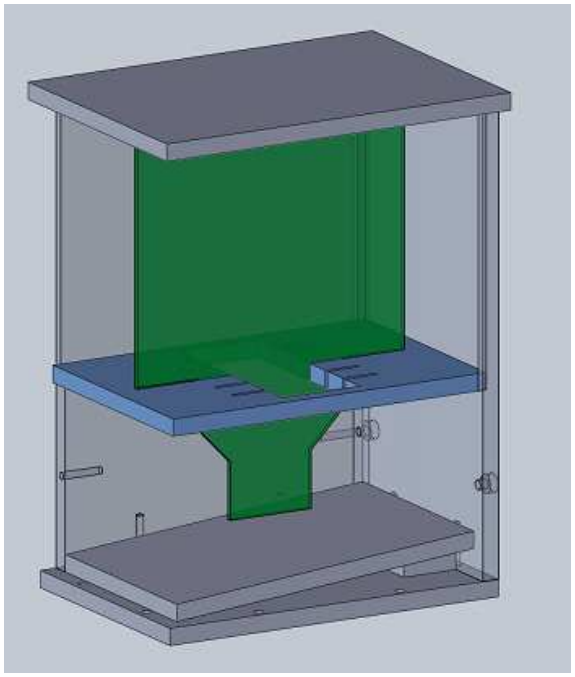

Figure 43: Overall geometry of the bench (configuration for 5 PCBs)

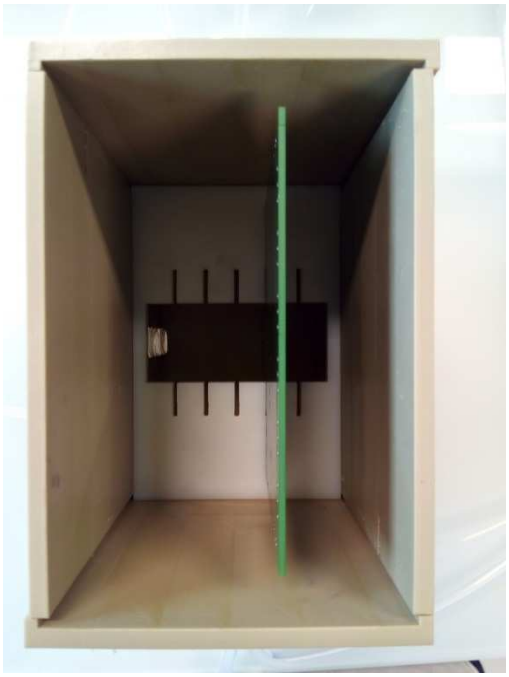

Figure 44: Pcture of the bench – top view (configuration for 5 PCBs)

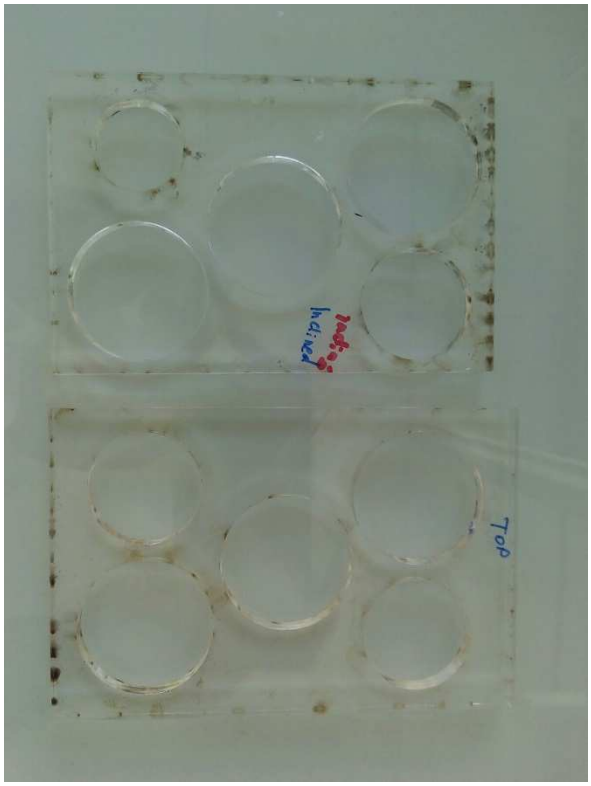

Figure 45: Plexiglas rack for 3 sensor caps and 2 reference sensors

Figure 46: Picture of the bench (configuration for 3 sensor caps and 2 reference sensors)

3.3.4 Distribution of liquid and cleaning process

A system is proposed to distribute a set of 6 pre-prepared solutions into the bench (Figure 47 to 50). Elevated glass containers are connected via six independent solenoid valves to the bench. Upon control from the computer, they release the analytes from the storage bottles into the box in a gravity-driven process.

To monitor continuously the volume of water (and hence the level of water in the bench) a photoelectric distance sensor is placed in one of walls of the bench. The photoelectric distance sensor provides a dynamic continuous analogue output signal that corresponds to the level of water in the bench.

To homogenize continuously the solution (chemically and thermally), a stirring system is implemented. After the experiment is finished and the batch of water is no longer needed, a solenoid valve located at the bottom of the bench is activated and the water is flushed to drainage.

The automated cleaning process consists in rinsing the bench with ultrapure water several times. During the process, the bench is filled with clean water (contained in one of the six glass containers from section 4.2) delivered from the inlet port. After the distance sensor detects that the bench has been completely filled with clean water, the drainage solenoid valve is activated and the water is flushed. This process is repeated at least 3 times.

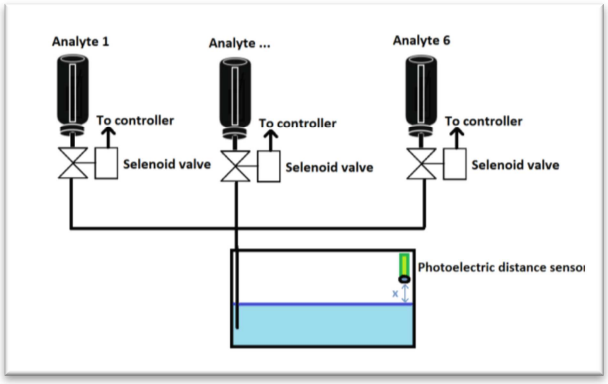

Figure 47: Principle of the distribution system

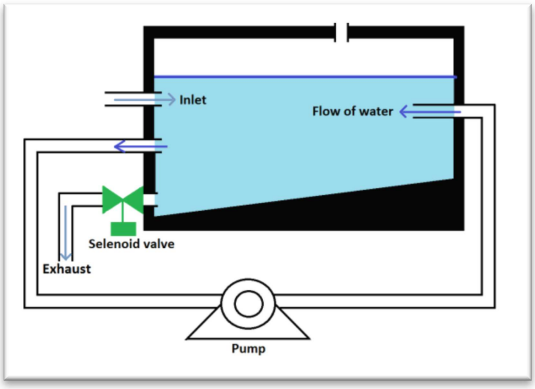

Figure 48: Principle of the stirring system

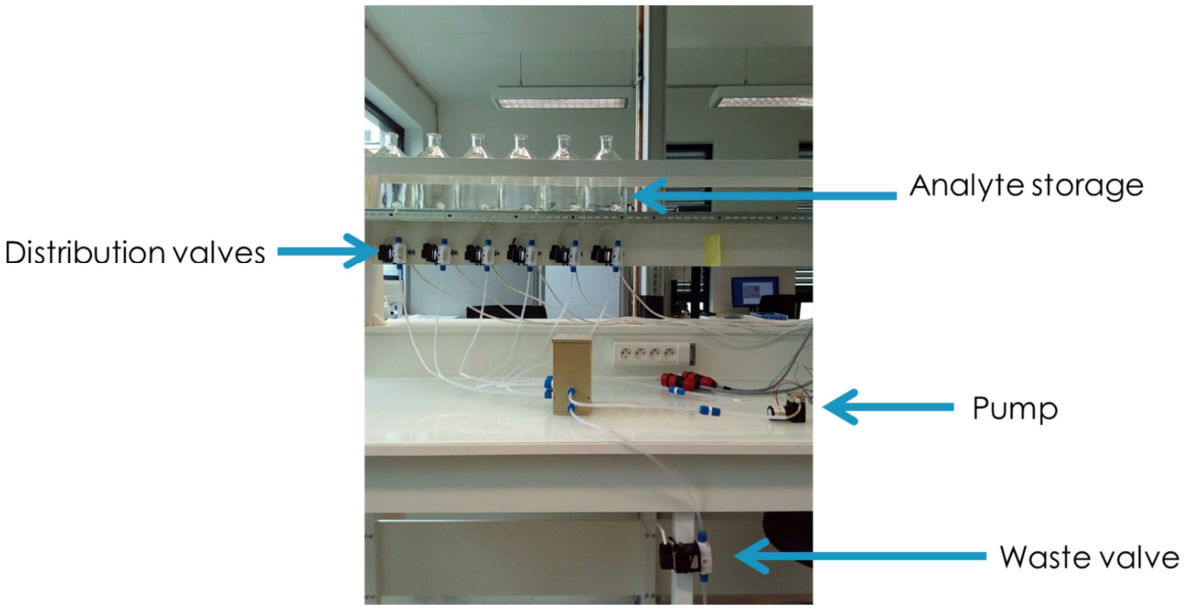

Figure 49: Picture of the distribution and waste disposal system

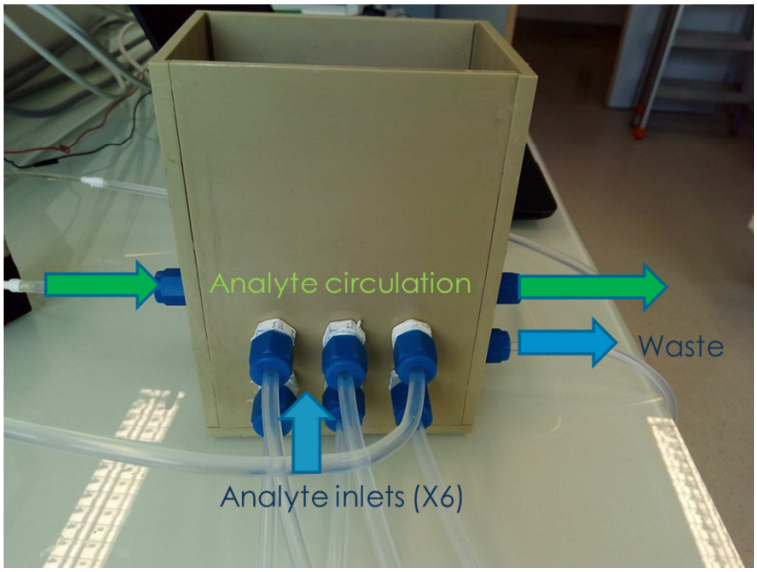

Figure 50: zoom on the bench inlets and outlets

3.3.5 Thermal management

For thermal management, the full bench is placed into a dedicated chiller system (Fisher scientific AC200), as shown in Figure 51.

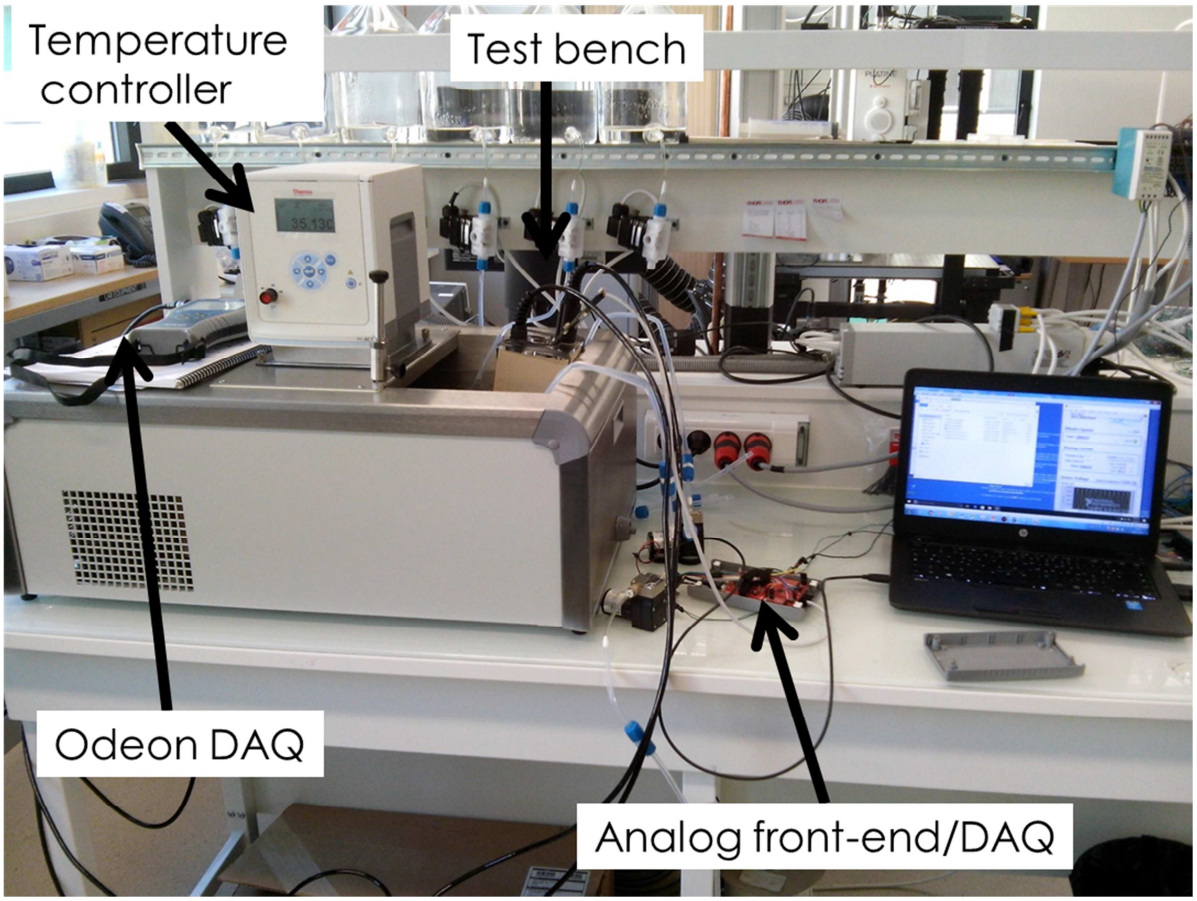

Figure 51: Testbench within its chiller for thermal control.

3.3.6 Pressure control

A pressure control system was designed (see Figure 52), but is not implemented yet, as the pressure sensors were not the focus of the first run, and as the pressure benchmarking can be carried out in the Sense-City experiment.

The idea is to enclose the current bench into a rigid metallic frame and increase the air pressure in the headspace above the liquid interface (atop the rack) so the pressure in the water increases as well. An electro-pneumatic pressure regulator is mounted in a closed loop control scheme for this purpose.

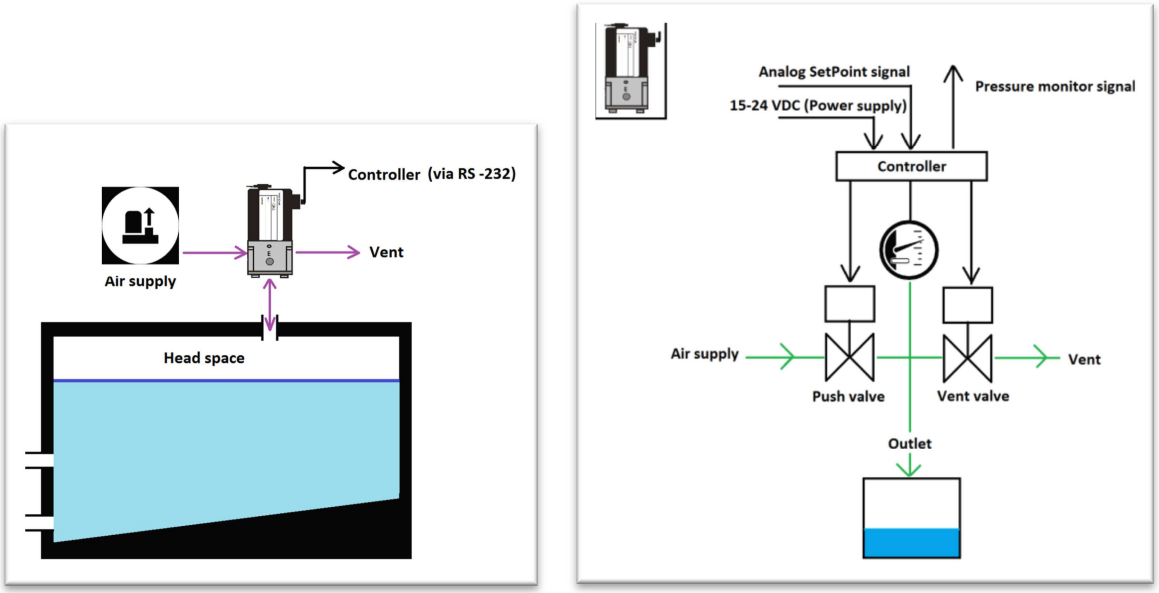

Figure 52: Pressure control; left: general outline of the electro-pneumatic pressure regulator device connected pneumatically and electronically to the characterization bench, right: internal layout of the pressure regulator. The green and black arrows depict the pneumatic and electrical lines respectively.

3.3.7 Reference measurements

During experiments, the status of the solution in the bench is controlled by two reference sensors:

- The PHEHT pH and temperature sensor from Aqualabo
- The C4E conductivity, salinity and temperature sensor from Aqualabo

In addition, periodic sampling of the solution is carried out to monitor Chlorine level evolution between start and end of testing. Free and total chlorine levels are determined using Aqualabo ODEON spectrophotometer (with the appropriate reagents).

3.3.8 Bench control

The fluid control system (fluid delivery, stirring, evacuation) is controlled by Labview (Figure XXX). The chiller system is compatible with Labview, but is presently programmed directly via the Fischer interface. The data from Aqualabo reference sensors are gathered via the provider's software and exported under the .csv format.

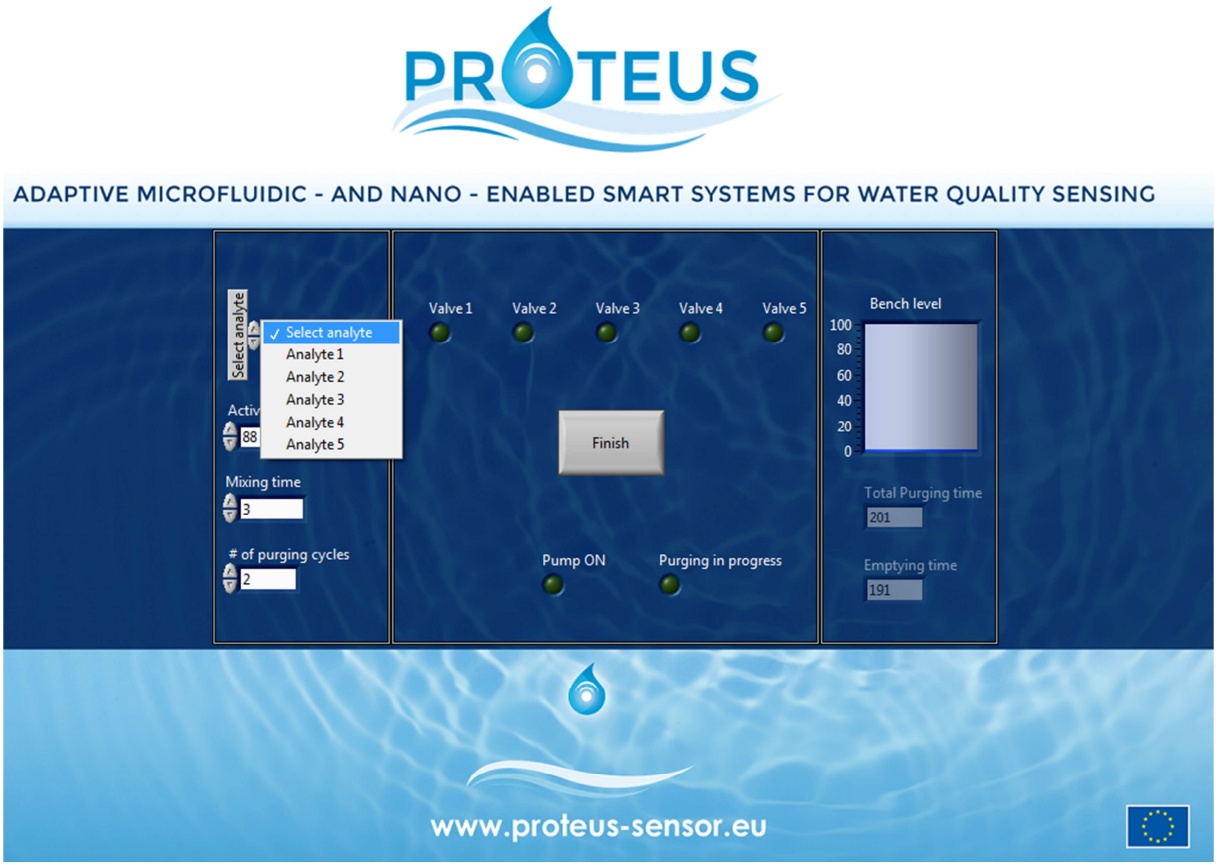

Figure 53: Labview based GUI for the testbench

3.4 Sensitivity results

3.4.1 Temperature

The trial for the temperature sensor is done on cap #6, temperature sensor 1, in deionized water. Figure 54 shows the very good correlation between sensor data and actual temperature (time step: 10s). Figure 55 shows the calibration curve between actual temperature and sensor output, yielding the calibration relationship of $T_{calculated}(°C)=0.52U_{temp1}(mV)-460$. Figure 56 shows the comparison between the calculated temperatures using the calibration relationship and the actual temperatures; as well as the absolute value of the error between the two temperatures. The mean error is 0.32°C but the maximal error is 1.9°C. Errors larger than 0.6°C appear when strong positive temperature gradient (>0.001°C/s) are applied, suggesting a slight delay in sensor response time.

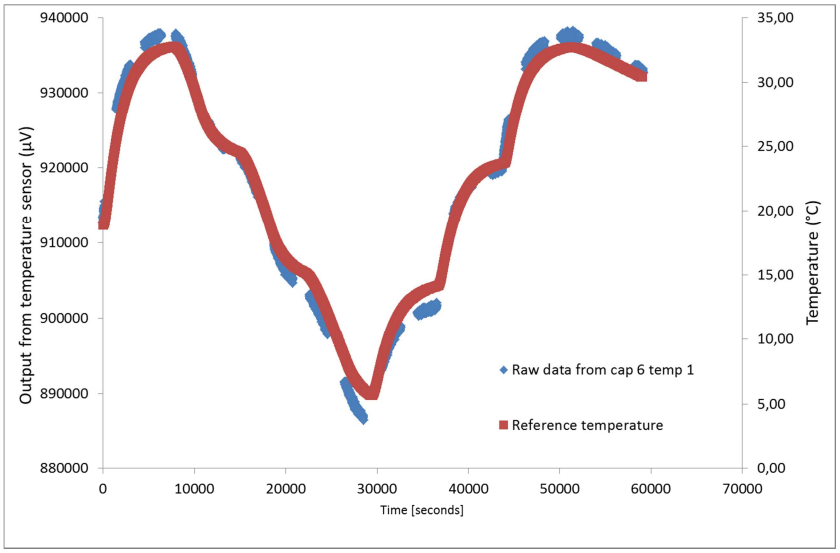

Figure 54: Comparison between reference temperature and output from temperature sensor 1 in cap #6

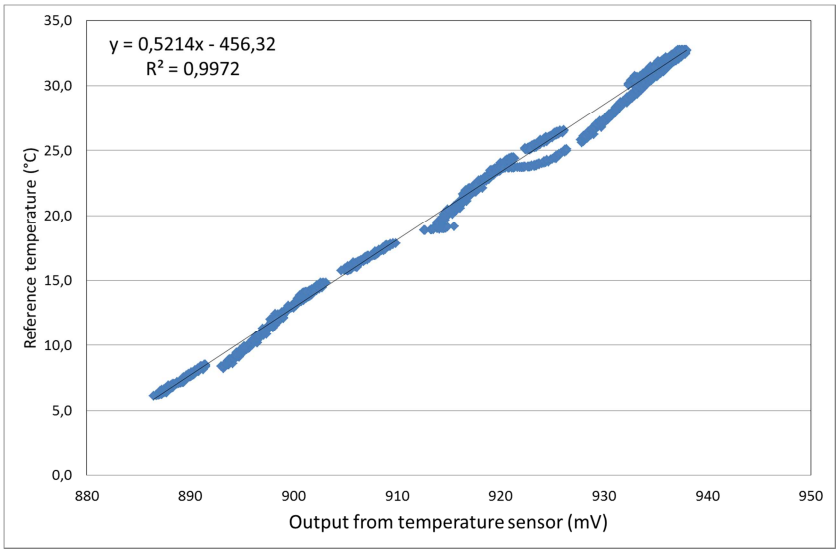

Figure 55: Linear relationship between actual temperature and sensor output: $T(°C)=0.52U_{temp1}(mV)-460$.

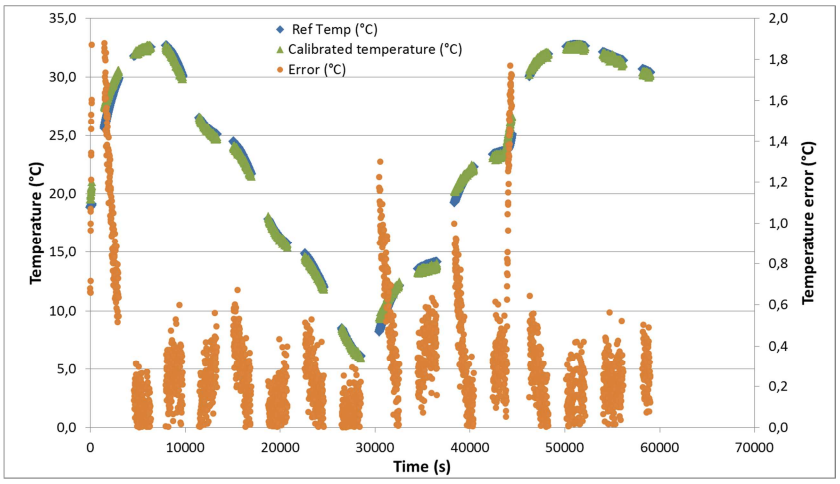

Figure 56: Error in temperature evaluation

To improve on this result and compensate for the time delay, the exact same procedure is applied, discounting data achieved with temperature gradient larger than 0.001°C/s. The calibration curve is much more linear (Figure 57), yielding the relationship $T_{calculated}(°C)=0.52U_{temp1}(mV)-450$ with still better correlation factor. Over this (reduced) set of data, the mean error is now 0.17°C, and maximal error is 0.75°C only, much improved from before. It confirms the hypothesis that the main source of error is due to higher rates of temperature increase. Further studies should be conducted to estimate the actual response time of the sensor.

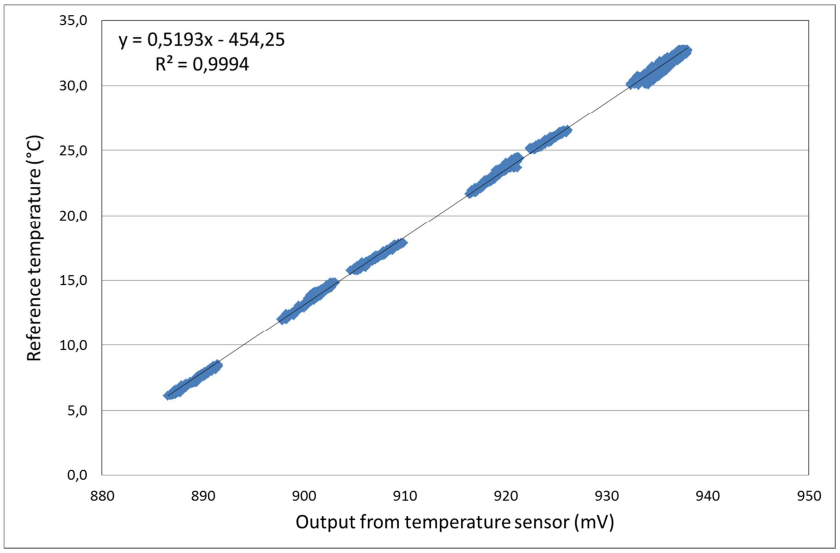

Figure 57: Linear relationship between actual temperature and sensor output for data subset with small thermal gradient $T(°C) =0.52U_{temp1}(mV)-450$.

3.4.2 CNT sensors

Data on CNT sensors sensitivity is gathered on cap #6. Current of 1µA is applied to the CNT sensors using rectangular waveform at frequency 0.15 Hz, duty cycle 10%. For each solution, all of the CNT sensor outputs are measured successively. CNT1, 2 and 3 sensors are respectively designed for chloride (CNT functionalized with FF-UR-14 polymer), chlorine (CNT functionalized with CF-OX-14 polymer) and pH sensitivity (non-functionalized CNT).

3.4.2.1 pH sensing

Solutions with different pH are prepared:

- for acid solutions (pH 3.6, 3.9, 4.3, 4.7, 5.7), acetic acid is dissolved in DI water;
- for basic solutions (pH 8.4, 8.9, 9.1, 9.4, 9.6, 10.3, 10.3), sodium hydroxide is used.
- for pH between 7.5 and 7.9, ten different solutions are prepared: two solutions at pH 7.7 with acetic acid, pH 7.5 and pH 7.9 with sodium hydroxide, pH 7.6, 7.7, 7.8, 7.9, 7.9 with potassium acetate. The average pH over these 10 solutions is 7.8. The sensor output displayed for 7.8 is the average of the outputs for the 10 solutions. Relative standard deviation on the outputs is below 5.4% for CNT1 sensors, below 7.1% on CNT2 sensors, below 2.0% on CNT3 sensors.

Figures 58 to 62 show the sensitivity of all the sensors to pH below 6 and to pH above 7.8. During this trial, sensor CNT3-R1 was discounted, as it returned negative values. Briefly:

- CNT1 sensors have low sensitivity over the full range of pH (less than 20% relative variation around the pH 7.8 value)
- 2 out of 3 CNT2 sensor outputs are strongly sensitive to pH: decrease with pH for low pH between 1.3 and 0.5.; increase with pH for high pH between 1 and 1.4
- 2 out of 2 CNT3 sensor outputs are strongly sensitive to low pH (the 3rd is not functional): decrease between 1.1 and 0.5 with increasing pH up to pH 5.7.

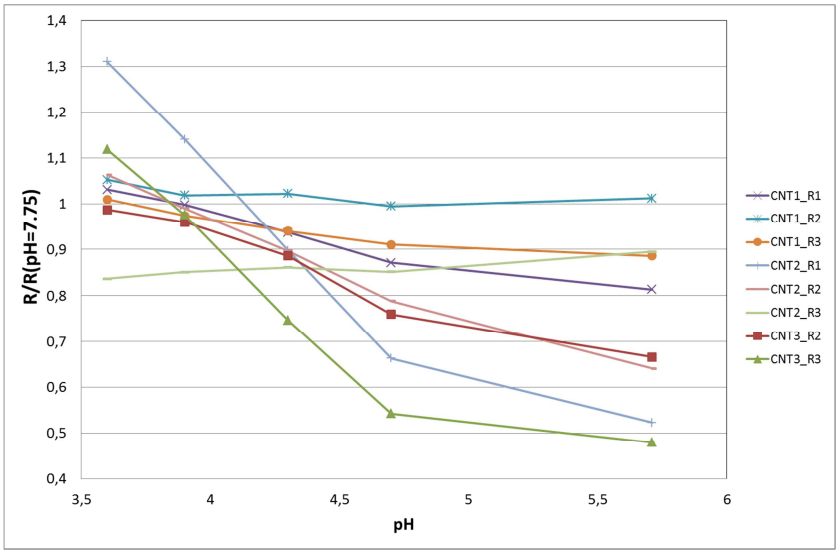

Figure 58: CNT sensor sensitivity to pH below 6

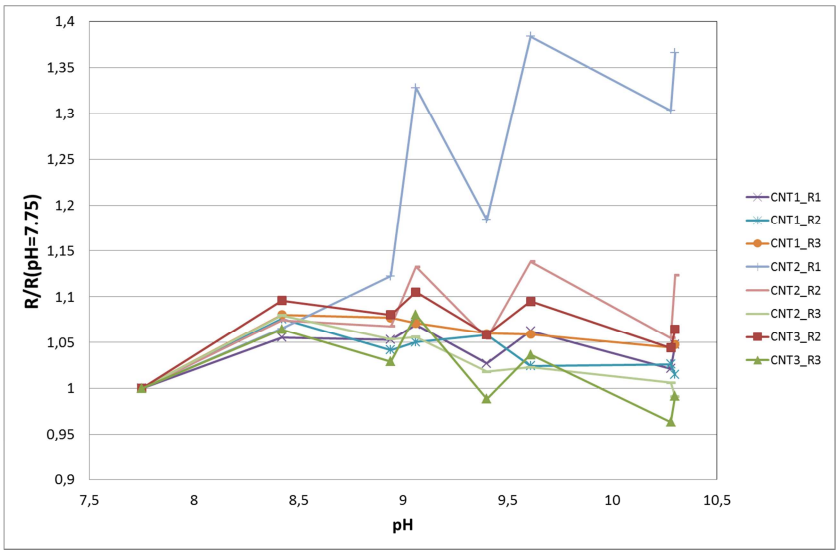

Figure 59: CNT sensor sensitivity to pH above 7.

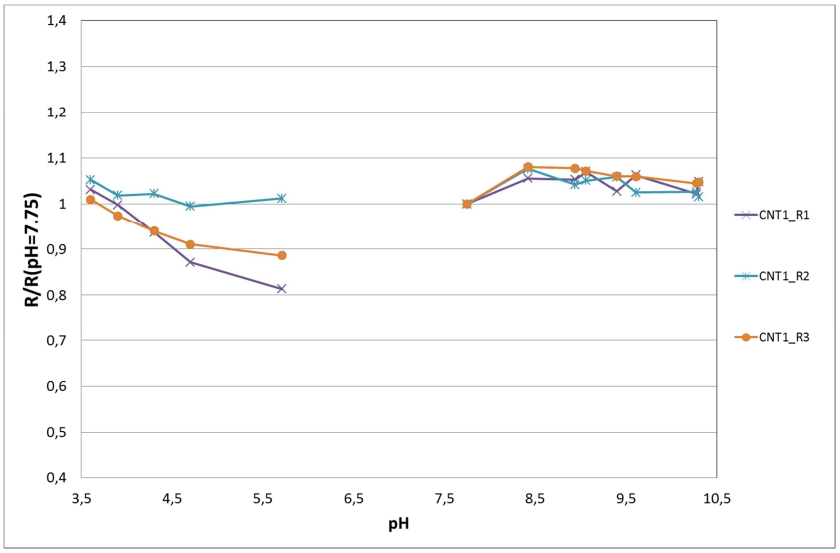

Figure 60: CNT1 sensor sensitivity to pH

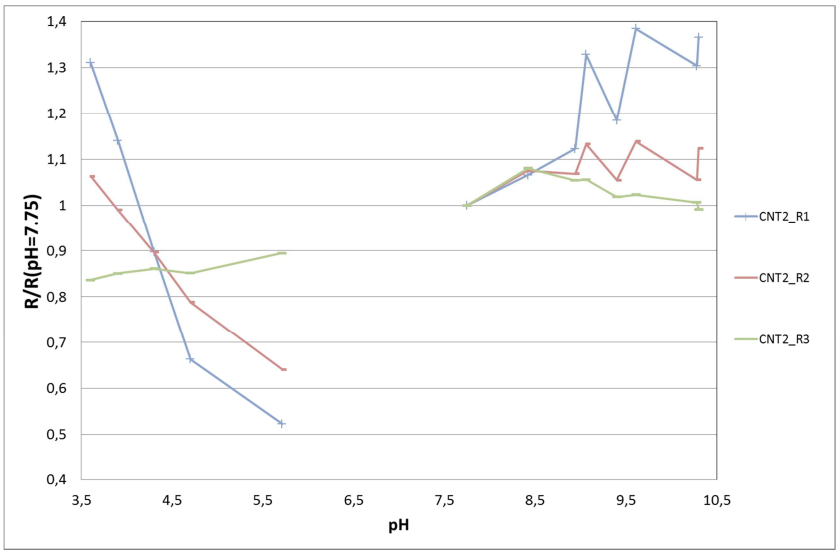

Figure 61: CNT2 sensor sensitivity to pH

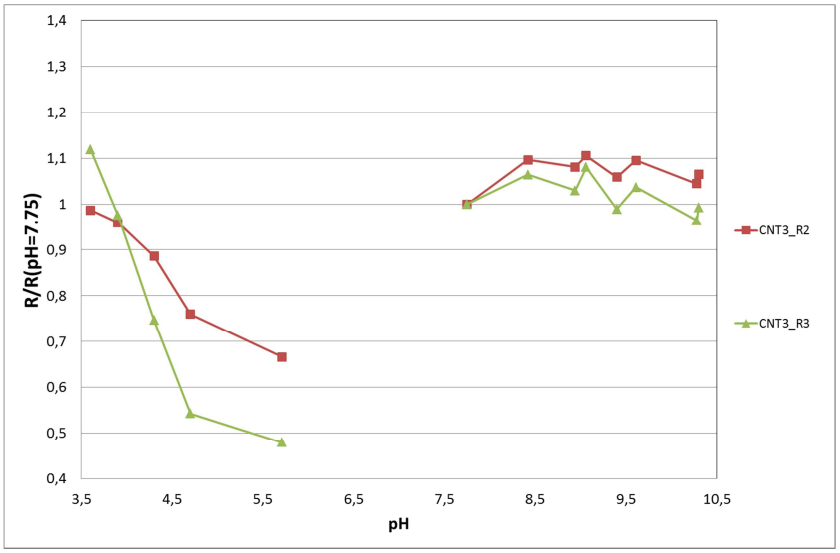

Figure 62: CNT3 sensor sensitivity to pH

3.4.2.2 Chloride sensitivity

Sensitivity to chloride is studied using 3 KCl concentrations in DI water (20mg/L, 120mg/L, 210mg/L). The reference solution is DI water. Note that the sensor outputs in DI water may not be representative of outcomes in tap water due to the very low conductivity of DI water. Note that in mg/L, we have [Cl-]=0.47[KCl].

From on solution to another, pH varies between 6.1 and 7.7. During the trials, temperature varies between 22.8°C and 24.0°C. CNT2-R2 has stopped operating.

Figures 63 to 66 show the results: there is a strong sensitivity to chloride levels for all the sensors up to 120mg/L. Between 120mg/L and 210mg/L, the sensitivity is limited (saturation effect). Briefly

- CNT1 sensor R2 output increases up to 5.6 times with chloride but R1 and R2 sensors have much smaller sensitivity with different directions of variation (respectively +30% and -30%).
- CNT2 sensors have both about 30% sensitivity to chloride.
- CNT3 sensors have between 40% an 60% sensitivity to chloride

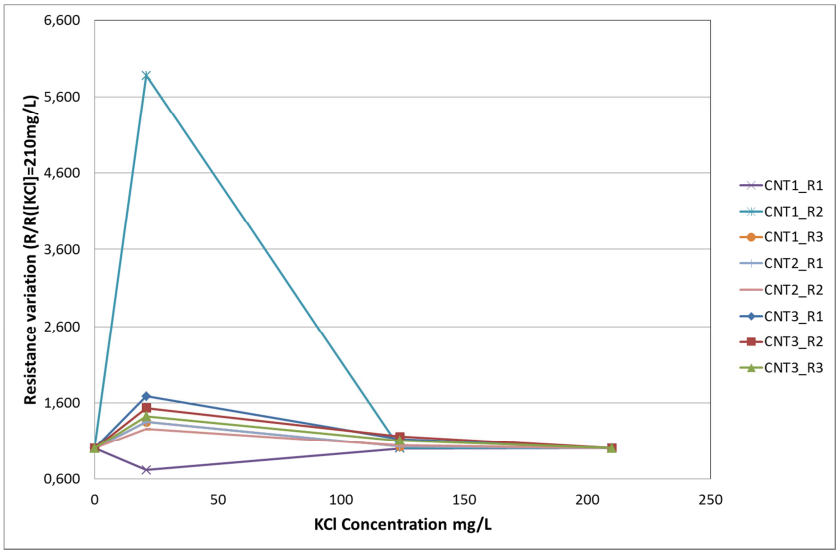

Figure 63: CNT sensor sensitivity to KCl concentration

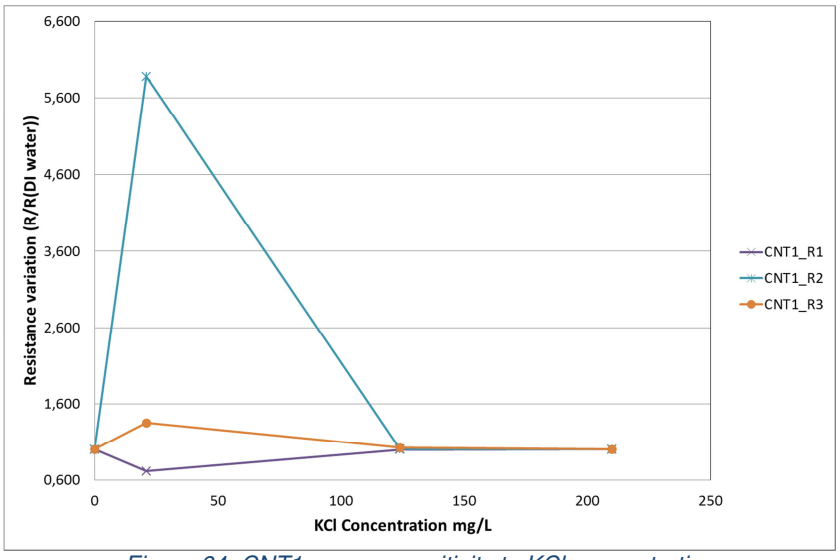

Figure 64: CNT1 sensor sensitivity to KCl concentration

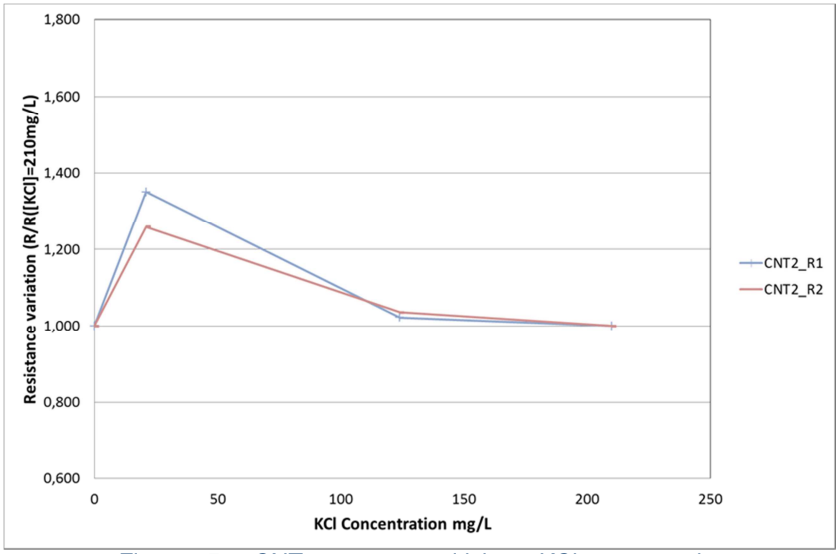

Figure 65:8. CNT2 sensor sensitivity to KCl concentration

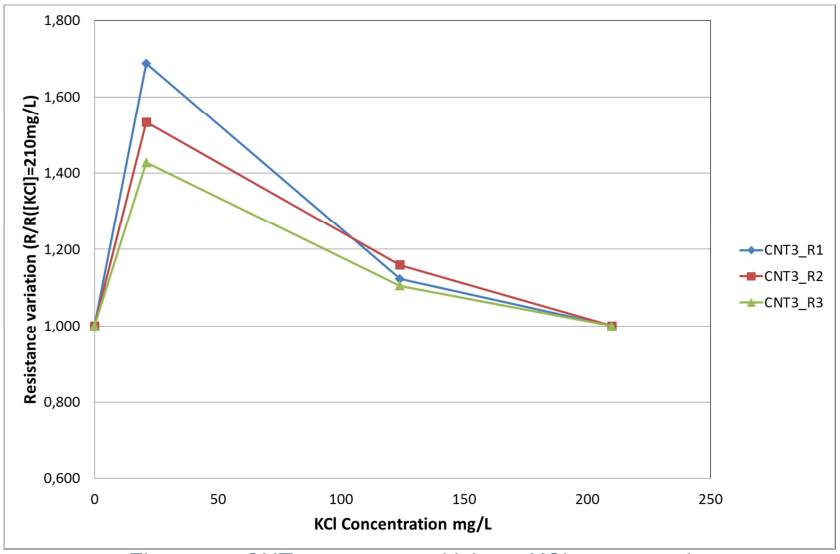

Figure 66: CNT3 sensor sensitivity to KCl concentration

3.4.2.3 Chlorine

Sensitivity to chlorine (HOCl) is studied using bleach diluted in DI water at different pH levels around 5 and around 6 (pH 5 solutions: 2 solutions 5.02 and 5.03 pH; pH 6 solutions: 2 solutions at pH 5.8 and 6.1). At this pH, the majority form of chlorine is HOCl, in other words active chlorine, and the active chlorine concentration is equal to the free chlorine concentration. The reference solution is DI water. Note that the sensor outputs in DI water may not be representative of outcomes in tap water due to the very low conductivity of DI water. During the trials, temperature varies between 22.4°C and 23.4°C. CNT2-R2 has stopped operating.

Figures 67 to 71 show the results. Sensitivity at pH 5 and pH 6 follow the same trends. In the figures below, the free chlorine level equal the active chlorine level due to the low pH. Briefly

- CNT1 outputs decrease by up to 25% with free/active chlorine concentrations.
- CNT2 outputs increase with chlorine (free/active) levels with a strong sensitivity to pH, and up to 200% at pH 6 (20% only at pH 5).
- CNT3 outputs increase up to 80% with (free/active) chlorine, with a low sensitivity to pH.

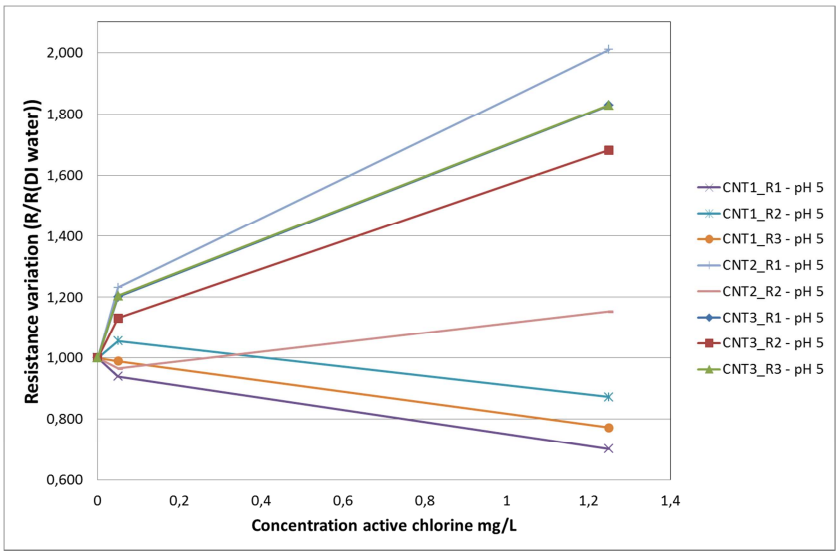

Figure 67 Sensitivity to active chlorine of all CNT sensors at pH 5

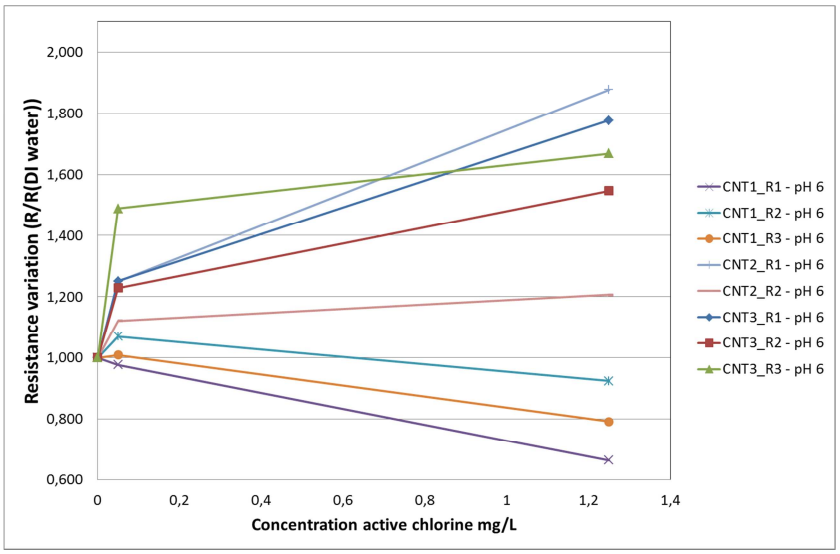

Figure 68: Sensitivity of all sensors to active chlorine at pH 6

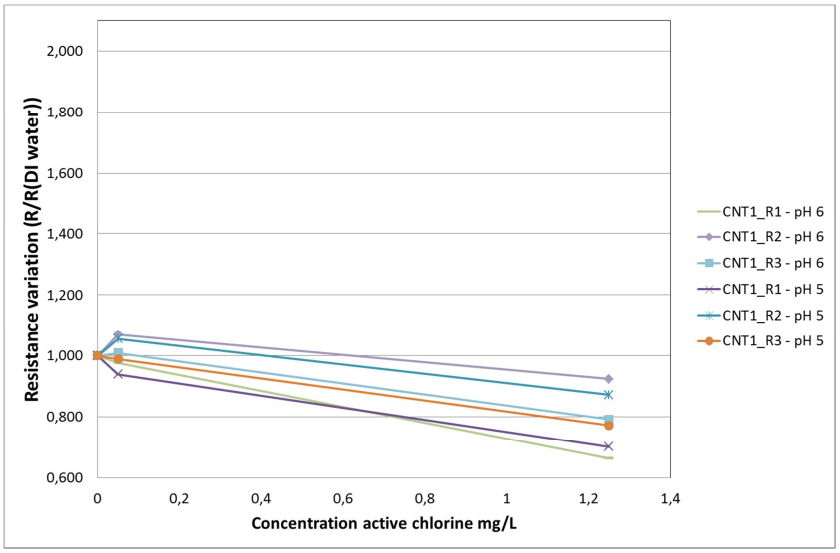

Figure 69: Active chlorine sensitivity of CNT1 sensor

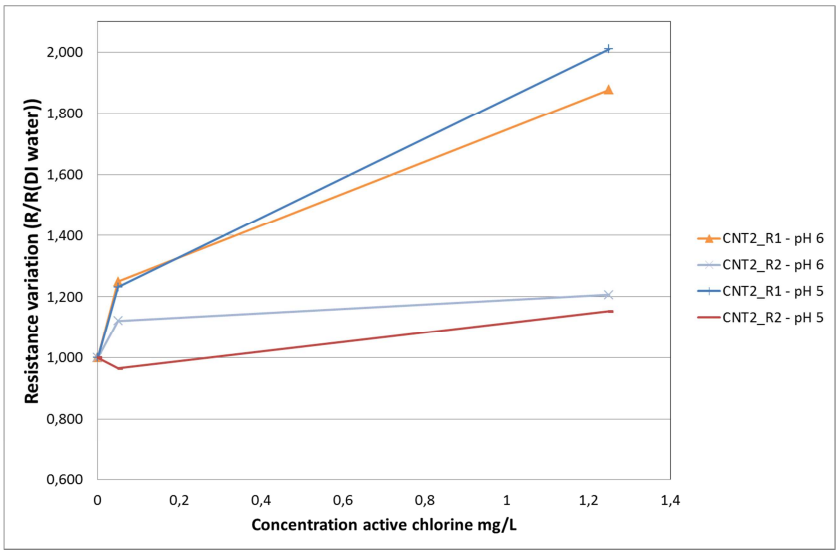

Figure 70: Active chlorine sensitivity of CNT2 sensor

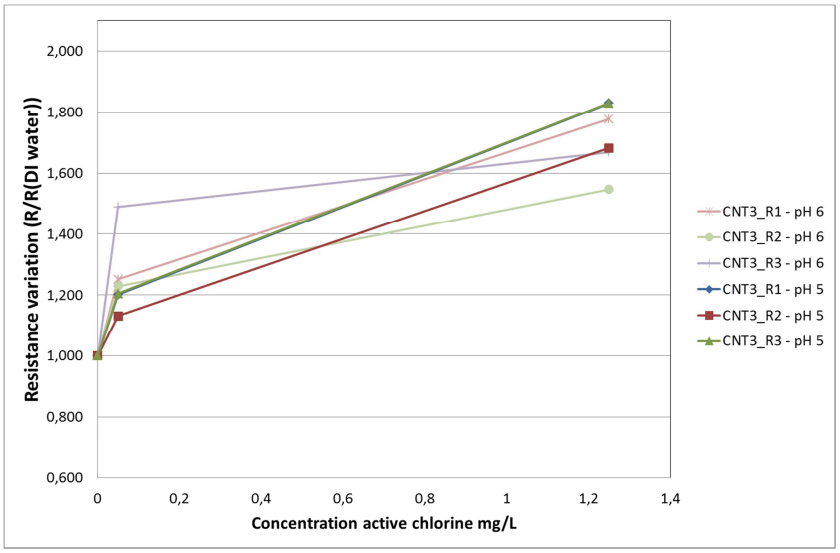

Figure 71: Active chlorine sensitivity of CNT3 sensor

3.4.2.4 Summary

The following table summarizes the results (reproducible refers to sensor-to-sensor reproducibility on the same chip – same trends, same ranges of magnitude of variation).

	CNT1 **(chloride sensor)**	**CNT2** **(chlorine sensor)**	**CNT3** **(pH sensor)**	**Complementary data needed**
pH sensitivity	-no clear trend -less than 20% variation -reproducible	-decrease at low pH, increase at high pH -sensitivity between -50% and +40% over the pH range -not reproducible (1 sensor not sensitive, 1 sensor very sensitive at high pH)	**-decrease at low pH, not sensitive at high pH.** **-sensitivity between +10% and -50% between -50% at low pH** **-not reproducible (1 sensor not sensitive)**	More data between 5.7 and 7.8 Confirm response of CNT2 sensors above pH 7.
Chloride sensitivity	**-Peak at 20mg/L** **-+560% for R2, ±30% for R1 and R3** **-not reproducible**	-Peak at 20mg/L -30% sensitivity -reproducible	-Peak at 20mg/L -40% to 70% sensitivity -reproducible	More data between 0 mg/L and 120mg/L Clarify differences between EDI and tap water as reference Reproduce result on CNT1-R2
Free/Active chlorine sensitivity	-Decrease -25% sensitivity (not sensitive to pH) -reproducible	**-Increase** **-sensitivity 200% at pH 6; 20% at pH 5** **-reproducible**	-Increase -80% sensitivity (not sensitive to pH) -reproducible	Data at pH 7 to 9 At pH <6, active chlorine=free chlorine, so both sensitivities cannot be differentiated

Regarding to CNT1 sensors, expected to sense chloride concentration, the only prominent sensitivity is actually chloride, but this result needs to be confirmed, as only one out of three sensors is responsive to chloride.

Regarding to CNT2 sensors, designed to sense chlorine, the main sensitivity is actually chlorine. The response to chloride is pH sensitive, and the sensor has also a pronounced response to pH in the absence of chloride.

Regarding to CNT3 sensors, designed to sense pH, sensitivities to pH (below 6) and chloride are of the same range of magnitude.

Regarding to chlorine sensitivity, the CNT2 sensors are as expected from design the most sensitive to free/active chlorine at higher pH (close to pH in tap water).

Regarding to chloride sensitivity, one of the CNT1 sensors is remarkably sensitive to chloride (as expected from design). Complementary data should confirm whether this result is an anomaly or a consistent result. In case the data is not confirmed, the CNT3 sensors also provide significant sensitivity to chloride.

Regarding to pH sensitivity, both CNT2 and CNT3 sensors are sensitive to pH below 6. Above pH 7, only one of CNT2 sensors is sensitive to pH.

Overall, these results show clear selectivity between the sensors and the analytes, though complementary data with other caps and additional solutions are needed for both confirming these results and establishing the calibration laws.

4 Deployment in Sense-City drink water loop

4.1 Proteus@Sense-City drink water loop

4.1.1 The Sense-City concept

The Sense-City [1] project was built in 2010 to help researchers to tackle the issues of smart technologies deployment for urban applications and to bring their innovations closer to industrial stakeholders. Sense-City is a project of Université Paris-Est, gathering in its consortium seven institutes, IFSTTAR, ESIEE, Ecole Polytechnique, CNRS, CSTB, UPEM and INRIA. Funded within the framework of the "Investment for the Future Program" since 2012, Sense-City focuses on the prototyping and validation of micro and nanosensors for sustainable cities applications. It enables researchers to explore the concept of "sensitive" city in a realistic manner, with the end goal to empower the city to constantly self-diagnose in order to save resources, preserve its environment and protect its inhabitants.

Sense-City is first and foremost a large experimental project. Its main feature consists on a large environmental chamber designed to host urban scenarios. These are full-scale realistic models of a city's main components: buildings, infrastructures, underground distribution networks. From 2017 onwards, this unique equipment will provide 4200m^3 of experimental volume over a 400m² surface area, with controlled environmental conditions (temperature and hygrometry, rain simulation, solar radiation, liquid or gas pollution, water saturation of the soil, etc.) (Figure 71).

Figure 72: Architect view of the upcoming Sense-City equipment, at the heart of Cité Descartes in Marne-La-Vallée.

In anticipation of the coming equipment, Sense-City first urban scenario, the so-called "connected district", was inaugurated in March 2015 (Figure 72). Since then, it has welcomed a wide range of smart city-related experiments, on the Internet of things for urban area, on urban air quality monitoring, building and neighborhood energy performances, on smart roads as well as on smart infrastructures and networks. Proteus@Sense-City drink water loop is the latest among these experiments deployed in the "connected district.

[1] http://sense-city.ifsttar.fr/

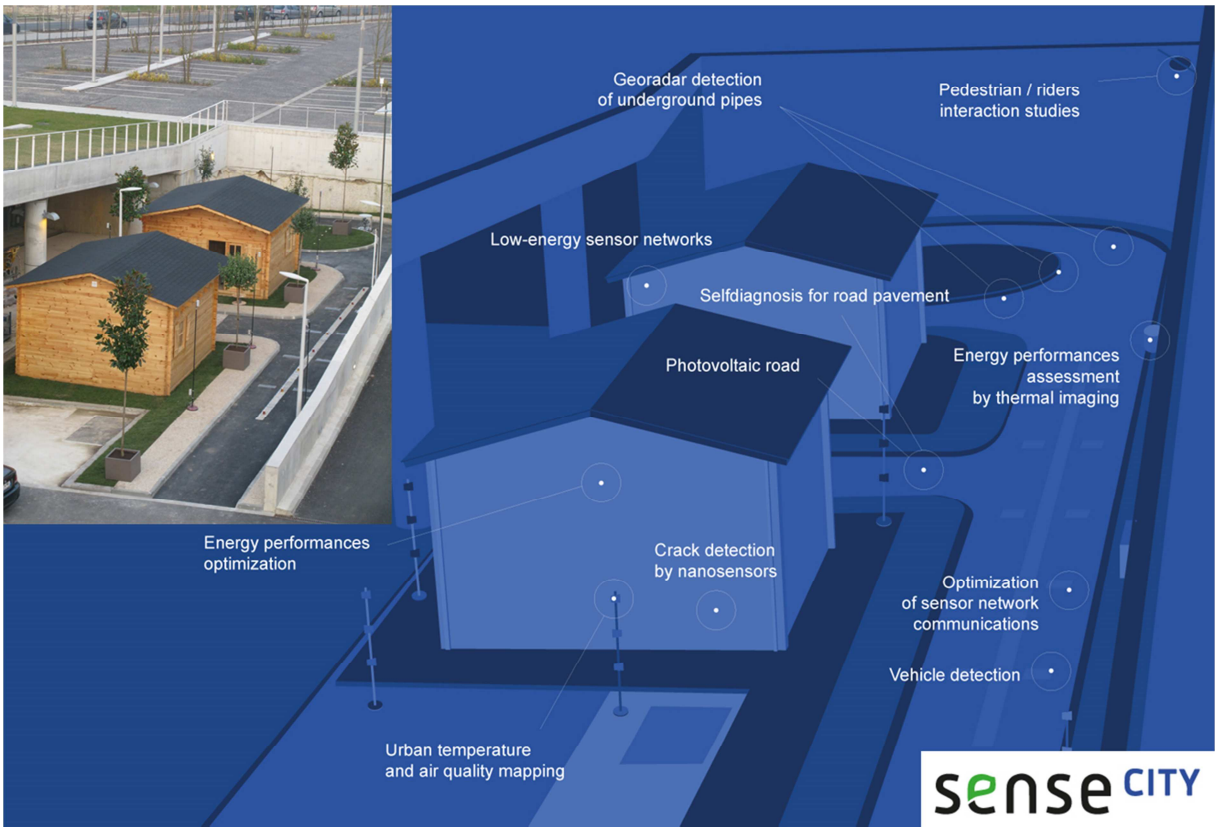

Figure 72: Ongoing experimentations in Sense-City connected district (inset). This urban scenario, located in IFSTTAR's Bienvenüe building, was inaugurated in March 2015.

4.1.2 Proteus drink water loop

Proteus@Sense-City drink water loop consists in 46m of above-ground PVC pipes connected in closed loop to a 1m3 water tank. Figures 73 to 78 show the implantation of the loop in Sense-City. The pressure in the pipe is controlled by a 30kW booster, while the flow is controlled by a manual valve. A thermal regulator with 14kW power enabled temperature control of the water in the tank.

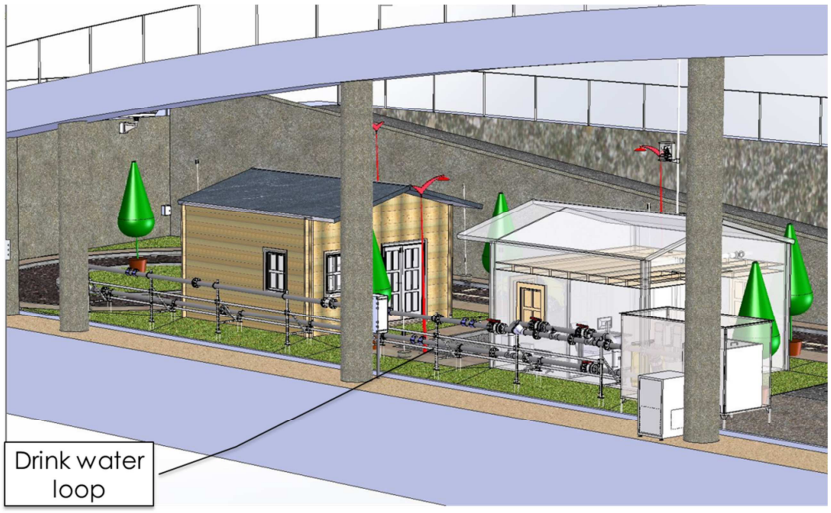

Figure 73: CAD representation of the Proteus@Sense-City water loop

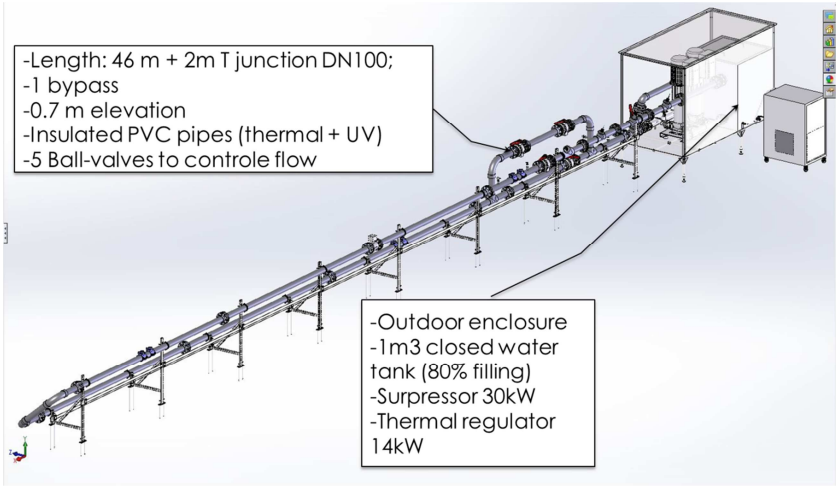

Figure 74: Focus on the characteristics of the water loop

Figure75: Water loop imaged from the booster side

Figure 769: Water loop pictured from its end, with the booster on the far side.

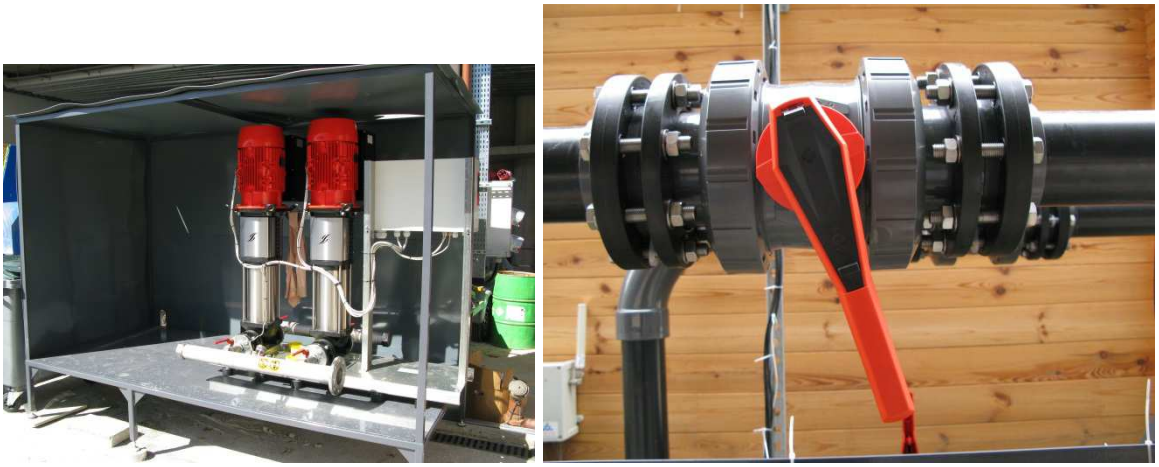

Figure 77: Left: Wilo Salmson Alti-nexis VE2207 booster in its outdoor enclosure (picture before installation of the water tank, now located to the left of the booster in the enclosure). Right: Manual valve enabling flow rate control

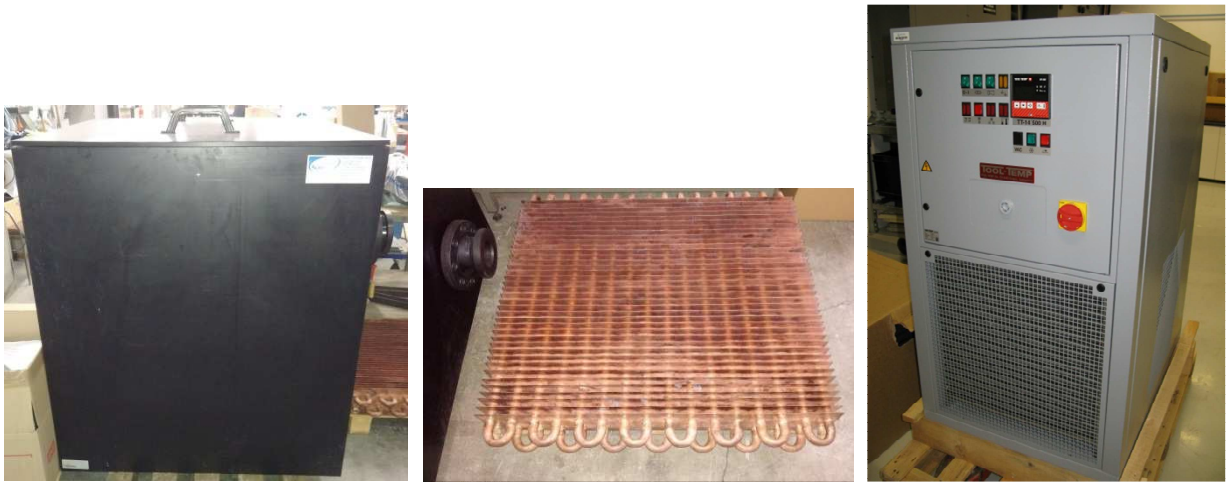

Figure 78: Left: 1000L water tank - Middle: Coper-based heat exchanger at the bottom of the tank – Right: Tool-Temp TT14500 water-based thermal regulator connected to the heat exchanger

The loop is fitted with the following reference sensors:

- Two T113 temperature sensors at the start and end of the loop.
- Aqualabo PHEHT pH and temperature sensor
- Aqualabo C4E conductivity, salinity and temperature sensor
- Optiflux 2100 electromagnetic flow rate sensor
- HSB0-UE-020-0-V-K-05 pressure transducer

All the sensors data are interfaced directly to the P400 PLC from Aqualabo and connected via the 4001 multichannel Modbus module (from Aqualabo also) (figure 79). The user-interface of the P400 PLC is the web-based version of the Arlequin SCADA.

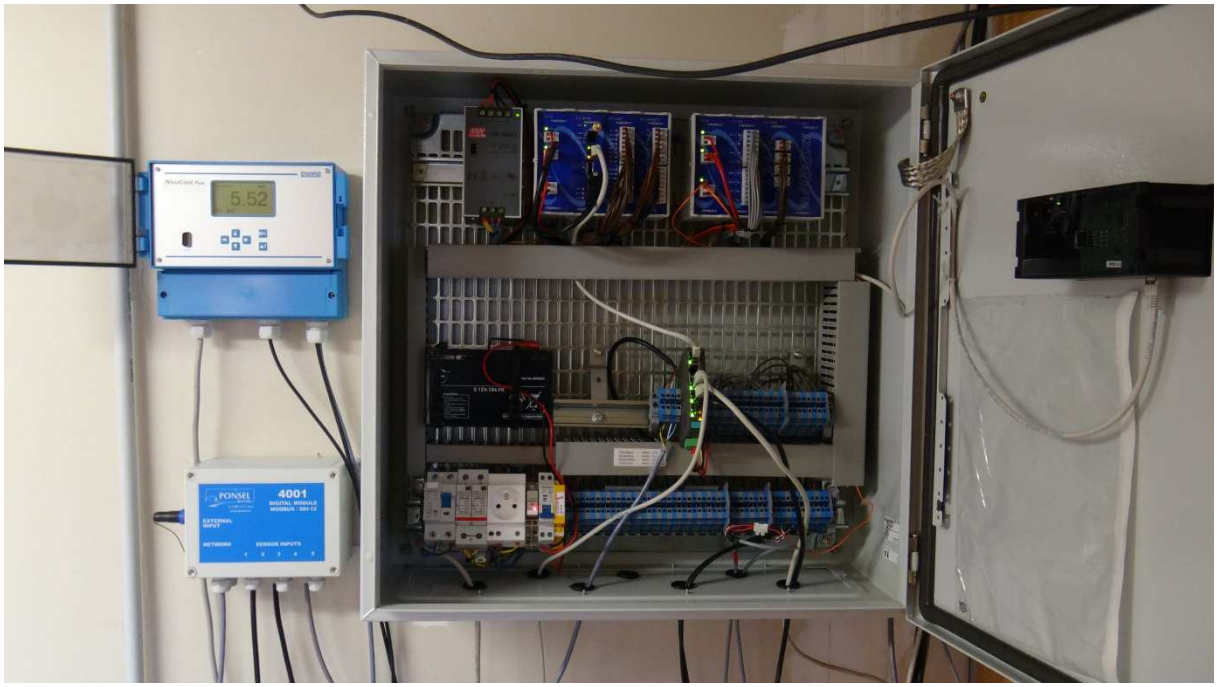

Figure 79: Flow rate sensor digital display (top left); 4001 module (bottom left); P400 PLC (right)

4.2 PNODE installation

Proteus@Sense-City water loop incorporates 6 clamping system to mount 3 pairs of PNODE and PNODE piezoelectric vortex generator. Figure 80 shows one PNODE installed in the loop. The AFE is installed directly in the housing.

Figure 80: PNODE deployed in Sense-City loop via the clamping system

In the current version of the deployment, the rest of the electronics (the MSP and the V1.1. board to operate the energy harvester) are located in a box below the PNODE (Figure 81). This solution is temporary, to be replaced by a single V1.2 board placed in the housing.

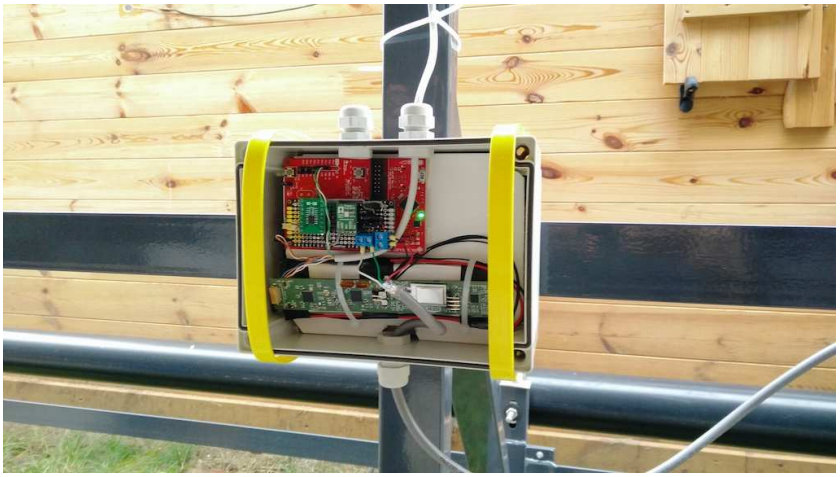

Figure 81 Connection box for the PNODE. It contains the temporary electronics (V1.1 electronic card to connect the harvester and external MSP to read the AFE and connect to the PLC) of the PNODE

4.3 PNODE sensor exploitation

4.3.1 Integration strategy

As shown in deliverable D51, Figure 82 depicts the integration between PROTEUS Node, PLC (P400 system), Production SCADA (Arlequin), OpenSCADA (Freeware) and PROTEUS Oracle.

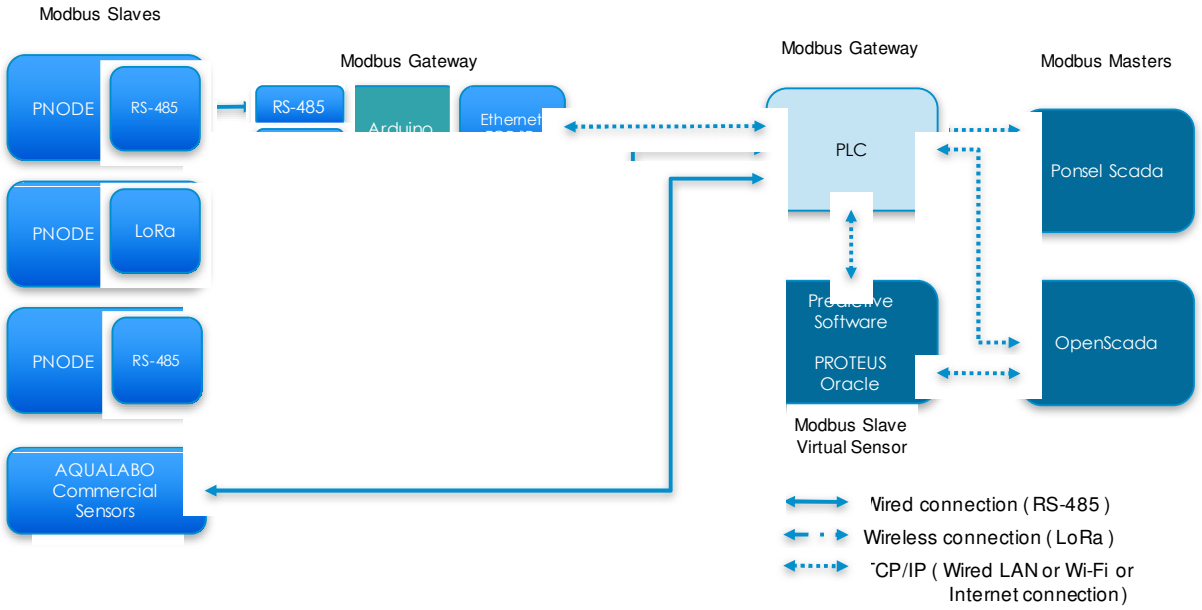

Figure 8210: Integration among Modbus Sensor Nodes, Modbus Gateway, PLC, SCADA, OpenSCADA and PROTEUS Oracle. Here the PLC is the P400 system and Ponsel/Aqualabo Scada is the Arlequin system.

As a reminder, the PNODE is connected directly to the PLC via Modbus over RS-485 or to a Modbus Gateway, via RS-485 or LoRa. The gateway converts Modbus over RS-485 or LoRa to Modbus over TCP/IP Ethernet and then connects to the PLC. Commercial sensors (from AQUALABO) serving as reference sensors are connected to the PLC via Modbus RS485. The PLC is feeding the Production SCADA with the retrieved measurements through Modbus over TCP/IP Ethernet. Similarly, the OpenSCADA is fed data by the PLC with the same manner.

The OpenSCADA acts as an interface between the PROTEUS Oracle (Predictive software developed by WINGS) and the PLC, since historical data record is required for the training of the predictive algorithms and not always available from a Production SCADA. The PROTEUS Oracle receives the historical data stored in the OpenSCADA SQL database through SQL queries over TCP/IP and then, it executes the predictive algorithms. The predictive algorithms can be applied to as many types of parameters as relevant (9 at most for Proteus configuration), and return the forecasted value for the selected parameter, according to past measurements. The predictive values are fed back to the PLC (as a virtual sensor) through Modbus over TCP/IP Ethernet, so as to appear in the Production SCADA. PROTEUS Oracle is a Modbus slave to the Production SCADA.

4.3.2 PNODE interrogation via AFE and MSP

Figure 83 shows the detail of the Sense-City deployment on the PNODE side. The AFE operation is described above, in section 3.2 of the present deliverable.

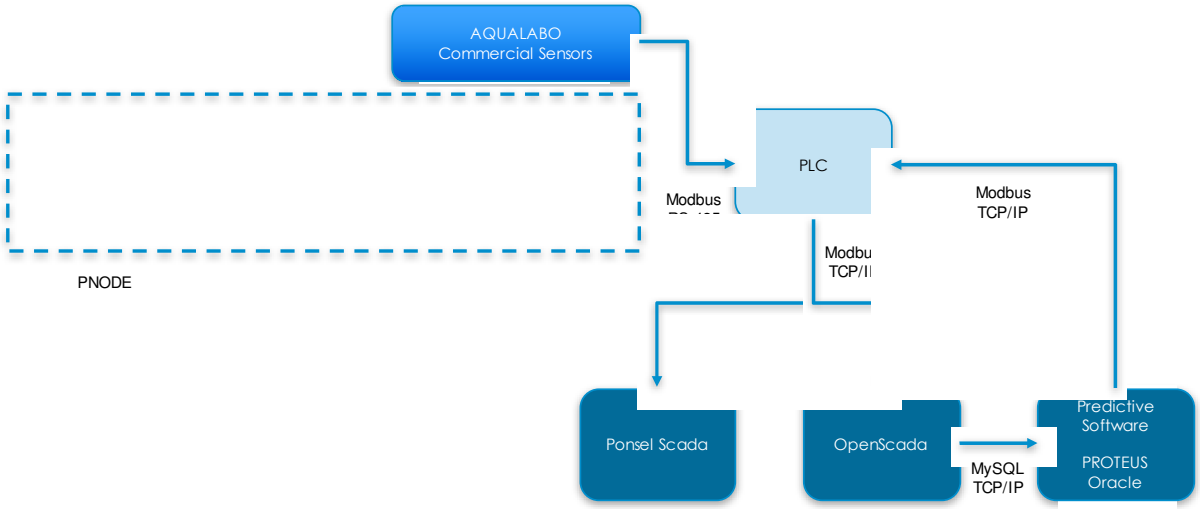

Figure 83: SenseCity deployment overview. Details on PNODE side

As a reminder of the deliverable D5.1, here is how the system operates for the temperature sensors in the caps: the PNODE reads the temperature sensor in a sensor cap via the Analog Front End. The AFE API is defined with a set of commands that are described below. The AFE periodically sends the measured value for the selected sensor to the MSP via Serial UART. The MSP can send commands to the AFE to select the sensor to be read or to change the biasing configuration. The MSP converts the read values to a physical parameter thru linear equations or calibration tables and stores the values in internal Modbus register.

Analog Front-End (AFE) API - V125 - Protocol over UART

< 1byte command > < 1byte length > < length bytes of data > < 1byte termination >

Commands

- ***Sensor Selection*** *(5 bytes)*
- ***DAC Period*** *(2 bytes) (0.076 Hz - 500 Hz)*
- ***DAC Duty Cycle*** *(1 byte)*
- ***DAC Range*** *(1 byte) (0 uA to 31.875 uA or 255 uA or 2048 uA)*
- ***DAC Value*** *(1 byte) (0 to 255 (1/8 uA/bit or 1 uA/bit or 8 uA/bit)*
- ***Measure*** *(2 + 4 = 6 bytes)*
    - *sample_sequence_number: 2 bytes (max samples for a session: 65536)*
    - *sample_value: 4 bytes*

The current MSP software now supports the following sensors in the caps:

- Two temperature sensors
- Two pressure sensors

- Two conductivity sensors
- Two flow rate sensors (not supported yet by the AFE)
- Three sets of three CNT sensors

For each sensor, the PNODE can send both raw data and calibrated values, when the calibration relationship is available at PNODE level (calibrated values can be also derived at the PLC level).

Due to memory limitations in the current version of the MSP, only 7 sensors out of the 17 can be read at the same time. Figure 84 shows an example of sensor data read out on the OPENSCADA software (only the temperature sensor is calibrated on the PNODE°

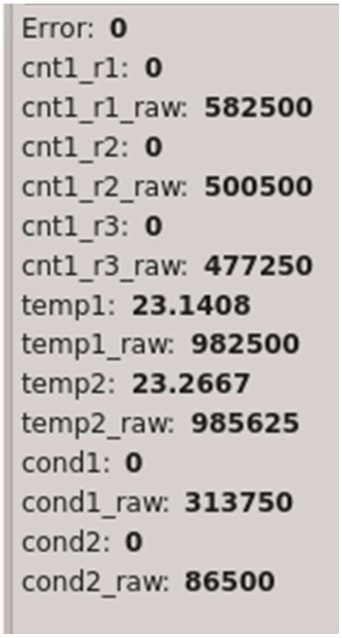

Figure 84: OpenScada readings of seven of the Pnode sensors with Raw and Calibrated values.

4.3.3 PNODE interrogation by the PLC

The P400 PLC is configured to read the 17 sensors of one PNODE with a predefined slave ID (currently ID #10). Each sensor in a PNODE is affected 2 modbus registers, one for the raw data (a signed integer coded over 32 bit – 4 words of 2 characters in hexadecimal – with µV unit), one for the calibrated data (signed, floating number, with the appropriate unit depending on the type of sensor).

Only the non-calibrated data are exploited currently: initially, each sensor data in µV frame is read as a positive integer and displayed in a first channel. For each sensor, a second channel is created to convert the positive integer into a signed integer via a dedicated function. Finally, a third channel is created to display the calibrated data (via an additional function) when calibration coefficients are available.

4.4 Results on packaging

The robustness of the mechanical housing of the sensor cap was first evaluated under various pressure conditions.

For this trial, the complete mechanical structure of the prototype (sensor cap linked to node housing) was implemented in the loop using the saddle clamp and its adaptor (Figure 85).

Figure 85: PNODE mounted in the saddle clamp with adaptor

The pressure in the loop was increased step by step from 3 to 10 bars at stable flowrate (5m3/h). Each pressure step is maintained for over 20 minutes (see blue curve in Figure 86). The flow is stopped after each step to remove the prototypes and evaluate visually their state.

Figure 86 Profile of pressure applied in the loop.

Figure 87 shows an image of a cap after these trials. It appears that the cap withstands properly the various pressure levels on a mechanical level: the PCB stays fully in place; the silicon membrane of the pressure sensor does not seem affected; the encapsulation resist (here EPO-TEK 730) appears

well in place. However, ageing of the globtop (EPO-TEK H70E-4) is observed, yielding to exposure of the bonding directly to water.

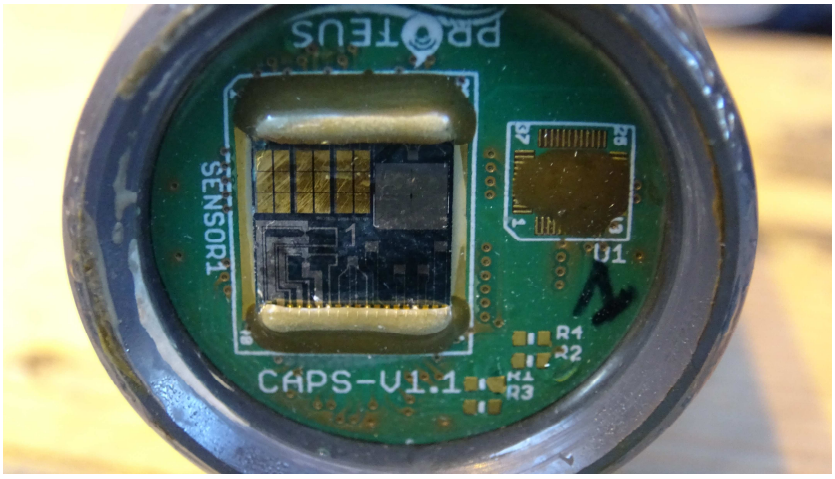

Figure 87: Image of a cap after exposure to 10bar showing possible delamination of the globtop resist.

4.5 Results on sensing

The sensing performances were analyzed on sensor cap #5 installed in Sense-City loop since Feb. 3rd, 2017.

4.5.1 Temperature

Figure 88 shows a comparison over 845 min (on Feb. 8th) between the raw output of the temperature sensor T2 and the actual reference temperature in the loop, while Figure 89 shows the reference temperature plotted as a function of the T2 sensor data; one observes the expected linear dependence between T2 outputs and the real temperature.

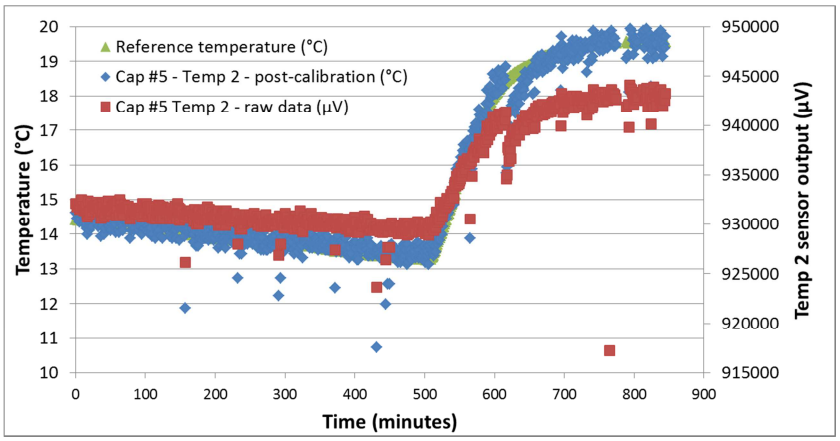

Figure 88: Comparison between the raw data from the temperature sensor 2 of cap #5, the calibrated data from temperature sensor 2 of cap #5 and the reference temperature.

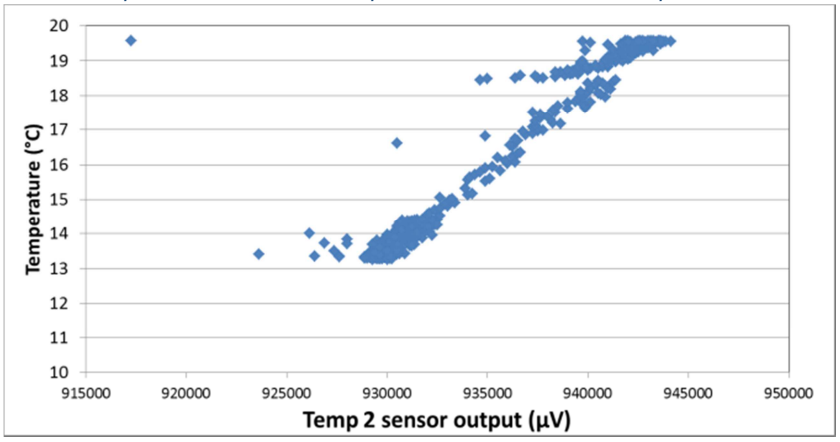

Figure 89 Reference temperature as a function of the raw data from the temperature sensor 2 of cap #5, showing a linear dependence

A linear regression is used to establish the relationship between reference temperature and raw data, yielding

$$T_{calibrated}\ (°C)=0.46U_{T2}(mV)-0.41$$

(where U_{T2} is the raw voltage measured by the AFE). The quantity $T_{calibrated}$ is the calibrated output for the sensor T2. Figure 88 also displays jointly the reference temperature and the calibrated output of T2, and shows the very good agreement between both sets of data. The average error is 0.25°C over the whole set of data (845min).

The noise level in the sensor output is about 0.32mV (standard deviation) for a reference temperature measured as varying by less than 0.03°C. Based on the previous relationship, the noise-related error on the temperature estimation is 0.15°C.

A significant contribution to this error stems from a clear misfit around 617 min. At this exact time, chemicals (NaOCl) were added suddenly into the water loop and changed the conductivity. Return to normal for the temperature sensor occurred in about 40min; maximal error on temperature estimation during this period is 2.5°C.

The sensor T2 stopped sending significant data after about 6 days in the loop (while other sensors in the cap kept operating). Post mortem analysis of the caps will be carried out to understand the cause for this failure.

4.5.2 Pressure

The response of the pressure sensor 1 of cap #5 is evaluated over a full day (Feb 17th, 2017). The raw data are negative; for simplicity sake, in the following section, we plot the opposite of the raw sensor output.

At 1bar of pressure, 5m3/h of flow rate (0.14L/s), the sensor shows temperature sensitivity (Figure 90):

$$U_{pressure1}(mV)=-2.0T(°C)+98.$$

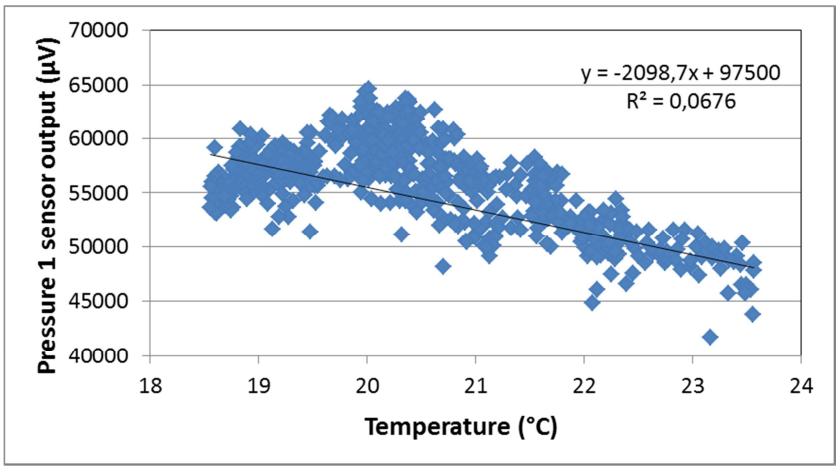

Figure 90: Temperature sensitivity of pressure 1 sensor

Then, the following pressure and flow rate steps are applied:

- T0: Pressure 0.5 bar; flowrate 5,0m3/h
- T0+66min: Pressure 2.0 bars; flowrate 4.9m3/h
- T0+139min: Pressure 3.0 bars; flowrate 4.8m3/h
- T0+239min : Pressure 1.0 bar; flowrate 5.0m3/h
- T0+307min: Pressure 1.0 bar; flowrate 9.7m3/h
- T0+387min: Pressure 1.0 bar; flowrate 20.4m3/h
- T0+466min : Pressure 1.0 bar; flowrate 5.0m3/h

The sensitivity to flow rate is of the same order of magnitude as the noise (1.3mV variation between 5m3/h and 20m3/h). Figure 91 shows the sensitivity to pressure (after temperature compensation):

$$P_{pressure1}\ (bar)= -0.25(U_{pressure1}(mV)-2.0T(°C))+5.6.$$

The noise in the sensor output is about 2mV. So (discounting additional errors on temperature estimation) the expected error on the pressure estimate is 0.5 bar, which is relatively large considering that the calibration relationship is evaluated between 1 and 3 bar. Reduction of noise in the pressure sensor output is clearly needed. One of the causes for this high noise level may be the ageing of the cap, as the pressure testing were done 2 weeks after installation of the cap in Sense-City.

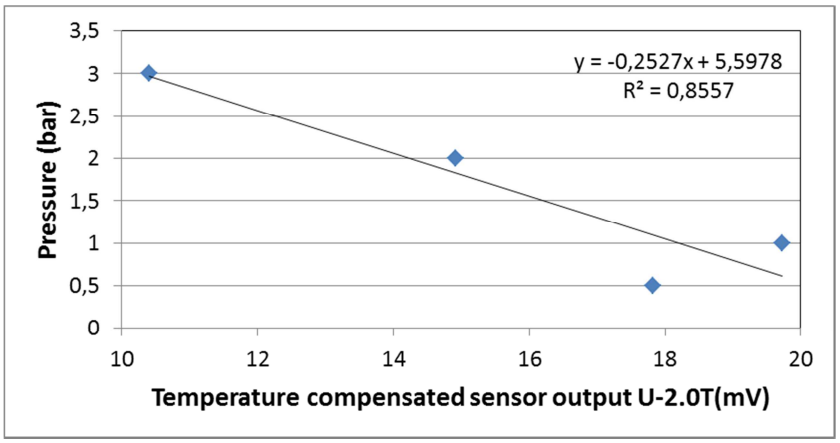

Figure 11: Pressure sensitivity

4.5.3 Chemical sensors

The response of the following sensors in cap # 5 is studied: conductivity 2, CNT1-R1 (Chloride), CNT2-R2 (Chlorine), CNT3-R1 (pH). The response of these chemical sensors was studied between Feb 8th, 00:40, and Feb 13th, 22:42. Figure 92 shows an example of the conductivity 2 sensor response as a function of time during the first day of sensor operation. In the figure, the numbers correspond to series of actions achieved on the loop (addition of chemicals, change in temperature).

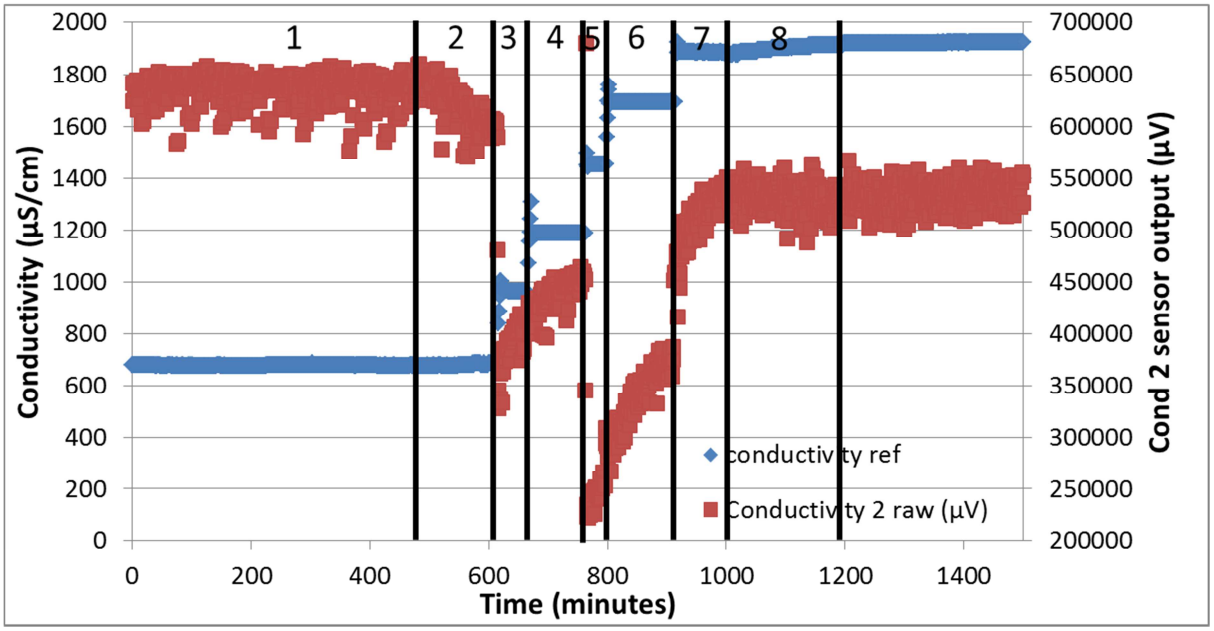

Figure 92: Conductivity 2 sensor response as a function of time, compared to the reference conductivity. Step 1: initial condition. Step 2: 1.2°C temperature increase. Step 3 & step 4: addition of 2.5L of NaOCl at 3.6% in 1000L. Step 5: addition of 0.5L HCl at 23% in 1000L. Step 6 & step 7: addition of 2.5L of NaOCl at 3.6% in 1000L. Step 8: temperature increase from 19°C to 27°C. The sensor stops working between step 7 and step 8.

The following table summarizes the responses of the sensors to these different actions.

	Parameters	Cond 2	CNT1-Cl-R1	CNT2-Cl2-R2	CNT3-pH-R1
1	-Initial conditions - Feb 8th -Duration: 470 min -Parameters: conductivity 680µS/cm pH 8.2, temperature between 13.3°C and 14.5°C – average 13.8°C, flow rate 4.9m3/h pressure 0.95bar	-Stable -No temperature correlation -Response Avg: 637mV Std dev: 13mV (2%).	-Stable -No temperature correlation -Response: Avg 305mV Std dev 7.7mV (2.5%).	-Stable -No temperature correlation -Response: Avg 861mV Std dev 8.0mV (0.9%).	-Stable -No temperature correlation -Response: Avg: 144mV Std dev: 6.2mV (4.3%).
2	-Temperature increase between 16°C and 18.5°C -Duration: 61min -Parameters: conductivity 680mS/cm pH 8.1, temperature average 17.4°C, flow rate 12m3/h pressure 0.96bar	U_{Cond2}(mV)= -12T(°C)+830	-Stable -No temperature correlation -Response: Avg: 296 mV Std dev: 9.9mV; (3.3%)	-Stable -No temperature correlation -Response: Avg: 828 mV Std dev: 12mV; (1.4%)	-Stable -No temperature correlation -Response: Avg: 143 mV Std dev: 8.4mV; (5.8%)
3	2.5L of NaOCl (bleach) at 3.6% in 1000L tap water -Duration: 37 min -Stabilized duration: 13min -Parameters: conductivity 960µS/cm pH 8.6, temperature average 19.0°C, flow rate 12m3/h pressure 0.96bar	-Instantaneous response (drop by about 200mV). -No stabilization	-Stable -Response: Avg: 248 mV Std dev: 5.0mV; (2.0%)	-Stable -Response: Avg: 607 mV Std dev: 4.7mV; (0.8%)	-Stable -Response: Avg: 129 mV Std dev: 3.9mV; (3.0%)
4	2.5L of NaOCl (bleach) at 3.6% is added to 1000L tap water -Duration: 88 min -Duration with stabilized -values: 18min -Parameters: conductivity 1190µS/cm pH 8.9, temperature average 19.4°C, flow rate 12m3/h pressure 1.0bar	-Stabilization after 1h -Response: Avg 453mV, Std dev 6.3mV (1.4%).	-Stable -Response Avg 250mV Std dev 8.3mV (3.3%)	-Stabilization after 1h -Response: Avg: 619mV Std dev: 2.9mV (0.5%).	-Stable -Response Avg: 137mV, Std dev 3.7mV (2.7%).
5	0.5L of HCl at 23% added to 1000L tap water -Duration: 26 min -Duration with stabilized	-No stabilization -Sensor output increasing	-Stable -Response Avg: 171mV Std dev: 11mV (6.7%)	-Stabilization after 15min -Response Avg 423mV Std dev: 8.3mV	-No stabilization. -Sensor output and noise increasing

	-values: 10min -Parameters: conductivity 1460µS/cm pH 6.1, temperature average 19.5°C, flow rate 12m3/h pressure 0.97bar			(2.0%)	
6	2.5L of NaOCl (bleach) at 3.6% is added to 1000L tap water -Duration: 99 min -Duration with stabilized values: 19min -Parameters: conductivity 1690µS/cm pH 6.4, temperature 19.6 °C, flow rate 12m3/h pressure 0.97bar	-Stabilization after 1h -Response: Avg: 367mV, std dev 7.8mV (2.1%)	-Stabilization after 1h -Response: Avg: 214mV std dev 15.0mV (7.0%)	-Stabilization after 1h -Response: Avg: 601mV, std dev 13.5mV (2.2%)	-Stabilization after 1h - Response Avg 146mV, std dev 12.6mV (8.7%)
7	2.5L of NaOCl (bleach) at 3.6% is added to 1000L tap water -Duration: 75 min -Duration with stabilized values: 23min -Parameters: conductivity 1690µS/cm pH 6.7, temperature 19.5 °C, flow rate 12m3/h pressure 0.97bar	-Rising, Stabilization uncertain after 1h -Response Avg: 533mV Std dev 9.4mV (1.8%) -Sensor assumed dead (average output identical to the value at next stage where sensor is dead)	-Stabilization after 1h -Response Avg 270mV std dev 12.6mV (4.7%).	-Stabilization after 1h -Response Avg: 701mV std dev: 15.8mV (2.2%).	-Stabilization after 1h -Response: Avg: 205mV; std dev 11.5mV (5.6%)
8	Temperature increase from 19.7°C to 27°C -Duration: 173 min -Parameters: conductivity 1900µS/cm pH 6.7, temperature average 23.9°C, flow rate 12m3/h pressure 0.98bar	-No change upon temperature variation -Response Avg 531mV Std dev 13.8mV (2.6%) -Sensor assumed to be dead	$U_{CNT1\text{-}R1}$(mV)= 9.5T(°C)+99	$U_{CNT2\text{-}R2}$(mV)= 20T(°C)+300	$U_{CNT3\text{-}R1}$(mV)= 8.5T(°C)+43.
Renewal of tank water					
9	Tap water; -Duration: 398 min -Parameters: conductivity 773µS/cm pH 7.5, temperature average 22.0°C, flow rate 5.1m3/h		-Stable -Response Avg 478mV Std dev 9.1mV (1.9%)	-Light temperature sensitivity -Response: 914mV, std dev 12mV (1.3%)	-Stable -Response Avg 300mV Std dev 8.7mV (2.9%)

	pressure 1.9bar				
10	83g of NaCl in 1000L -Duration: 112 min -Parameters: conductivity 910µS/cm pH 7.5, temperature average 22.1°C, flow rate 5.1m3/h pressure 1.9bar		-stable -Response Avg 469mV std dev 12.4mV (2.6%).	-stable -Response Avg 929mV std dev 12.5mV (1.3%).	-No stabilization (decrease).
11	83g of NaCl in 1000L -Duration: 267 min -Duration with stabilized values: 116min -Parameters: conductivity 1040µS/cm pH 7.4, temperature average 21.6°C, flow rate 5.1m3/h pressure 1.9bar		-stable -Response Avg 462mV std dev 13.8mV (2.7%)	-stable -Response Avg 934mV std dev 14.1mV (1.5%)	-stabilization after 2hours -Response Avg 182mV std dev 7.5mV (4.1%)
12	83g of NaCl in 1000L -Duration: 115 min -Parameters: conductivity 1150µS/cm pH 7.5, temperature average 21.1°C, flow rate 5.3m3/h pressure 0.95bar		-no stabilization (decrease)	-stable -Response Avg 905mV, std dev 3.8mV (0.4%)	-no stabilization (decrease)
13	Step 12 condition, lower temperature -Duration: 200 min -Parameters: conductivity 1150µS/cm pH 7.5, temperature average 19.4°C, flow rate 5.3m3/h pressure 0.95bar		-stable -Response Avg 396mV, std dev 17.6mV (4.4%)	-stable -Response Avg 399mV, std dev 23.4mV (2.5%)	-stable -Response Avg 55.8mV, std dev 2.6mV (4.7%)

4.5.3.1 Temperature responses

The cond2 sensor sensitivity to temperature is evaluated during step 2: Increase of temperature under stable conductivity: Under temperature increase between 16°C and 18.5°C in stable water condition (conductivity 680mS/cm), the sensor output decreases roughly linearly by 6.7% (Figure 93). The relationship is approximately

$$U_{Cond2}(mV)=-12T(°C)+830.$$

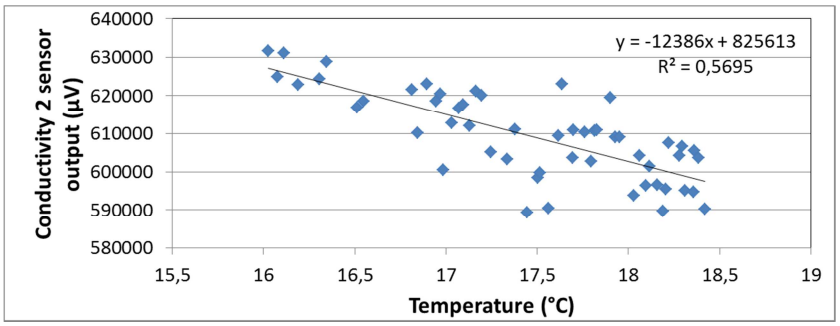

Figure 93: conductivity sensor temperature response

The CNT1-Cl-R1 sensor sensitivity to temperature is evaluated during step 8: for an increase of temperature from 19°C to 27°C, the sensor output increases roughly linearly (Figure 94):

$$U_{CNT1\text{-}R1}(mV)=9.5T(°C)+99.$$

With 6.2mV noise on the conductivity sensor, the error on temperature estimate here is about 0.65°C (6.2mV/9.5°C/mV).

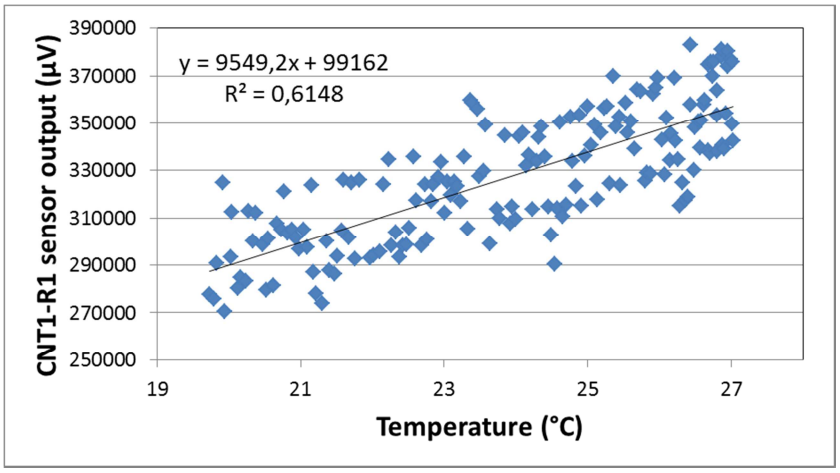

Figure 94: CNT1-Cl-R1 sensor temperature response

The CNT2-Cl2-R1 sensor sensitivity to temperature is evaluated during step 8: for an increase of temperature from 19°C to 27°C, the sensor output increases roughly linearly (Figure 95):

$$U_{CNT2\text{-}R2}(mV)=20T(°C)+304.$$

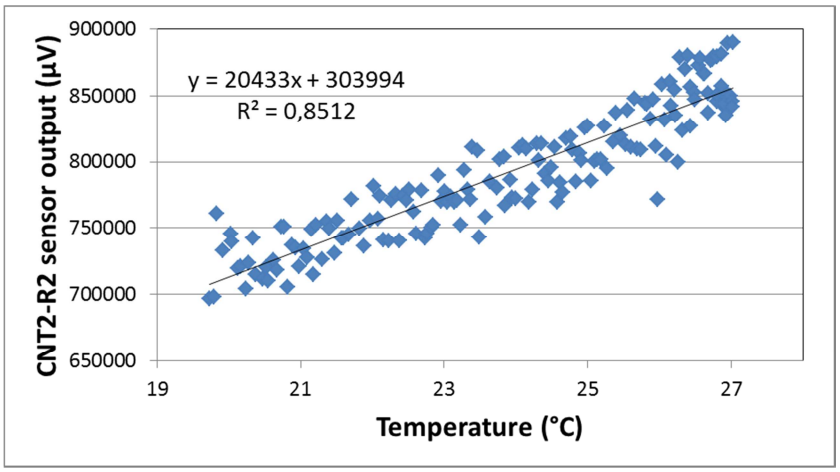

Figure 95: Temperature sensitivity of CNT2-R2

The CNT3-pH-R1 sensor sensitivity to temperature is evaluated during step 8: for an increase of temperature from 19°C to 27°C, the sensor output increases roughly linearly (Figure 96):

$$U_{CNT3\text{-}R1}(mV)=8.5T(°C)+43.$$

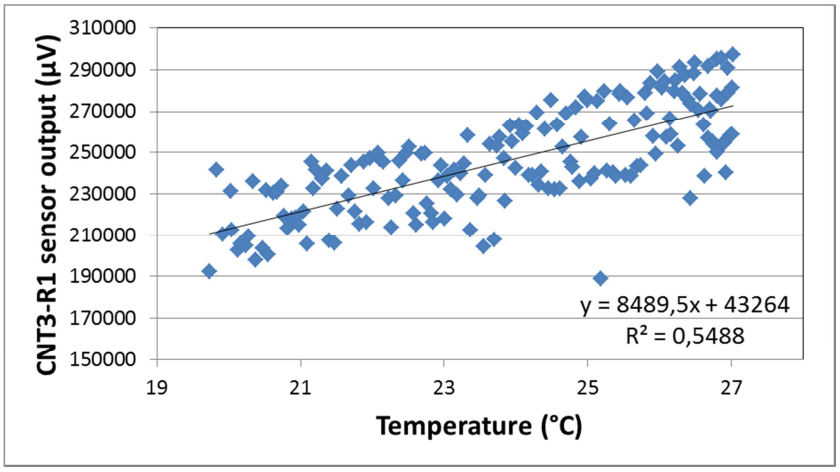

Figure 9612: Temperature sensitivity of CNT3-R1

Standard deviation on thermal sensitivity: A further step should be carried out for all the sensors to estimate the error on thermal sensitivity. A possible method to be used is the bootstrap method, which consists in randomly creating subsets of the data set and calculating the thermal sensitivity for all these subsets. The actual sensitivity is the average of the sensitivity for all the subsets, while the error is the standard deviation over these datasets.

4.5.3.2 Conductivity sensor

Based on the three reliable sensor outputs obtained at 677µS/cm, 1187µS/cm and 1684µS/cm (respectively 13.8°C; 19.5°C and 19.6°C), and on the temperature dependence expressed as U_{Cond2}(mV; at 680µS/cm)=-12T(°C)+830, we obtain (Figure 97) the following relationships enabling calibration of the conductivity 2 sensor data. These relationships are valid after about 1h of stabilization of the conductivity.

$$Conductivity_{cond2}\ (\mu S/cm) = -5.0(U_{Cond2}(mV) + 12T(°C)) + 4700$$

Considering noise level at about 13mV, the noise-related error on conductivity evaluation is around 50µS/cm. To this error should be added the error on temperature estimate (0.25°C with Temp2 sensor), and the error on estimation of the thermal sensitivity.

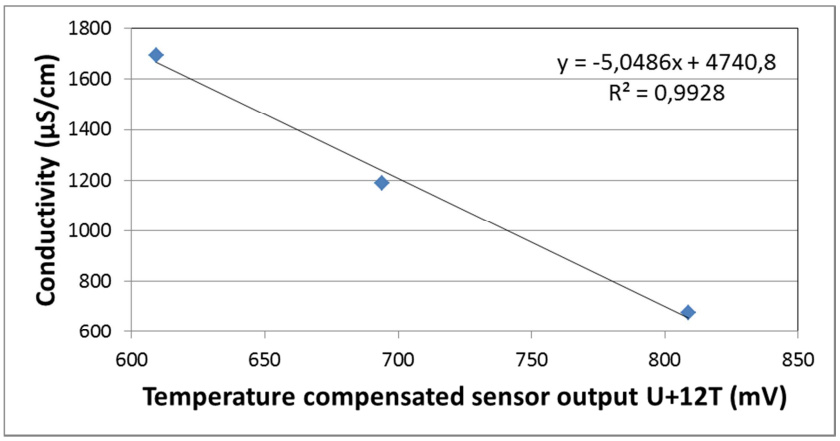

Figure 97: Conductivity sensitivity curve

End of sensor operation: The cause of the sensor failure might be precisely due to a destructive effect caused by the relative high conductivity value reached at stage 7, or by an irreversibility issue, or by a failure in the electronics. Further lab studies will be carried out to check possible irreversibility issue at higher conductivity values.

4.5.3.3 CNT1 (Chloride) sensors

The sensitivity is shown in Figure 98: there is 21% relative variation for an increase in salt concentration between 0 and 250mg/L. The sensitivity is linear up to 160mg/L, then a saturation effect appears to set in. This is completely consistent with lab data where a saturation effect was also observed. The range of linearity needs to be investigated further. Note that in mg/L, [Cl-]=0.6[NaCl].

Up to 160mg/L, the calibration relationship is the following

$$[NaCl]_{CNT1\text{-}R1}(mg/L) = -11(U_{CNT1\text{-}R1}(mV) + 9.5T(°C)) + 2900.$$

However, with 7.7mV of noise, the noise on [NaCl] estimate is about 85mg/L (51mg/L for [Cl-]), which is fairly large compared to the range of variation of [NaCl] concentration (0 to 160mg/L).

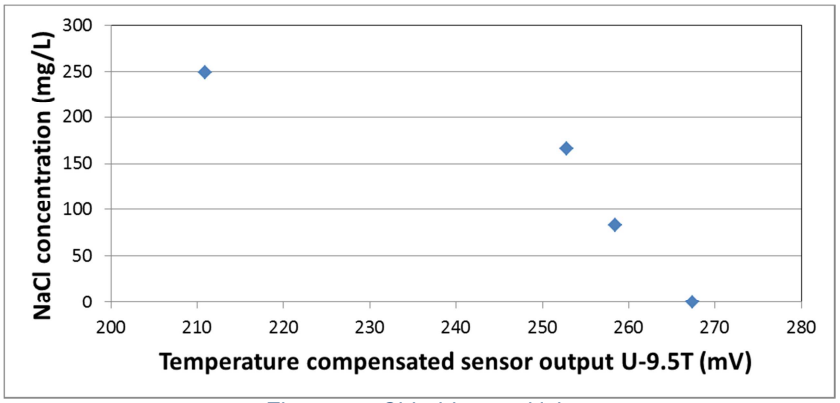

Figure 98: Chloride sensitivity

The sensor features similar trends with chlorine as the chlorine sensor, with smaller sensitivity:

- At pH>8, sensitivity to the addition of NaOCl (20% variation up to 90mg/L NaOCl, compared to 54% for the chorine sensor)
- At pH<8, linear sensitivity to the increase in active chlorine (HOCl): 100mV variation over the range, compared to 300mV for the chlorine sensor. The relationship is (Figure 100)

  $$[HOCl]_{CNT1\text{-}R1}(mg/L) = 1.2(U_{CNT1\text{-}R1}(mV) + 9.5T(°C)) + 200.$$

  With 7.7mV of noise, the error on [HOCl] estimate is about 9.2mg/L (5% of the range considered here)

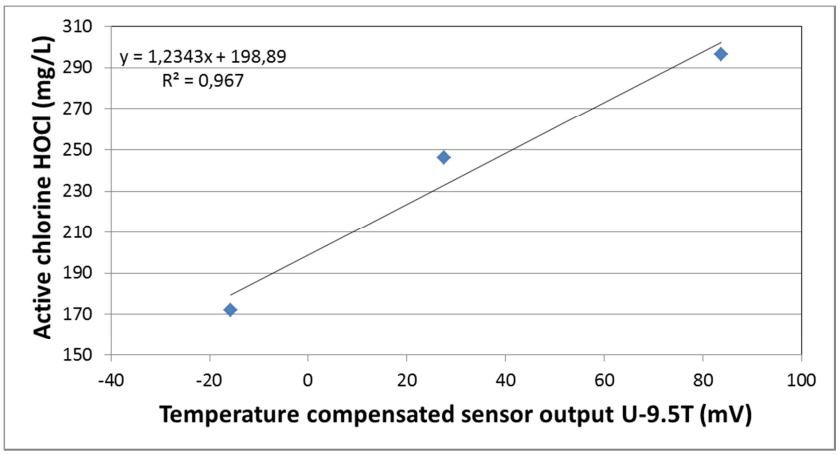

Figure 100: Chlorine sensitivity for CNT1 (chloride) sensor.

4.5.3.5 CNT2 (Chlorine) sensor

The (pH correlated) active (HClO) and available (ClO^-) chlorine sensitivities are shown in Figure 101:

- The concentration of ClO- (available chlorine, not active) and HOCL (active chlorine) is derived from the pH of the water and the total amount of added bleach (free chlorine).
- At pH around 8, the temperature-corrected sensor response decrease by 54% in less than 15min when bleach is added (2.5L of NaOCl at 3.6% in 1000L, i.e. 90mg/L free chlorine, yielding, at pH 8, 85mg/L of available chlorine, 5mg/L of active chlorine). This level is above saturation level for the sensor as no variation between 85mg/L and 174mg/L (addition of another 2.5L of free chlorine) is observed. Note that the amount of free and active chlorine added here are largely above Proteus target (5 times the amount of active chlorine).
- At pH around 6.5 (active chlorine=free chlorine), no saturation is observed. The temperature-corrected sensor response increases linearly by one order of magnitude with increasing level of HOCl between 170mg/L and 300mg/L, with the relationship

$$[HOCl]_{CNT2\text{-}R2}(mg/L) = 0.4(U_{CNT2\text{-}R2}(mV) + 20T(°C)) + 160.$$

  - Note that here, the level of free chlorine are widely out of range compared to Proteus parameters, so the relationship cannot be easily extrapolated to low chlorine level (figure XXX).
  - In lab testing at much lower active chlorine level and at pH 5 or 6, the same trend was however observed (rise of the resistance/voltage with the level of active chlorine).
  - Based on the 8.0mV noise estimate, the noise on active chlorine estimate is about 3.2mg/L (which is fairly small - 2% -compared to the levels of chlorine teste here).
  - Based on the 8.0mV noise measured here, and on the free chlorine sensitivity data reported in section 2.5 from lab experiments (Figure 16), the expected noise in the actual range of interest (up to 1.25mg/L) should be about 0.02mg/L.

These results clearly indicate the need to establish pH-dependant chlorine-sensitivity curves, and to investigate the effect of much smaller concentration of free chlorine.

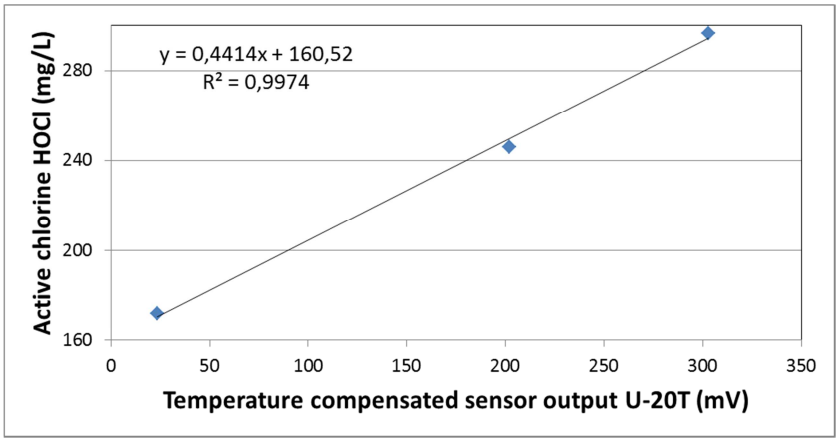

Figure 101: Free chlorine sensitivity at pH between 6 and 7

Chloride sensitivity: the sensitivity of the sensor to chloride is very low: between 0mg/L and 250mg/L of NaCl, relative variation below 2.2% (20mV), for a noise level larger than 1.2mV (1.3%).

4.5.3.6 CNT3 (pH) sensors

The sensitivity is shown in Figures 102 and 103:

- pH and temperature sensitivity: based on the data acquired during NaOCl and HCl addition (4 points) and on the temperature correction derived above, one can provide the calibration curve for pH sensors:

  $$pH_{CNT3\text{-}R1}\ (\text{pH unit}) = -0.029(U_{CNT3\text{-}R1}(\text{mV}) + 8.5T(°C)) + 7.9.$$

  The sensor outputs vary by about 30% between pH 6.7 and pH 8.9. Based on the noise level (6.2mV), the noise on pH estimate is 0.18 (discounting error on the temperature data provided by other sensors).
- Chloride sensitivity: the sensor displays a strong sensitivity to chloride level, with the relationship

  $$[NaCl]_{CNT3\text{-}R1}(\text{mg/L}) = -1.2(U_{CNT3\text{-}R1}(\text{mV}) + 8.5T(°C)) + 140.$$

  The sensor outputs vary by about 80% between concentrations of dissolved NaCl ranging from 0 to 249mg/L. Accounting for 6.2mV of noise, the error on [NaCl] concentration in mg/L is 7.4 (discounting error on the temperature data provided by other sensors).
- There is no sensitivity to flow rate.

Remarks and recommendations:

- The sensitivity to both pH and chloride of CNT3 was also observed in the lab testing of the cap #6.
- The analysis of sensitivity to temperature should be extended to the full range of temperature (presently only 20°C to 27°C).

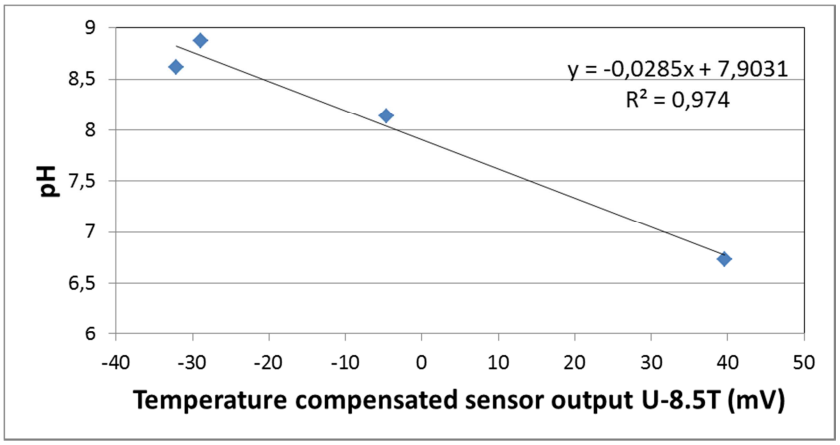

Figure 102 pH sensitivity calibration curve

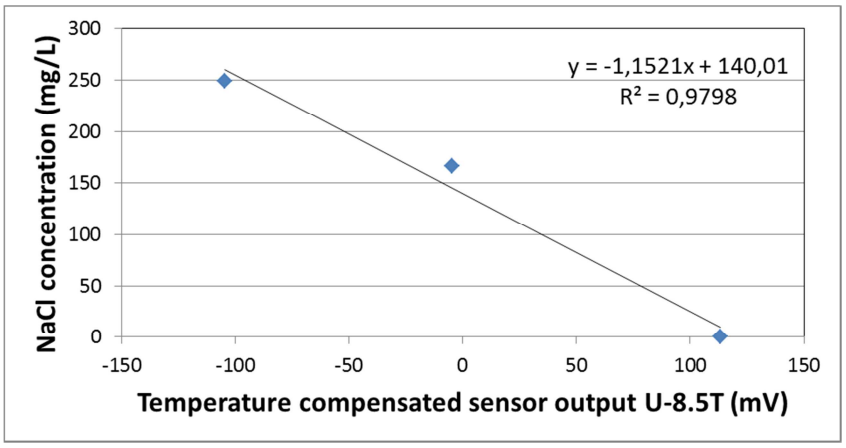

Figure 103 chloride concentration calibration curve

4.5.3.7 Response time

The response times observed here are in general similar for both CNT and conductivity sensors. Though a detailed analysis of response time is needed, this suggests that the response time is not controlled by the sensors themselves, but by the geometry of the caps (time of diffusion of chemicals from the water in the loop to the sensor surface) or by the behavior of the water in the loop itself (homogenization time of the water after chemical additions). Among these two factors, the fact that the response times vary widely from one chemical scenario to the other (from instantaneous to 1h), suggest that the dominant factor is actually the time of homogenization in the loop, and not the caps geometry.

4.5.4 Remark on noise levels

The data presented above, notably the noise levels, are obtained from data that have been partially cleaned by post-processing before analysis. Indeed, the raw outputs from the node present significant noise patterns which are easily identifiable and removable from the data by software-based approach:

- Signal drops to zero over a few minutes, and then goes back to its initial level.
- Wrongly signed output: negative signal for temperature, conductivity and CNT sensors; Positive signal on pressure sensors.
- Crosstalk between channel: the output measured on a given channel is actually the output from another channel

Among these three types of noise, the last two appeared to clearly worsen along the life of the cap in the loop, suggesting an effect of ageing at cap level (for instance loss of waterproofing of the wirebonding due to the observed ageing of the globtop), or at AFE level. Subsequent analysis will be carried out to understand better and correct these noise issues.

4.5.5 Synthesis

The following table summarizes the different results obtained in Sense-City loop for cap #5.

	Temperature T(°C)	**Pressure P(bar)**	**Conductivity C(µS/cm)**	**pH (pH unit)**	**Chloride [NaCl] (mg/L)**	**Active Chlorine [HOCl] (mg/L)**	**Comment**
Temp2 T2 U_{T2}(mV)	$T=0.46U_{T2}-0.41$ Error: 0.25°C (among which, sensor noise accounts for 0.15°C)		Temporary increased response time with conductivity jump				
Pressure1 Pr1 U_{pr1}(mV)	$U_{pr1}=2.0T+98$	$P=-0.25(U_{pr1}-2.0T)+5.6$ Noise: 0.5bar					No flowrate sensitivity
Cond2 U_{Cond2}(mV)	$U_{Cond2}=-12T+830.$		$C=-5.0(U_{Cond2}+12T)+4700$ Noise: 50µS/cm				
CNT1-R1 (chloride) $U_{CNT1-R1}$(mV)	$U_{CNT1-R1}=9.5T+99$			pH sensitive [HOCl] sensitivity	Up to 160mg/L, $[NaCl]=-11(U_{CNT1-R1}+9.5T+2900$ Error (on [Cl-]): 51mg/L	At pH<8, linear sensitivity; up to 300mg/L $[HOCl]=1.2(U_{CNT1-R1}+9.5T)+200$ Error: 9.2mg/L	Chlorine sensitivity cannot be univocally separated from pH sensitivity with the current set of data
CNT2-R2 (chlorine) $U_{CNT2-R2}$	$U_{CNT2-R2}$(mV)= 20T(°C)+304			pH-sensitive [HOCl] sensitivity No correlation with pH independantly from [HOCl]	<2.2%	At pH<7, up to 300mg/L, $[HOCl]=0.4(U_{CNT2-R2}+20T)+160.$ Noise on [HOCl]:3.2mg/L Noise projection in range of interest (<1.25mg/L): 0.02mg/L	Chlorine sensitivity cannot be univocally separated from pH sensitivity with the current set of data
CNT3-R1 (pH) $U_{CNT3-R1}$	$U_{CNT3-R1}$(mV)= 8.5T(°C)+43			Between pH 6 and 9 $pH_{CNT3-R1}=-0.029(U_{CNT3-R1+}8.5T+7.9$ Noise: 0.18 pH unit	$[NaCl]=-1.2(U_{CNT3-R1}+8.5T)+140$ Noise (on [Cl-]): 4.4mg/L	Only 2 data points available	Chlorine sensitivity cannot be univocally separated from pH sensitivity with the current set of data
Comment	The error estimate on temperature sensitivity remains to			CNT3-R1-pH has the clearest sensitivity to pH,	Both CNT3-R1-pH and CNT1-R1-Cl are sensitive to chloride,	Both CNT2-R2 and CNT1-R1-Cl are sensitive to chloride,	

	be determined using the bootstrap method. For all the sensors, the range of estimation of the temperature sensitivity should be expanded			independent from the other parameters.	but CNT3-pH R1 has much less noise. Remark: [Cl-]= 0.6[NaCl]	but CNT2-Cl2-R2 has much less noise. Remark: [HOCl] is the active chlorine concentration (close to the available chlorine concentration at pH<7)	

General comments:

-Noise levels do not account for the error on the temperature sensitivity or for the error on the temperature. To evaluate the error on the estimation of temperature sensitivity, the bootstrap method should be applied to all the data on temperature sensitivity.

-The chlorine and pH sensitivity are not easily decorrelated with this set of data. Additional experiments with HCl and NaOH only (without NaOCl) should be carried out to enhance the analysis.

-The CNT sensor data are well differentiated from one sensor to the other, but still correlated with one another (selectivity is not ideal). Data from the other sensors will be needed to decorrelate between variation in pH, in active chlorine and in chloride levels. Notably a change in the conductivity would signal preferentially a change in chloride, while a change in pH or chlorine level with small or negligible conductivity change would be more directly correlated with a change in chlorine level.

4.6 Energy harvesting

In Sense- City we tested the piezoelectric vortex generator (PVG) already tested in the laboratory test bench, having made suitable the covering cap to the Sense-City loop hydraulic connections. In Figure 104, it is shown the field deployment of the device: it is placed at a distance of about one meter from a second hydraulic connection which could accommodate the PROTEUS sensor cap. At the moment, the device is tightly kept in position using the external PVC collar for pressing the cover cap. The second version will adopt the same connection scheme of the PROTEUS head, with a device, which can be put in the operating position after raising the watertight closure.

Figure 104 – Deployment of the Piezo Vortex Generator in Sense -City

Moreover, a standard (3.3 V – 4 W) solar panel was deployed inside the cabin and in some cases connected to the power circuit in order to test the multisource alimentation.

A t first, in order to test only the device we acquired the signal coming from the electrical termination of the piezoelectric cantilever varying the speed of the water circulating in the loop at a fixed pressure equal to 1 bar. In a second moment, the device was connected to the energy management circuit, alone or together with the solar panel.

Figure Figure Figure shows the signal acquired from the harvester on a 196 kΩ resistive load for different speeds of the water.

Note that the speed is actually an average speed of the water running inside the loop as it is obtained dividing the measured volume flux by the pipe section, while it is known the speed profile inside a pipe is usually parabolic. In any case it is apparent that there is a significant increase of the voltage as the the speed increases.

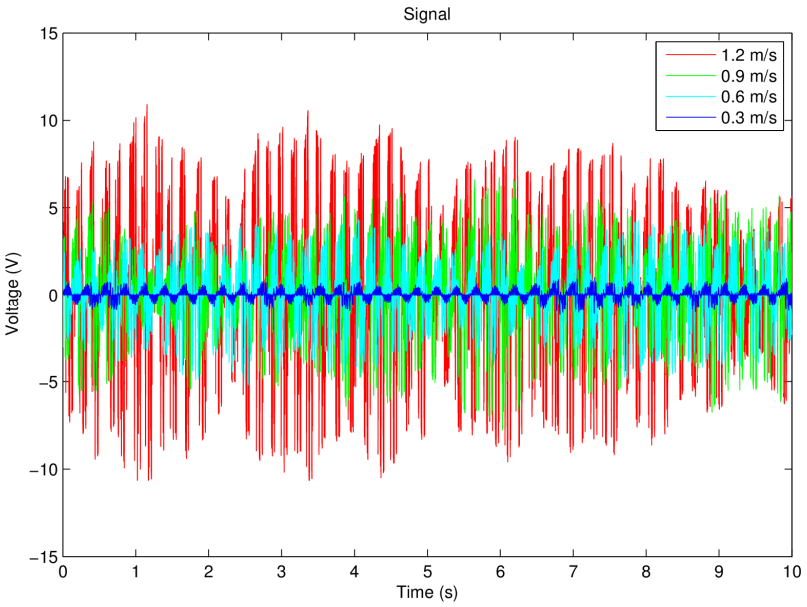

Figure 105 – Piezoelectric cantilever signal at various water speeds.

The power spectrum of the collected signal (Figure 106**Erreur ! Source du renvoi introuvable.**) shows that most of the energy transferred from the water flux is confined at low frequency. In fact, as the transversal size of the oscillating cylinder is 24 mm, we expect that the frequency driving force, f_w, is about 2.5 Hz at 0.3 m/s and it increases linearly with the velocity up to 10 Hz at 1.2 m/s. The observed frequency peak is however at first higher and then consistently below the driving force frequency (Figure 07). We can explain such result considering the behavior of a real cantilever with a certain resonance width (due to viscous losses), stimulated by an external forcing with a finite bandwidth (due to the spread of velocities inside the pipe). Assuming linear conditions, the mechanical interaction can be described as the product of the stimulus and the response of the cantilever, which is fixed. Let us assume further, for sake of simplicity, that both the cantilever resonance and the driving force can be described by Gaussian functions. The result is still a Gaussian curve with an average (weighted by the variance) value of the central frequency, which is therefore less responsive to the external stimulus frequency. The resonant frequency of the cylinder is 4.8 Hz in air and 3.8 Hz in still water, due to the increased friction, thus explaining both the behavior at low and high water speed.

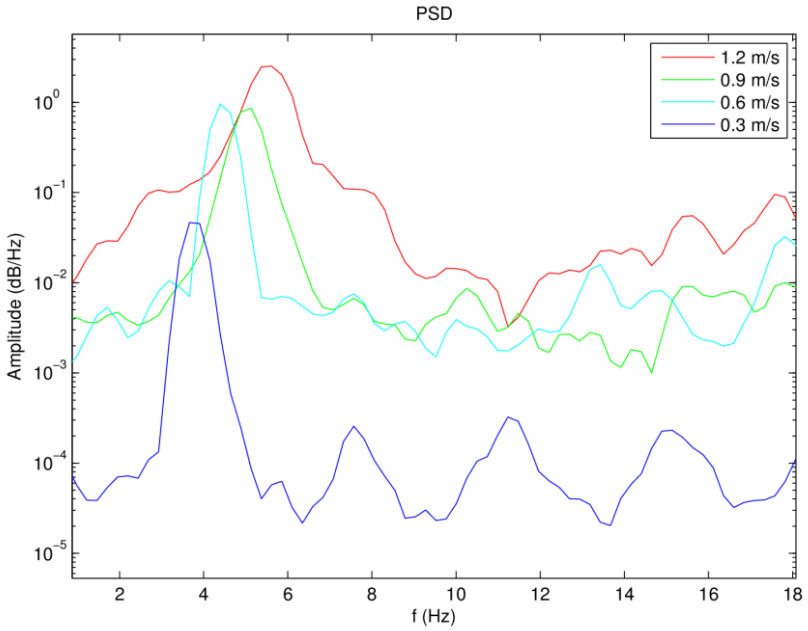

Figure 106 – Power spectrum of piezoelectric cantilever signal at various water speeds.

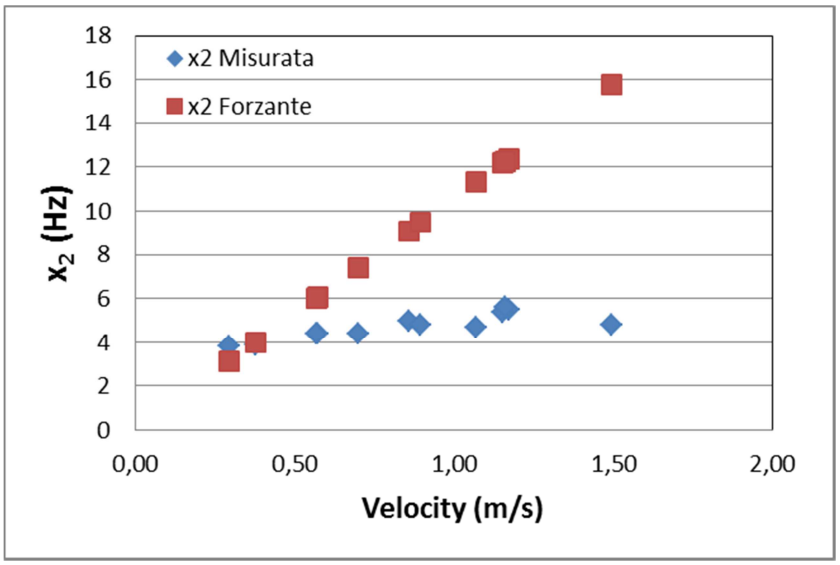

Figure 107 – Comparison the frequency of the driving force and that of the oscillating cylinder.

The power generated by the harvester is reported in Figure 108Figure . The values can be fitted to a power law with 2.4 exponent in quite good agreement with the power increase of the water flux, modified by the frequency dependence of the cantilever resonance, the effect being weak as the resonance is quite broad (FWHM ~1 Hz). The values are, for the actual device tested in Sense-City, very low (efficiency<.0001), nearly two order of magnitude lower than what obtained for an analogous device tested in laboratory. The efficiency can be increased (about 1 order of magnitude) using a better matched impedance load, which subsequent measurements in lab have shown to be about 1 MΩ, but still this transduction scheme (by piezoelectric, i.e.) has an inherent weak efficiency, highly dependent on the actual assembly of the physical pieces. In these conditions, we expect that the piezoelectric scheme could be adopted only for the higher range of water speeds expected in the

network. In order to exploit more aptly the energy of the water flux, different transduction schemes (electromagnetic or electrostatic) should be employed.

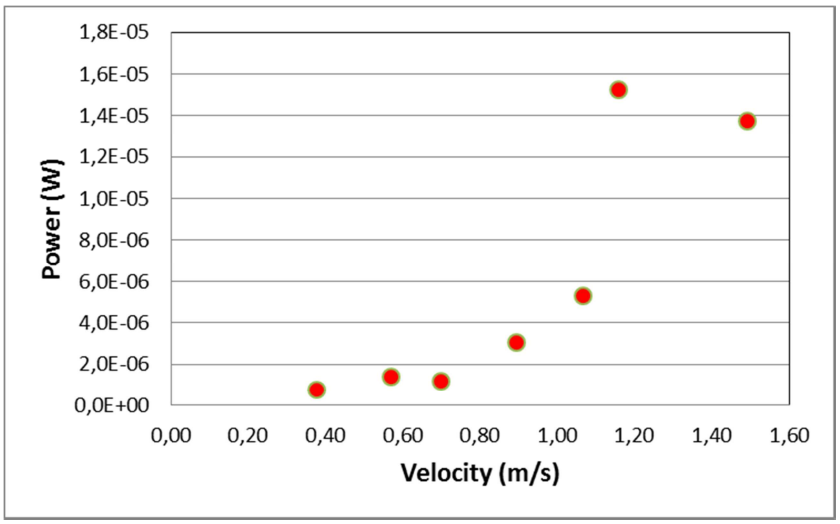

Figure 108 – Power generated by the piezoelectric harvester as a function of water speed.

As a final test, the device was connected to the conditioning circuit provided by UNINOVA. After the rectification the amplitude is practically the same. The output voltage and rectified one are showed in Figure 09.

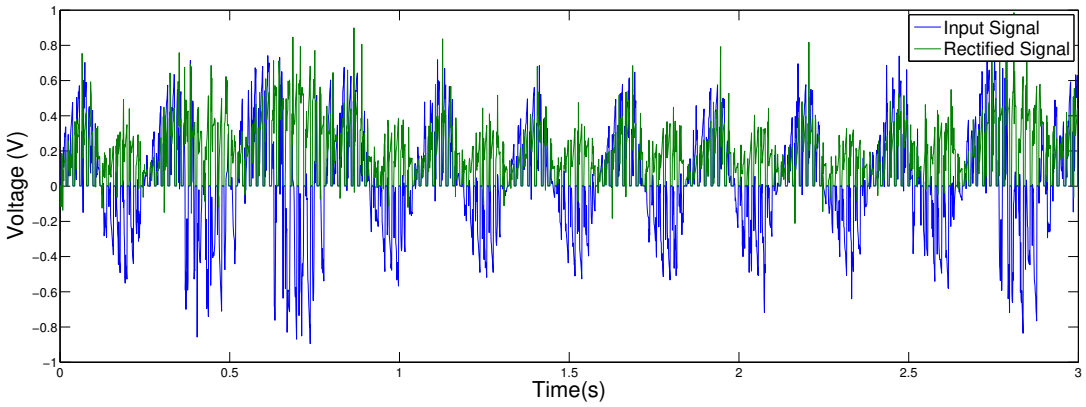

Figure 109 – Output voltage and rectified signal from the piezoelectric generator.

4.7 Proteus oracle

In this section, we present the results of the application of the predictive algorithm in the data obtained by each sensor deployed in the Sense-City. The sensors can be classified as either commercial sensors or Pnode sensors. As an evaluation criterion, for the performance of the algorithm, the Mean Square Error (MSE) was used. The MSE is the average of the difference between the predicted value and the actual value, thus lower MSE values means that the predictions are accurate.

In the following subsections, we present the predicted results indicating the MSE of the algorithm, and a set of graphs which illustrate the data gathered and the predicted values for the commercial sensors and the Pnode. The data were gathered from the Sense-City loop considering the last 1500 samples measured from each of the following nine commercial sensors: *Flow rate, PH, Conductivity, PH-Temperature, 1st Pressure, 2nd Pressure, 1st Temperature, 2nd Temperature, Conductivity-Temperature*.

4.7.1 Results on the commercial sensors

If we have n samples of sensor measurements , and for each one of them we correspond a predicted value h, then the Mean Square Error (MSE) between the predictions and the measurements is defined as:

$$MSE = \frac{1}{n}\sum_{i=1}^{n}(y_i - h_i)^2$$

where y_i ,h_i are the measurement and the predicted value for the i[th] period respectively. An MSE value close to zero means that the predictions are nearly the same as the measurements.

To find the accuracy of the algorithm, we use the Mean Absolute Percentage Error (MAPE) evaluation criterion. MAPE is a measure of accuracy in predictions used in statistics, for predictive algorithms, and it is expressed as a percentage. A MAPE value close to 100% means that we have achieved great accuracy in our predictions.

MAPE is defined by the following formula:

$$MAPE\ \% = 100 - \frac{100}{n}\sum_{i=1}^{n}\frac{y_i - h_i}{y_i}$$

Where y_i , h_i are the same as previously.

For a successful training and prediction, we will have the MSE value close to zero and the MAPE value close to 100.

The following table and Figures 110 to 118 show the results:

Sensor Parameters	Mean Square Error	MAPE
Flow rate	*0.0005*	*99.84%*
PH	*0*	*99.99%*
Conductivity	*0.6718*	*99.96%*
PH-Temperature	*0*	*99.99%*
1st Pressure	*0.0011*	*98.95%*
2nd Pressure	*0.0008*	*99.1%*
1st Temperature	0.0003	99.92%
2nd Temperature	0.0004	99.92%
Conductivity-Temperature	0	99.99%

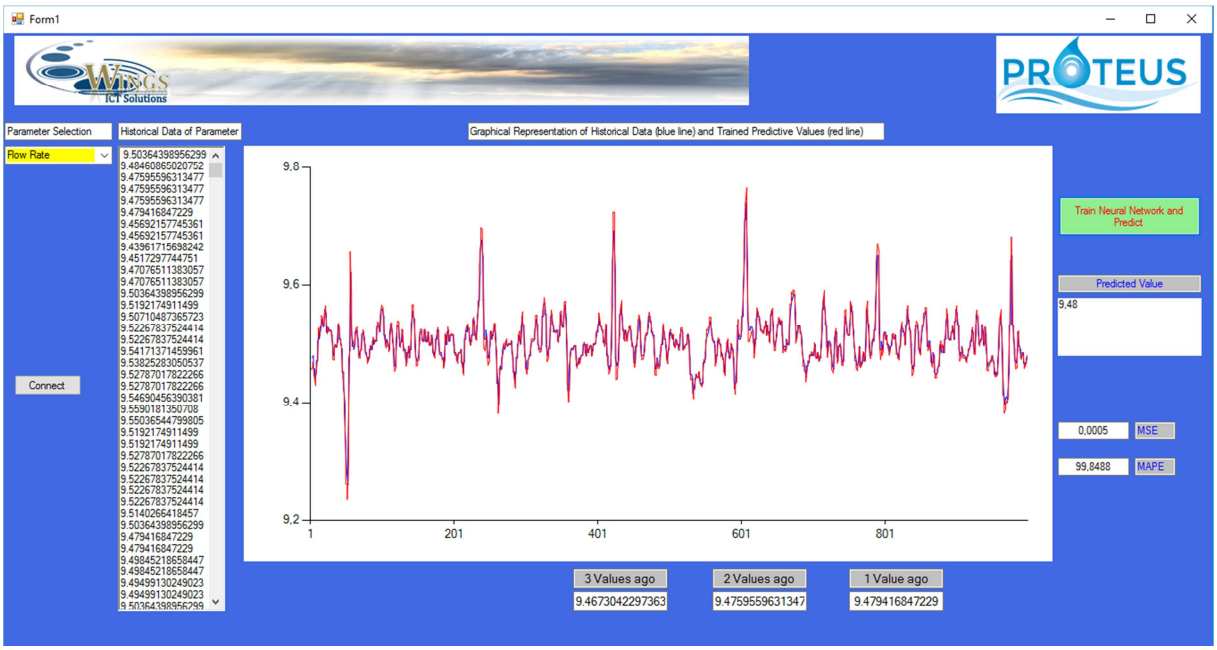

Figure 110 - *Result of the predictive algorithm for the flow rate sensor, MSE = 0.0005, MAPE = 99.84%*

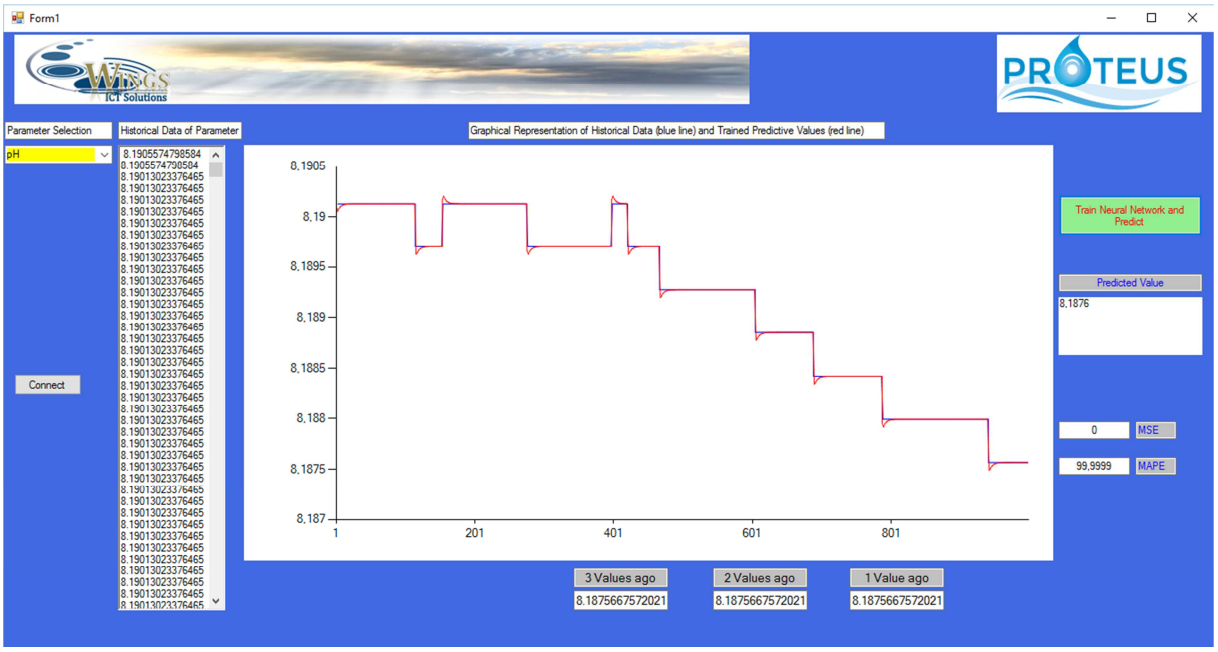

Figure 111 - Result of the predictive algorithm for the pH sensor, MSE = 0, MAPE = 99.99%

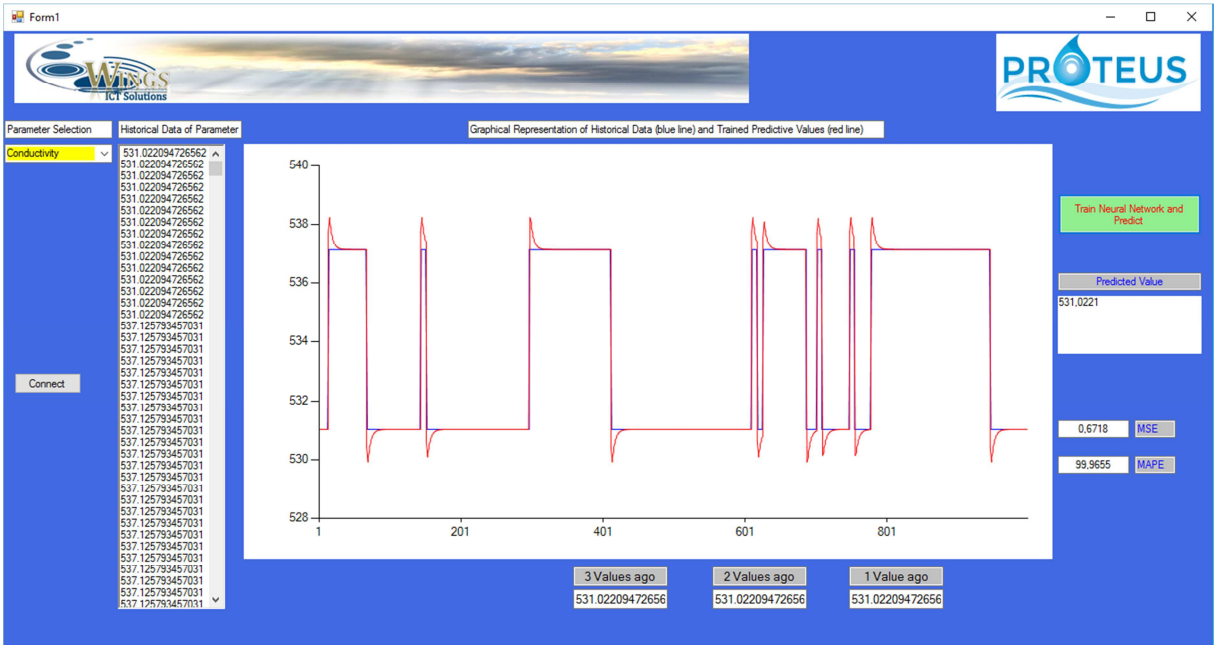

Figure 112- Result of the predictive algorithm for the conductivity sensor, MSE = 0.6718, MAPE = 99.96%

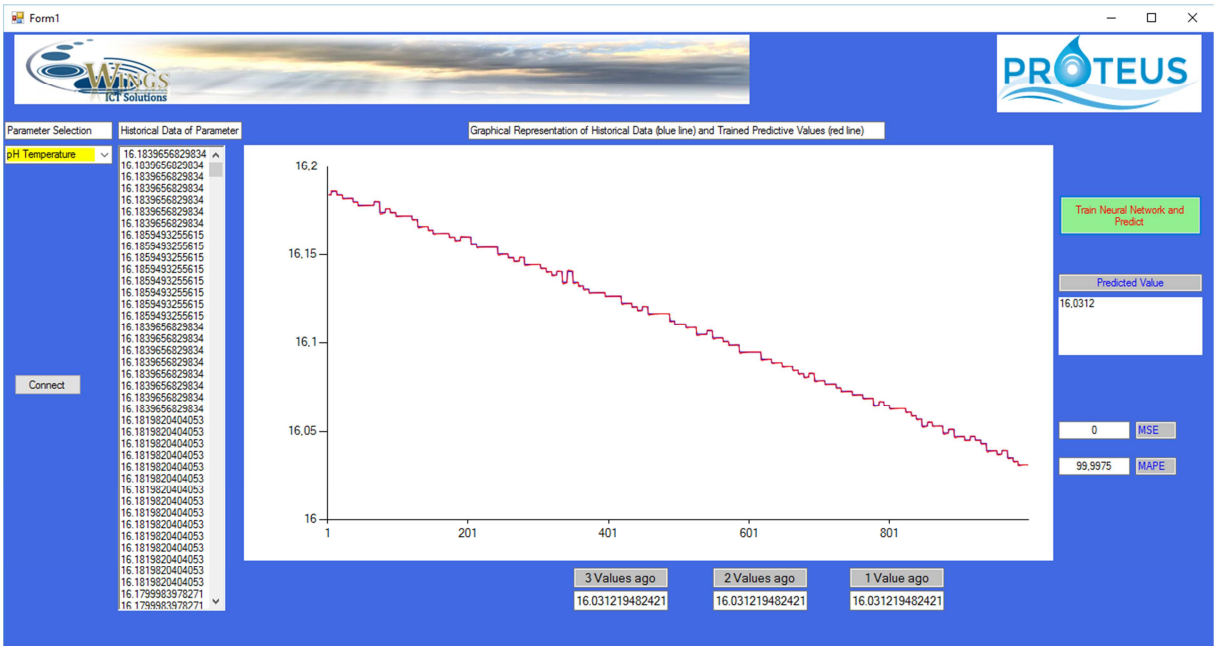

Figure 113 - Result of the predictive algorithm for the pH temperature sensor, MSE = 0, MAPE = 99.99%

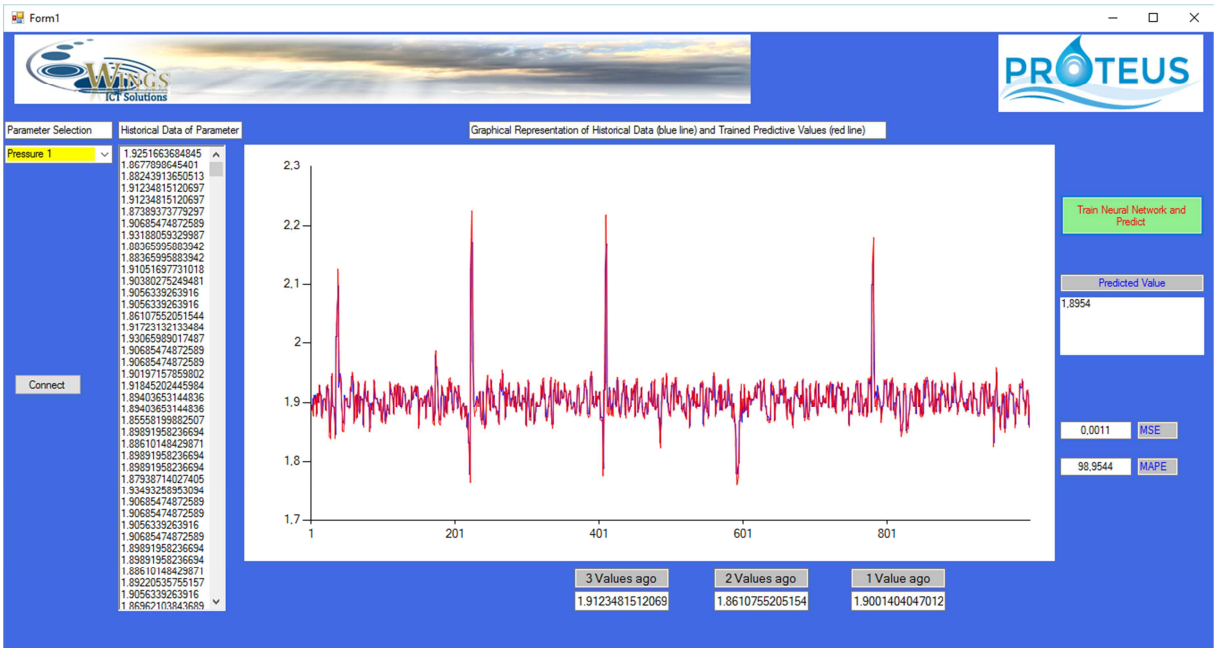

Figure 114 - Result of the predictive algorithm for the 1st pressure sensor, MSE = 0.0011, MAPE = 98.95%

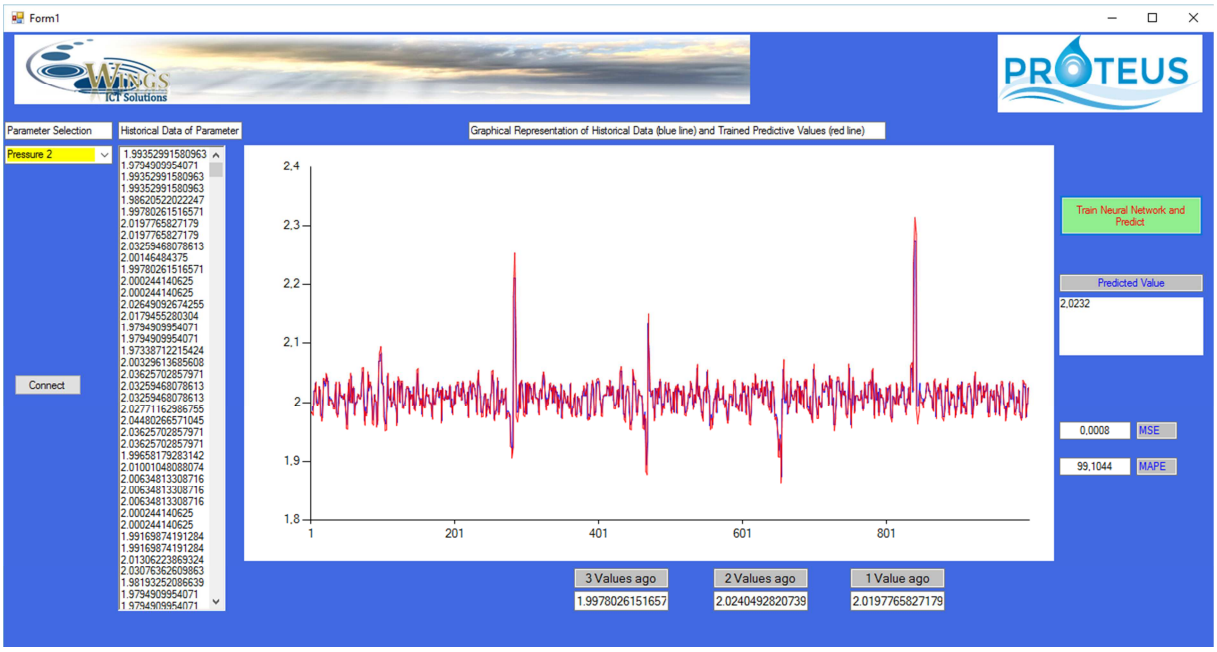

Figure 115 - Result of the predictive algorithm for the 2nd pressure sensor, MSE = 0.0008, MAPE = 99.1%

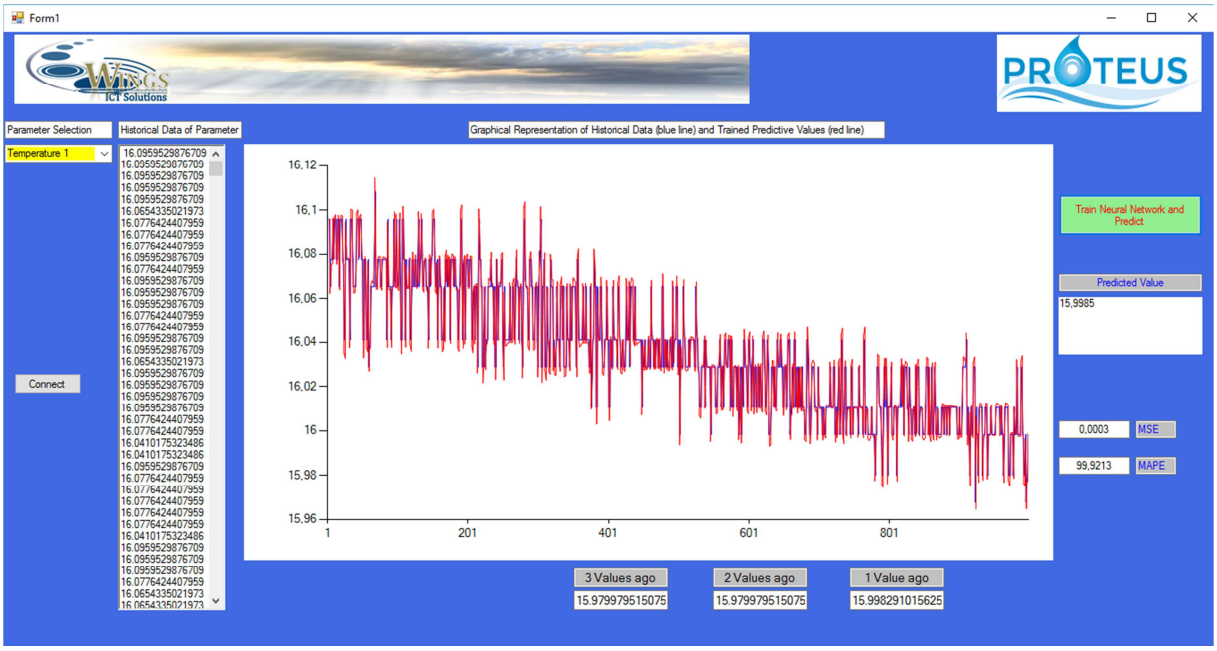

Figure 116- Result of the predictive algorithm for the 1st temperature sensor, MSE = 0.003, MAPE = 99.92%

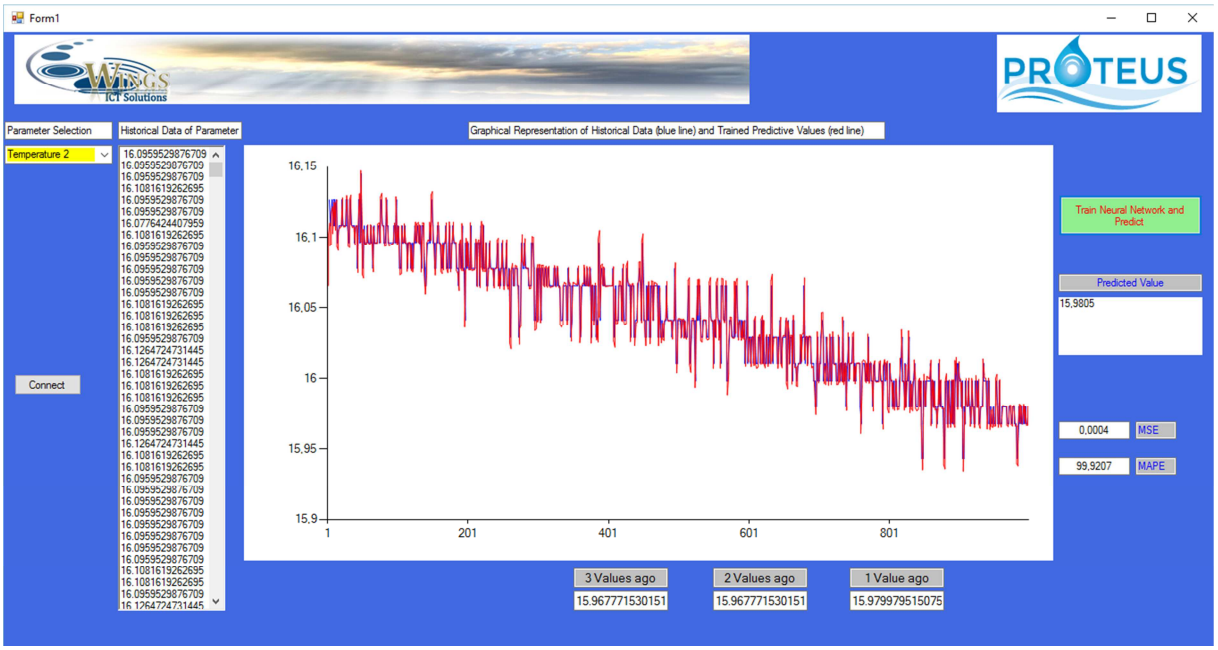

Figure 117 - Result of the predictive algorithm for the 2nd temperature sensor, MSE = 0.0004, MAPE = 99.92%

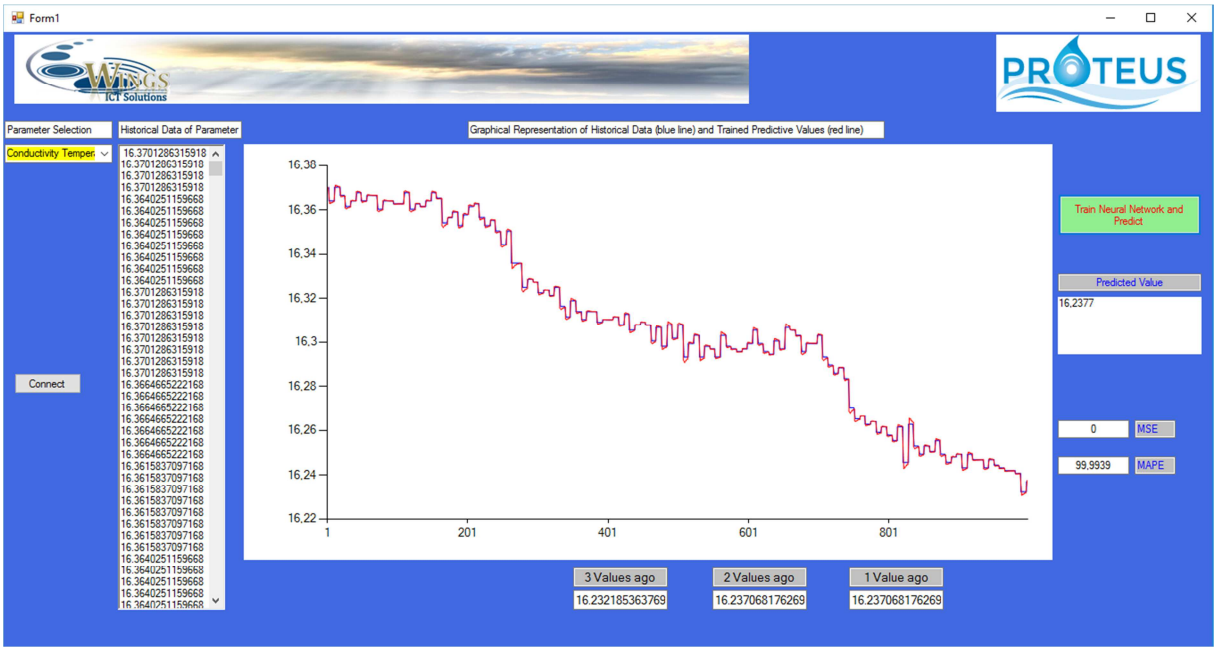

Figure 118 - Result of the predictive algorithm for the conductivity temperature sensor, MSE = 0, MAPE = 99.99

4.7.2 Results on the Pnode temperature sensor

Finally, we present the results of the algorithm on the Pnode temperature sensor that was installed on Sense City (Figure 119). The MSE in this case is 0.0359 and the corresponding MAPE is 99.79%.

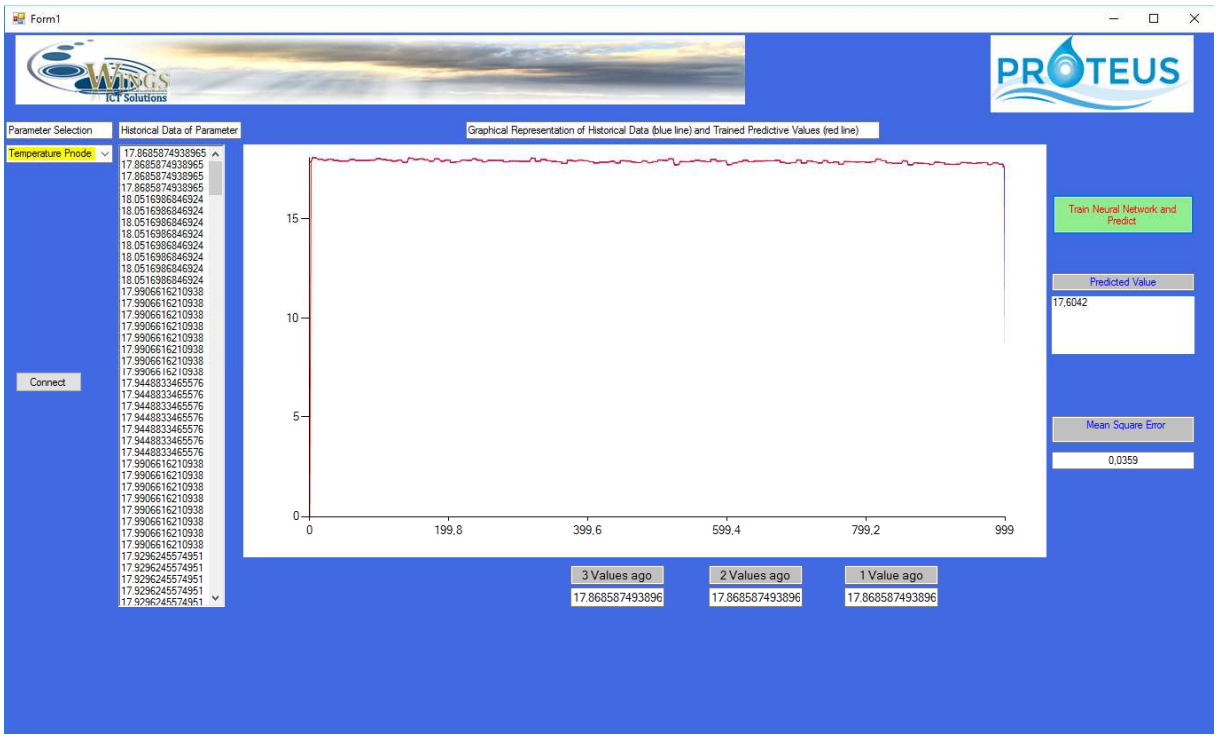

Figure 119 - *Result of the predictive algorithm for the Pnode temperature sensor, MSE = 0.0359*

The results of the predictive algorithm present a high level of accuracy. It would be interesting to test the algorithm in datasets with large variations.

5 Synthesis and prospects

5.1 Summary of results

The following paragraphs summarize the results (positive and negative) of the different stage of validation (separate building blocks and assembled caps in the lab, assembled system in SenseCity)

5.1.1 Lab validation of separate building blocks

	Results	Limitations	Comments
Temperature sensor	Linear relationship between temperature and resistance (increase)		Calibration parameters different from models
Conductivity sensor	Linear relationship (increase) between conductivity and sensor conductance (1/V)	Linearity only for device versions 2 and 3	
Flowrate sensor	Nonlinear decrease of resistance with flow rate	Only exploitable for devices on glass (not usable for subsequent assembly into Proteus node)	Flow rates considered are much lower than Proteus Second version being developed (see D2.2)
Pressure sensor	Linear relationship between temperature and resistance (increase)	The rectangular pressure sensor more sensitive than the square one	Two versions available
pH sensor	Not sensitive below pH 8 Linear relationship between pH and resistance (increase) pH 8 (50% variation)	No cross sensitivity study (including in temperature)	Device to device reproducibility to enhance
Free Chlorine sensor	Linear relationship between free chlorine concentration and	No cross-sensitivity study (including in	Device to device reproducibility to

	resistance (increase) Sensitivity low (10% variation only)	temperature)	enhance Only the dependence to free chlorine is studied
Chloride sensor	Linear relationship between NaCl concentration and resistance (increase) (50% variation)	No cross sensitivity study (including in temperature)	Only 0.5% of range of interest for chloride variation Device to device reproducibility to enhance
CMOS chip (analog to digital conversion)	Successful Analog to digital conversion with simulated conductivity sensor output	Low pass filter decimation via MATLAB	
Pizeo electric vortex generator as energy harvester	Maximum power of 230µW available at 0.78m/S		Evaluation of PVG frequency as a function of water velocity

5.1.2 Sensitivity analysis of assembled caps

	Results	Limitations	Comments
Temperature sensor	Linear relationship between temperature and sensor output (increase) Mean error. 0.32°C (0.17°C when discounting data with high rate of temperature rise)	Larger errors when high rates of temperature increase Suggests limitations in response time	Response time should be analyzed
pH sensor	50% decrease between pH 4 and pH 6 No sensitivity above pH 8	Significant cross sensitivity to chloride (up to 70% variation) 1 out 3 sensors not responsive to pH	Data between pH5.7 and pH 7.8 needed. Optimal choice of solutions for pH testing still remain unclear
Chloride sensor	Over 500% relative variation (increase) with chloride addition (at 20mg/L) Saturation above 120mg/L	Only 1 sensor out of 3 with very strong sensitivity Moderate (25%) cross sensitivity to chlorine	More data needed between 0 and 120mg/L KCl.
Active chlorine sensor	pH sensitive increase with HOCl concentration (active chlorine) 200% relative variation at pH6	Strong cross sensitivity with pH (expected, as active chlorine levels are highly depending on pH) and moderate (30%) sensitivity to chloride)	Data at pH 7 to 9 are needed to decorrelate HOCl (active chlorine) and OCl (available chlorine) sensitivity

5.1.3 Assembled system validation in Sense-city loop

	Results	Limitations	Comments
Packaging	Up to 10 bars No mechanical failure: PCB in place, no degradation of the chips Encapsulation resist stable, but degradation of globtop exposing wirebonding	No testing with variable flow rate	New choice of gloptop resist is planned for version 2 of sensor caps assembly (see. D2.2)
Noise level (from sensor caps to WMS level)	Different noise patterns observed at WMS level: Signal drops, Wrongly signed output, crosstalk between channels	Noise correction achieved via data post-processing	Need to include code for noise correction in the PNODE software, and to identify cause for noise at hardware level
Temperature sensor	Linear relationship (increase) between temperature and sensor mV output Accuracy: 0.25°C; Precision: 0.15°C	Temporarily increased response time when conductivity jumps up	Calibration parameters different from models D1.1 requirements: 1.5°C precision
Conductivity sensor	Linear relationship (increase) between conductivity and sensor mV output Precision: >50µS/cm	Inverted trend compared to lab data.	Testing only achieved for increasing conductivity, on version 3 conductivity sensor D1.1 requirements: 30µS/cm
Pressure sensor	Temperature decorrelated linear relationship between pressure and resistance (increase) Presicion: >0.5bar	Precision low (>0.5bar) compared to range of variation of pressure (1 to 10 bar)	Rectangular pressure sensor; tested from 1 to 3bar. D1.1 requirements: 0.8bar
pH sensor	Temperature-decorrelated linear relationship between pH and sensor output between pH 6 and 9 Precision: >0.18pH unit	Linear cross-sensitivity to chloride (precision >4.4mg/L) Possible cross sensitivity to chlorine	Chlorine sensitivity cannot be univocally separated from pH sensitivity with the current set of data D1.1 requirements: 0.25 pH unit

Active chlorine sensor	Temperature-decorrelated, pH sensitive, linear relationship between HOCl (active chlorine) and sensor output Projection on precision: >0.02mg/L No cross sensitivity to chloride	Cross sensitivity to pH	Range of active chlorine considered here 2 ranges of magnitude larger than Proteus range Chlorine sensitivity cannot be univocally separated from pH sensitivity with the current set of data D1.1 requirements: 0.06mg/L
Chloride sensor	Temperature-decorrelated linear relationship between chloride and sensor output Precision: >51mg/L	Linear cross sensitivity to HOCl (precision 9.2mg/L) Possible pH cross sensitivity	Chlorine sensitivity cannot be univocally separated from pH sensitivity with the current set of data
Pizeo electric vortex generator as energy harvester	Power generated increase from 1µW at 0.4m/s to 15µW at 1.2m/s Successful connexion as power supply for the the PNODE electronic card (V1.1)	No power generation at 0.1m/s, which is the maximum level of flowrate measured in several points in Almada network.	A new harvester design is proposed to be compliant to lower flowrate (see D2.2) D1.1 requirements: 13mg/L
ORACLE (predictive software)	Successful prediction for reference sensors (error: less than 0.9%) and for the PNODE temperature sensor (error: 0.2%)		Error: mean of absolute value of point by point error

5.1.4 Additional experiments for sensitivity analysis

The synthesis above suggests the following complements of validation for sensitivity analysis

- Lab testing of caps:
  - Testing of conductivity sensors
  - Chlorine sensitivity analysis at higher pH
  - Temperature sensitivity analysis
  - Response time analysis
- Sense-City scenarios
  - Extended steps durations to ensure all sensor stabilization
  - Enhanced testing of conductivity sensor (notably with decreasing conductivity level)
  - pH variation without change in chlorine level
  - much smaller range of chlorine variations
  - temperature sensitivity analysis over extended ranges of temperature

Regarding to the Sense-City sensor validation stage, considering the mass of data to process and the complexity of trials, an automated data processing approach would be highly beneficial, as well as an automated noise correction software.

5.2 Directions of optimization

Even without these additional data, the synthesis above suggests the following routes for optimization of the PNODE:

- Sensors
  - Change the design of the flow rate sensor (a new design is already available and described in the D22 deliverable)
  - Improve on the device-to-device reproducibility and on the selectivity on the CNT sensors
  - Increase the range of sensitivity to pH
- Electronics:
  - Identification & correction of hardware causes for noise
  - Software level correction of noise
- Packaging:
  - Improvement of the gloptop strategy
- Energy harvester
  - New strategy for harvesting at low flow rate